Flow as a Mediator of Ecosystem Engineering: Hydrodynamics Shape Chemical Modification by Kelp and Mussel Beds

Kindall Murie

A dissertation

submitted in partial fulfillment of the

requirements for the degree of

Doctor of Philosophy

University of Washington

2025

Reading Committee:

Emily Carrington, Chair

Jennifer L. Ruesink

Thomas L. Daniel

Program Authorized to Offer Degree:

Biology

Abstract

Flow as a Mediator of Ecosystem Engineering: Hydrodynamics Shape Chemical Modification by Kelp and Mussel Beds

Kindall Murie

Chair of the Supervisory Committee:

Emily Carrington

Department of Biology

Ecosystem engineers are organisms that modify their physical and chemical surroundings in ways that shape the structure and function of ecological communities. Physically, they build biogenic structures that modify flow, light, and habitat complexity. Chemically, they change oxygen and pH levels through metabolic processes such as photosynthesis and respiration. These modifications can either facilitate the presence of associated species by creating favorable microhabitats or inhibit them by amplifying environmental stress. Understanding the circumstances under which and how these shifts occur has become increasingly important as climate change intensifies environmental variability in coastal ecosystems. Advancing our understanding of how ecosystem engineers shape their communities requires considering how external factors, particularly flow, mediate their influence on the surrounding environment. Driven by tides, waves, and currents, flow regulates water residence time and thus the

accumulation or dispersion of biologically modified water. Yet despite its central importance, the role of flow in controlling the strength and direction of ecosystem engineering remains poorly understood.

This dissertation examines how local hydrodynamics influences the capacity of marine ecosystem engineers to modify their surrounding chemical environments. It focuses on two contrasting but complementary systems: an autotroph, bull kelp (*Nereocystis luetkeana*), and a heterotroph, mussels (*Mytilus spp*.). Looking across these systems provides a broader view of how different types of engineers—those that produce oxygen through photosynthesis and those that consume it through respiration—shape their local chemical environments. By studying both systems, this work links two aspects of ecosystem engineering: 1) oxygen production and depletion, and 2) explores how flow determines when these species have the potential to act as facilitators or inhibitors within their communities. I combined field observations with laboratory and field experiments to explore how flow dynamics interact with biological traits, such as canopy structure, density, and behavior, to determine when these engineers act as facilitators or inhibitors within their communities. Across chapters, the work progresses from identifying environmental controls on kelp-driven chemical modification (Chapter 1) to isolating mechanistic feedbacks between flow, mussel behavior, and chemistry (Chapter 2), and then investigating density effects on chemistry and behavior by out-planting manipulated mussel aggregations in natural conditions (Chapter 3).

Chapter 1 addresses a fundamental gap in understanding how hydrodynamic variability constrains the ability of kelp forests to alter seawater chemistry. Using high-frequency, long-term measurements of flow, light, dissolved oxygen (DO), and pH, this chapter quantifies how diel

and tidal cycles interact to control the timing, magnitude, and spatial pattern of kelp-driven chemical change within a tidally dominated bull kelp forest in the Salish Sea. The results show that kelp effects on local seawater chemistry are not static "hotspots" but dynamic, flow-dependent features that shift predictably across space and time. Kelp-driven increases in DO occur primarily during daytime slack tides, when reduced flow allows oxygen-enriched water to remain within the canopy before being rapidly replaced by the next tidal exchange. These findings demonstrate that even in a highly productive kelp forest, strong and variable tidal currents limit the persistence of chemical modification to only a few hours per tidal cycle. As a result, the capacity for kelp forests to function as chemical refugia depends less on their metabolic potential and more on the hydrodynamic context that influences water retention and exchange. By explicitly linking diel and tidal processes, this chapter reframes kelp-driven buffering from a static to a dynamic process and provides a framework for predicting when and where macrophyte canopies can locally ameliorate chemical stress.

Chapter 2 builds on this framework by examining how flow and organismal behavior mediate chemical modification in a heterotrophic engineer, the mussel. Valve gaping in mussels regulates the flow generated by their pumping activity, which drives water exchange between the ambient environment and the interstitial spaces within aggregations. This chapter presents an experimental approach that couples behavioral measurements from high-frequency gape sensors with real-time oxygen data to evaluate how valve activity and flow together shape interstitial water chemistry across three *Mytilus* species. Two consistent patterns emerged: oxygen depletion within mussel beds decreased exponentially with increasing flow speed, and gaping behavior remained largely static across flow and low-oxygen conditions. The absence of compensatory gaping under low-flow conditions indicates limited behavioral feedbacks between gaping,

chemistry, and flow, underscoring the dominant role of physical flow in driving oxygen dynamics within mussel aggregations. Variation in oxygen depletion among species was best explained by differences in biomass density, suggesting that morphometric traits, rather than behavior, primarily govern their capacity for chemical modification. These findings refine our understanding of ecosystem engineering by identifying the conditions under which structural and hydrodynamic factors outweigh behavioral influences.

Chapter 3 builds on insights from Chapter 2 by extending the work into the field, where mussel aggregations experience natural tidal flow and greater variation in density. The first goal was to determine whether higher mussel densities lead to stronger oxygen depletion under natural flow conditions. A second goal was to test whether the relationship between flow speed and dissolved oxygen follows the same exponential pattern observed in the steady-flow flume (Chapter 2), and whether mussel gaping remains insensitive to flow and oxygen variation across different aggregation positions in a more dynamic environment. The field experiment showed that oxygen concentrations declined sharply with increasing aggregation density, with the highest-density aggregations exhibiting the lowest mean DO levels, the largest diel fluctuations, and frequent short-lived hypoxic events. Gaping behavior varied with density and position within an aggregation, as interior mussels gaped wider and spent more time open than edge mussels, but showed little response to short-term changes in flow or oxygen availability. These results demonstrate that structural traits of an aggregation, such as density, amplify chemical modification, while flow regulates its magnitude and persistence. Moreover, there was no evidence that behavior provides any buffering capacity once physical exchange is constrained.

Across systems, this dissertation highlights a unifying principle: the capacity of marine engineers to alter their environment depends primarily on how their biological traits, such as metabolism, structure, and abundance, interact with hydrodynamic forces. By quantifying how flow controls oxygen variability across autotrophic and heterotrophic systems, this work advances a better understanding of when and where ecosystem engineers function as facilitators or inhibitors, emphasizing the central role of local physical dynamics in shaping their ecological influence.

Table of Contents

Acknowledgements

They say it takes a village to raise a child. Well, it took a village, a town, and roughly half a city to raise this PhD student—and I couldn't be more grateful for my people. It's taken a little over 25 years of school to reach this dream of mine, and there are so many people to thank that I know I won't be able to list them all here. So first, a BIG thank you to everyone who had a hand in this journey, big or small. I'm grateful for all the support, inspiration, and friendships along the way.

I want to begin by thanking my advisor, Dr. Emily Carrington. Over the past five years, you've shown me how to view and think about science in an entirely new light. It's a true gift to walk away with a new skill set—biomechanics, physics, electronics, and so much more—that will genuinely broaden how I approach future scientific endeavors. These skills have opened doors I never imagined myself walking through. Thank you for the countless hours and sweat you poured into this thesis as well. I truly appreciate all your effort and time in helping shape me into a better scientist and human, always down to be a paddleboard buddy.

Additionally, I want to thank my reading committee members. Dr. Jennifer Ruesink, thank you for your thoughtful comments and helpful conversations, especially the stats! Watching how hard you work is truly inspiring. Thank you to Dr. Thomas Daniel for encouraging me from day one and greeting me as 'Dr. Murie' well before I earned it. You've always made me feel like I deserve a seat at the table, and I truly appreciate that. I'd also like to thank Dr. Alex Gagnon for serving as my GSR; your questions and suggestions at every meeting helped shape many aspects of this thesis. I'm incredibly grateful to have had a committee full of such remarkable scientists.

Next, I would like to thank collaborators, or what I like to call my extended lab family. Both Dr. Michael Nishizaki (and lab) and Dr. Matthew Reidenbach (and lab) were such a pleasure to work with. I enjoyed every lab meeting, summer data-collection adventure, attempts at playing rec sports, and late-night convo. Thank you for always being willing to share equipment, review the data, and encourage me to keep going these last 5 years. I truly learned a ton from both of you and your students. I would also like to thank Dr. Luke Miller for his generous help with the instructions and for building the mussel tracking boards.

A big thank you to the Carrington lab post-doctoral scholars, Dr. Aaron Ninokawa, and Dr. Alli Cramer. You both are amazing and totally were right, no one should ever code alone! Aaron, I have always joked that I will have to name my firstborn after you for the countless hours you have spent helping me with R and seawater chemistry calibrations. Your enthusiasm for science and a good pun is contagious – I can't thank you enough for all your help. I have learned so much from you. Alli, thank you again for always taking the time to lend a hand, whether it was with R or reading over job applications and cover letters. Your encouragement was always appreciated. You both are top-tier scientists, and I was lucky to work with you both.

My lab mates, Robin Fales, Jack Litle, and Grace Leuchtenberger, you all are friends for life, and I can't stress it enough that without you all, I would have quit after year one. Thank you for the constant support, thoughtful feedback, and memories throughout the years. Thank you for picking me up when I was down and celebrating the wins along the way. I can't wait to collaborate on some excellent science in the future.

To my FHL family, you all were my home away from home, and each and every one of you makes FHL one of the best, most special field stations in the world. I already miss it and each and every one of you. I want to give a special thank you to Dr. Megan Dethier for her encouragement and for helping support my work at Friday Harbor Laboratories (FHL). You always went out of your way to help me achieve all my goals. Peggy Combs, you are amazing. Thank you for all your help with the logistics throughout the years. I hope you know how lucky FHL is to have you. And to Doug Engel, I know I kept you on your toes these last couple of years, to say the least, but thank you again for always coming to help me before I broke or burned down the lab. I have learned a ton of life skills from you, and I can't wait for you and Lee to meet Benson. Pema and Kristy, thank you for all your support with diving and boating over the years. Some of my best moments at FHL are on the water, and they wouldn't have happened without your help. To the countless boat tenders and scuba divers who braved the cold weather and early mornings, I couldn't have pulled any of it off without you! To Izzy Graham, Eleanor Rollins, Ava Martin, and Seila Lai, thank you for allowing me to be your mentor. I learned so much from each of you and am grateful for all the hours and hard work you put into helping me. You all brought so much laughter and joy to my days.

Finally, to my friends and family, there are not many people in life who truly, selflessly look out for your best interests. It's rare to find those who stand in your corner, not just in your circle—and to you all I am truly grateful. From my forever advisor, Paul Bourdeau, who thought he got rid of me in 2020, thank you for always answering my emails, calls, and texts. I would not have even known a Ph.D. in marine science was possible if it wasn't for you. If I become half the mentor/scientist you are, I will be stoked. Lily McIntire, Ande Fieber, Wes Hull, Tharadet Man, Becca Garcia, and Callie Woodall, thank you all for always being in my corner. Your support throughout this will always be something I cherish. Thank you to my family, you all are my rock and keep me grounded and remind me what's important in life. Thank you for believing in me. And of course, a special thank you to my Dad and my brother Wyatt, who got me into scuba diving so many years ago, it really was the start of me falling in love with the ocean and the natural world around me, who knows what I would have done if it wasn't for those moments underwater with both of you. And of course, my mom, my best friend. Your sacrifice, unconditional love, and support have allowed me to pursue this dream career, and I can't thank you enough for the opportunity. I am forever grateful for you. I love you all.

Tidal currents constrain a kelp forest's ability to modify its local chemical environment

Kindall A. Murie[1,2*], Aaron Ninokawa[3], Ross Whippo[4], Emily Carrington[1,2]

Institutional affiliations:
[1]Department of Biology, University of Washington
W Stevens Wy NE, Seattle, WA 98195

[2]Friday Harbor Laboratories, University of Washington, 620 University Rd, Friday Harbor, WA 98250, USA

[3] College of Environmental Science and Forestry, State University of New York, Environmental Science and Forestry, 1 Forestry Dr, Syracuse, NY 13210

[4] Oregon Institute of Marine Biology, University of Oregon, 63466 Boat Basin Rd, Charleston, OR 97420

Abstract

Kelp forests can locally alter seawater chemistry through photosynthesis and respiration, potentially buffering marine organisms from ocean acidification and hypoxia during the day. How hydrodynamic conditions shape biogeochemical modification within kelp forests by influencing the movement and persistence of kelp metabolic signals (i.e., diel fluctuations in pH and DO) remains poorly understood, partly because most research has focused narrowly on a few outer-coast species. We measured the temporal and spatial variation in dissolved oxygen (DO) and pH in a bull kelp (*Nereocystis luetkeana*) forest in the Salish Sea, WA, an inland sea with strong mixed semi-diurnal tidal currents. Spectral analysis of long-term, high-frequency sensor data from seven locations within and outside the kelp forest during its growing season revealed the combined influence of light-driven kelp metabolism and tidally driven water exchange. The largest changes in DO and pH occurred when daytime coincided with low-flow periods (e.g.,

‘slack’ tides), which followed semidiurnal/diel (< ~24hr) and circasemilunar cycles (~ 14 days). The precise timing and magnitude of these changes shifted within the canopy, depending on where and for how long current speeds were reduced. Across the 17-week deployment, the average difference in DO and pH between the different kelp canopy locations and outside surface water was 8.0–20.0 μmol L^{-1} and 0.03–0.05 pH units, respectively, while that between the kelp canopy and benthos was only 2.7–4.3 μmol L^{-1} DO and 0.01–0.02 pH units. Differences of this magnitude or greater typically persisted for less than two consecutive hours on a given day, depending on the duration of tidal condition (ebb, slack, or flood). Overall, strong tidal currents constrained the accumulation of light-driven kelp metabolic signals, resulting in small differences in DO and pH that are likely not biologically relevant for buffering hypoxia or ocean acidification compared to less dynamic systems. Our findings highlight that the potential for kelp forests to serve as chemical refugia can be limited and context-dependent, shaped by day length, tidal phase, and local hydrodynamics.

Introduction

Kelp forests are among the most productive, ecologically diverse, and economically important marine ecosystems on Earth (Steneck et al. 2002, Smale et al. 2013). As ecosystem engineers, canopy-forming kelps actively alter their environment through various biophysical processes, influencing light availability, nutrient retention, sedimentation, hydrodynamics, and seawater chemistry (Rosman et al. 2007, Nederlof et al. 2022, Masteller et al. 2015, Valle-Levinson et al. 2022, Kosek & Kukliński 2023), thus providing habitat, shelter, and food for a wide array of marine organisms, including commercially valuable fisheries worth millions of USD annually (Jones et al. 1997, Eger et al. 2023). Due to these strong ecological effects, kelps

have been globally included as contributors to climate adaptation and mitigation strategies (Krause-Jensen & Duarte, 2016; Filbee-Dexter, K., & Wernberg, T., 2020).

Through photosynthesis, kelps increase local dissolved oxygen (DO) and pH levels during the day, while their nighttime respiration decreases both, leading to predictable daily fluctuations in seawater chemistry (Frieder et al. 2012; Pfister et al. 2019; Murie & Bourdeau 2020). Because daytime photosynthesis typically exceeds nighttime respiration during the growing season (late spring–autumn), this has generated interest in the potential for kelps to mitigate stressors such as ocean acidification and hypoxia (Raven et al. 2008, Cornwall et al. 2012; Hurd 2015; Duarte 2017; Cyronak et al. 2018; Kosek & Kukliński 2023). However, studies across different kelp forest ecosystems and different kelp species have shown mixed results regarding the ability of kelps to mitigate acidification and low oxygen conditions (Hoshijima and Hofmann 2019, Traiger et al. 2022).

The inconsistency observed across studies and systems may, in part, be explained by differences in water motion, which directly influence kelp physiology and the persistence of chemical signals (Koehl et al. 2008; Hurd 2000). For example, factors like upwelling, wave exposure, turbulence, and current velocity strongly influence the residence time of water within kelp canopies, potentially affecting the magnitude and duration of any chemical changes (Hirsh et al. 2020; Koweek et al. 2017; Kapsenberg & Hofmann 2016; Gaylord et al. 2012; Traiger et al. 2022). Recent reviews of the role of kelp forests modifying local seawater chemistry highlight hydrodynamics as a critical yet often under-quantified driver of seawater chemistry variability in these biogenic habitats (Kosek & Kukliński 2023, and Strain et al. 2024). Noisette et al. (2022) identify four key priorities for studies examining the capacity of ecosystem

engineers, like kelp, to alter their local chemical environment: (1) clearly report the dominant hydrodynamic regime (e.g., tidal, wave-driven, oscillatory) and its intensity; (2) link hydrodynamics to *in situ* measurements of metabolism and seawater chemistry; (3) capture the temporal and spatial variability of flow and chemistry; and (4) characterize the magnitude, extent, and frequency of chemical habitats created by flow–metabolism interactions.

Most studies quantifying local chemical changes driven by kelp compared conditions inside and outside forests, a practical and widely used approach (Kosek & Kukliński, 2023; Strain et al., 2024). Across most of these studies, differences in DO and pH vary considerably, ranging from 0.13–2.89 mg L^{-1} (4.1–90.3 μmol L^{-1}) for DO and 0.01–0.8 units for pH, likely reflecting unique biotic and abiotic factors such as canopy density and hydrodynamic conditions in each system. Few studies directly test how hydrodynamic conditions influence the magnitude and persistence of kelp-driven chemical modification (e.g., Hirsh et al. 2020; Traiger et al. 2022; Koweek et al. 2017), and even fewer quantify the type and intensity of water motion. Additionally, over 70% of studies focus on giant kelp (*Macrocystis pyrifera*), with relatively few examining other canopy-forming species. These studies converge on the need for integrated approaches that combine detailed hydrodynamic characterization with biological and chemical measurements to determine when and where kelp forests can act as localized chemical refugia.

To date, studies of how flow affects the ability of kelp to modify its chemical environment have mainly been conducted along wave-exposed coastlines, such as central California (Graham et al., 1997; Navarrete et al., 2022; Strain et al., 2024), or in high-latitude regions with prolonged photoperiods and pronounced seasonality (Krause-Jensen & Duarte, 2016; Filbee-Dexter et al., 2022). In wave-dominated coastal systems, flow is largely oscillatory

and driven by swell (~10 s period). Under calm conditions, water can be entrained and chemically modified by the kelp for extended periods, elevating DO and pH within the canopy for hours to days (Murie and Bourdeau, 2020). The temporal variation in this signal follows a diel cycle, due to the light dependence of photosynthesis.

By contrast, relatively few studies have examined kelp forests in estuarine or inland sea environments, where tidally-driven currents dominate and flush the canopy with new, unmodified water with each ebb and flow of the tide (~6-12 hour period). When currents slow or pause during periods of 'slack", however, water can remain within the canopy long enough for photosynthesis and respiration to alter local DO and pH (Traiger et al. 2022). In this manner, tidally-driven flow conditions have the potential to shape the magnitude, timing, and spatial distribution of kelp-driven changes in seawater chemistry. Studying kelps in these tidally energetic systems, therefore, provides a valuable opportunity to test the limits of their capacity to modify local chemistry and to understand how the hydrodynamic setting constrains or enhances their role as ecosystem engineers.

The Salish Sea, with its strong and variable tidal currents, offers a natural laboratory for testing how hydrodynamic forces shape kelps' ability to alter their surrounding chemical environment. This fjord estuary system in the eastern North Pacific hosts 22 of the region's 26 kelp species, including canopy-formers such as giant kelp (*M. pyrifera*) and bull kelp (*Nereocystis luetkeana*) (Guiry 2012). Here, kelps experience strong mixed semi-diurnal tidal currents, with velocities reaching up to ~1 $m \cdot s^{-1}$ during peak ebb and flood tides, when water flows seaward and landward, respectively. These currents decrease substantially during slack tide, when flow temporarily pauses between tidal reversals (Sutherland et al. 2011; Banas et al.

1999, Gaylord et al. 2007). While the magnitude and timing of current speed and direction follow a semidiurnal cycle (~12.4 hrs), the light intensity necessary to drive photosynthesis in a kelp canopy follows a diel cycle (~24 hrs). These two signals interact to create a 'beat frequency', or circasemilunar cycle (~14.8 days), over which they fall in and out of phase; the timing and magnitude of kelp canopy modification of water chemistry is therefore expected to follow this longer-term periodicity in the Salish Sea.

Here, we provide a detailed *in situ* study of how the flow environment influences chemical conditions within a Salish Sea bull kelp forest by combining high-frequency (15-minute intervals) DO and pH monitoring with hydrodynamic measurements. We examine how diel and tidal cycles interact with the kelp canopy to influence kelp-driven changes in seawater chemistry and how these patterns vary spatially and temporally. Specifically, we aim to: (1) characterize the magnitude, duration, and timing of local diel and tidal conditions across the 17-week deployment; (2) determine how temporal variation in light and flow drives fluctuations in DO and pH inside and outside the kelp canopy and identify whether dominant frequencies in DO correspond to periodic patterns in these physical drivers; (3) evaluate how the magnitude and timing of kelp-driven chemical differences vary across canopy locations under different flow and light conditions.

We hypothesize that large differences in DO and pH between the kelp canopy and outside surface waters occur when slack tides coincide with daylight. At these times, low current speeds lack sufficient energy to remove photosynthetic metabolites faster than they can be produced within the canopy. We further hypothesize that this interaction between light availability and tidal flow creates consistent cyclical temporal patterns across canopy locations, such as increased

differences between the kelp canopy and outside surface waters during daytime slack compared to nighttime slack. Additionally, strong tidal currents during non-slack periods that pull buoyant blades underwater, streamline their shape, and contract the canopy will decrease the time water masses stay within the canopy (Britton-Simmons et al. 2008, Koehl et al. 2008). Depending on current strength and direction, this effect is likely to vary across the canopy, with some regions experiencing greater modifications than others. We therefore hypothesize that tidal dynamics alter the spatial extent of kelp-driven changes, resulting in stronger DO and pH signals in areas where flow is reduced at a given time. In this system, kelp-driven changes in DO and pH are expected to be smaller and more transient than those seen in wave-dominated environments, with significant spatial and temporal variability in seawater chemistry driven by interactions between dynamic tidal currents and diel cycles.

Methods

Site characterization and sensor deployment

Our study site, Turn Rock (48°32′05.9″N 122°57′52.4″W), sits ~400 m off the northeast side of Turn Island Marine State Park, near Friday Harbor, Washington, USA (Fig. 1). Turn Rock is a small rocky islet in the San Juan Channel that experiences strong tidal currents and has submerged rocky outcrops that provide habitat for bull kelp (*Nereocystis luetkeana*) and many other marine species. Bull kelp surrounds Turn Rock at depths of ~3–12 m (Fig. 2) and extends farther from the rock on the south, east, and north sides where the seafloor slopes gradually. In contrast, the west side drops steeply, forming a channel with strong currents between Turn Rock and Turn Island Marine State Park. We leveraged these predictable, cyclic tidal flow patterns to test how hydrodynamic conditions influence kelp-driven changes in seawater chemistry by

strategically deploying chemical sensors outside and throughout the kelp forest for 17 weeks (June 1–September 23, 2022).

Prior to sensor placement, we observed the dynamics of tidal currents in and around the kelp forest for multiple days under each of the different tidal conditions (i.e., ebb, flood, and slack during both high and low tides). For example, a flood tide brings water south to north through the San Juan Channel (landward). As water diverges at Turn Rock, the kelp on the south end of Turn Rock is pulled under the surface, while the kelp on the north end remains at the surface. This effect is reversed during an ebb tide, when water runs north to south (seaward); kelp on the north end of Turn Rock is dragged under, while kelp on the south end remains at the surface. During slack tide, when currents momentarily slow as the tide shifts direction, kelp at Turn Rock rises to the surface, maximizing visible canopy exposure. Because the San Juan Islands experience mixed semidiurnal tides, slack typically occurs four times a day. Simulation studies like those conducted by the Salish Sea Modeling Center have shown that tidal currents in the San Juan Islands are highly dynamic, capturing how local bathymetry and coastline complexity influence the strength and direction of surface currents. (https://www.youtube.com/watch?v=EPSnXWfcPQE).

We estimated current speeds during the study using NOAA tidal current predictions (cm s^{-1}, every 6 minutes) at Pear Point (east–PUG1746: 48°30’41.0"N, 122°57’10.4"W) and light (µmol m^{-2} s^{-1}, reported as 15 min average) from the Friday Harbor Laboratories (FHL) weather station, located less than a mile away (NOAA 2022, Carrington, E. 2025). We verified the timing and magnitude of the predicted current at the site by deploying a current sensor (TCM-1 Tilt Current Meter Lowell Instruments LLC) outside the kelp forest at a depth of 32 ft for one

week (July 21- 27, 2022), recording current speed and direction every second. The current sensor was positioned on the south end of Turn Rock, an area directly exposed to flood currents but sheltered from ebb currents (Fig. 2).

We quantified temporal variation in DO and pH within and outside of Turn Rock's kelp forest by deploying sensor arrays on four moorings in the north, middle, and south regions of the forest, as well as outside the kelp forest (Fig. 2B and C). All moorings supported a sensor array positioned near the surface (1 m below the surface, m.b.s.). Additionally, the outside and middle mooring supported a benthic sensor array (~4m, or 1 m above the bottom m.a.b.). The middle mooring supported a third sensor array midway between the surface and benthic array (~2.5 m below the surface). We therefore deployed sensor arrays in seven locations: Outside Surface (OS), Outside Bottom (OB), North Canopy (NC), Middle Canopy (MC), Middle Mid-Water (MM), Middle Bottom (MB), and South Canopy (SC).

We placed moorings based on our observations of tidal currents interacting with the kelp canopy at Turn Rock under different tidal conditions (Fig. 2). The Middle Canopy (MC) and its associated Middle Mid-water (MM) and Bottom (MB) sensors were placed in the forest interior, where flow was observed to be slowest and kelp blades generally stayed at the surface, even during moderate ebb and flood tides. The South Canopy (SC) sensor was positioned ~5 m inside the southern edge of the kelp canopy, where currents were strong during flood (flowing northeast) but were dampened by the canopy and Turn Rock's topography during ebb, as evidenced by kelp blades remaining at the surface. Similarly, the North Canopy (NC) sensor was positioned ~5 m inside the northern edge, where currents were strong during ebb (flowing southeast) but dampened by the canopy during flood, evidenced by kelp blades remaining at the

surface. Finally, we placed the Outside Surface (OS) and Outside Bottom (OB) sensors ~30 m north of the canopy edge, where any water modified by the kelp was unlikely to influence the sensors. These sensor locations allowed us to make specific comparisons: (1) using OS as a 'no-kelp control' against in-canopy sites (NC, MC, SC) and (2) using MC, MM and MB to assess depth differences within the middle region of the forest.

We conducted surveys to (1) estimate kelp density at each sensor location, verifying that biomass did not differ among sites and therefore would not confound comparisons of chemical change, and (2) measure the overall size (area) of Turn Rock's bull kelp forest using SCUBA and kayak surveys, respectively. In August 2022, we completed subtidal transect surveys using SCUBA, first by positioning a 30 m × 2 m transect so the 15 m mark aligned with the sensor mooring. We placed two additional transects 5 m parallel to the first—one toward the edge of the kelp bed and the other toward the center of the islet. Each transect followed a depth gradient to avoid crossing paths. Divers counted bull kelp stipes >1 m tall following PISCO protocols (https://piscoweb.org/kelp-forest-sampling-protocols). In September 2022, we measured the canopy area by tracing its perimeter during a low tide slack from a kayak using a handheld GPS unit (Descent Mk1, Garmin, KS, US). We recorded canopy perimeter coordinates every ~3 m until completing a full loop around the forest, then imported the points into Google Earth to delineate the canopy boundary and estimate its area, shape (elliptical), and linear dimensions (length and width).

Sensor Deployment and Calibration

Each sensor array contained a pH, DO, and conductivity logger, each with *in situ* temperature measurements (HOBO MX2501, U26-001, and U24-002-C, respectively; Onset,

USA) that recorded continuously at 15-minute intervals. We calibrated all sensors at each deployment following the manufacturer's instructions. In total, we used 14 loggers of each sensor type; while seven of each type were deployed in the field, we cleaned, calibrated, and prepared the remaining loggers for redeployment. We swapped in a freshly calibrated set of sensors every two weeks to download data, verify calibrations, and minimize biofouling. Before and after deployment, sensors were cleaned of biofouling and then placed into holding reservoirs at the Friday Harbor Laboratories (FHL) for cross-calibration, as described in the supplemental materials

Statistical Analyses

All statistical analyses were performed in R (version 4.3.2). We compared NOAA-predicted tidal current speeds to *in situ* currents measured by the tilt sensor to verify the timing and magnitude of flow at Turn Rock. Tilt data were averaged to one-minute intervals and assigned directional sign (positive = northward/flood, negative = southward/ebb). NOAA predictions, reported at six-minute intervals, were linearly interpolated to a one-minute resolution to enable direct comparison. We computed cross-correlation functions (CCFs) over a ±60-minute window at 1-minute resolution to identify the temporal offset between the tilt sensor and NOAA predictions that maximizes the correlation between the two time-series. The NOAA series was then time-shifted accordingly, and linear regressions were used to assess agreement between predicted and measured flow speed during both flood and ebb tides. Our predicted current speeds for all subsequent analyses were the time-shifted NOAA predictions.

We used both predicted current speed and light to assign diel periods (day, night) and tidal conditions (ebb, slack, and flood) to each timestamp. We downsampled the predicted current speed time series from 6-minute to 15-minute intervals using linear interpolation with the

approx() function (package: *stats*) to align it with the sampling frequency of the light, DO, and pH datasets. We assigned diel periods (day, night) using the compensating irradiance for *N. luetkeana* (17 µmol m^{-2} s^{-1}; Poulson et al., 2011); values below this threshold were considered 'night', which meant that nighttime conditions did not occur at exactly the same time at all deployment stations. We assigned tidal condition to each time point based on a predicted current speed threshold of 30 cm s^{-1}; speeds ≥ 30 cms^{-1} as "flood" (northern, landward flow), speeds ≤ −30 cms^{-1} as "ebb" (southern, seaward flow), and speeds between −30 and +30 cm s^{-1} as "slack" (Figure S1). The threshold of 30 cm s^{-1} for slack aligns with previous studies (Viehman et al., 2023; Wünsche et al., 2024; Gunner et al., 2025) and with those that define slack as the hours before and after high and low tides (Brennan et al., 2002).

We then classified each 15-minute observation into one of six tidal–light conditions (ebb day, ebb night, slack day, slack night, flood day, flood night). Across consecutive periods within a given condition, we calculated both the mean duration (hrs) and mean current speed (cm s^{-1}).We then computed the overall mean values across each consecutive period for each tidal–light category (n per each category -Table 1) . We used a linear model to test whether duration differed across tidal–light conditions. We evaluated the significance of main effects and interactions using Type III ANOVA and performed post hoc pairwise comparisons where appropriate.

We calculated Pearson correlation coefficients (r) between DO and pH for each week (n = 17) and each sensor location (n = 7) using 15-minute interval data. We used a Kruskal–Wallis rank sum test to determine whether mean weekly correlations differed among locations, followed

by *post hoc* pairwise comparisons using Dunn's test with Benjamini–Hochberg (BH) *p*-value correction to control for false positives (Type I errors) from multiple comparisons.

We performed spectral analyses to identify dominant periodicities in our predicted, measured and derived time series (e.g., predicted current speed, light, salinity, temperature, DO/pH at each sensor location, DO/pH comparisons between locations). We used the absolute value of predicted current speed to assess magnitude, but not direction, and detrended all-time series using linear regression. We performed Welch-style FFT averaging using the *fft* package, using a segment length of 8192 with 90% overlap, with a Hanning window to reduce spectral leakage. The FFT amplitudes of each series were normalized to the power spectral density (PSD). The frequencies associated with peaks in each PSD spectrum were identified and compared to known diel and tidal frequencies common to the Salish Sea (e.g., 12.4 hr, 24 hr, 14.8 day). We also used the cross-correlation package *ccf* to examine low-frequency temporal offsets between select time series: MC-OS DO, salinity, and temperature compared to predicted current speed (absolute value) and PAR. Each series was smoothed with a 2-day rolling mean and the CCF was calculated for lags up to 7 days at 15-minute intervals. The temporal lag resulting in the greatest absolute correlation was identified.

We used Linear Mixed-Effects Models (LMMs; lmer package) to test our hypothesis that tidal conditions and diel periods affect DO in and out of the canopy at Turn Rock. We first calculated the differences in DO (ΔDO) between specific locations: (1) canopy-versus-outside surface comparisons, where we used the outside surface sensor (OS) as a reference for each canopy sensor—North Canopy (NC-OS), Middle Canopy (MC-OS), and South Canopy (SC-OS); and (2) within-forest depth comparisons, based on the difference between habitats—

between the surface and midwater (MC-MM), midwater and bottom (MM-MB) and surface and bottom (MC-MB). Both models included all fixed effects and their interactions (location comparisons × diel period × flow condition). We included the deployment number as a random intercept to account for non-independence and baseline variation among deployments. We used AIC-based model selection to identify the best-fitting model for each set of habitat comparisons. Finally, we used the *emmeans* package to estimate marginal means and perform pairwise comparisons across combinations of sensor locations, tidal condition, and diel period. We applied Tukey-adjusted *p*-values to identify statistically significant differences in ΔDO across locations and diel–tidal interactions.

Because water masses at Turn Rock can differ markedly over small spatial scales due to variable mixing and freshwater influence, sensors positioned in different habitats may at times sample distinct water parcels (e.g., a freshwater plume affecting the OS sensor but not the MC sensor). Such heterogeneity can create apparent differences in seawater chemistry that are unrelated to kelp-driven modification. To reduce the influence of this mixing artifact, we filtered the dataset to include only periods when salinity differences between habitats were ≤ 1.0 PSU, and then reran the same linear mixed-effects model (LMM) described above to evaluate how ΔDO magnitudes compared with the unfiltered dataset. This conservative approach minimizes the risk of attributing DO variation to kelp metabolism when it may instead reflect the advection of physically distinct water masses.

Results

Turn Rock kelp forest covered 2.7 ha and was approximately elliptical in shape, measuring ~241 m in length and ~159 m in width, with a perimeter of 685 m, with a bull kelp

density of 5.5 stipes m^{-2}. Predicted current speeds lagged the *in situ* current meter (Lowell Tilt sensor) by 30 minutes. Once adjusted for lag, the predicted current speeds and *in situ* measurements showed tighter alignment in both timing and magnitude of current speeds during flood tides (Fig. 3; Pearson correlation: $r = 0.83$, $p < 0.001$). During ebb tides, *in situ* measurements aligned in timing but not in magnitude, and although a significant relationship existed, it was weak (Pearson correlation: $r = -0.15$, $p < 0.001$). This was due to the sensor being located on the south side of Turn Rock, where it was directly exposed to flood tides. During ebb, current speeds are dampened by both the topography of Turn Rock and the kelp canopy.

Tidal duration was affected by the interactive effects of tidal condition (ebb, slack, or flood) and diel period (day or night; linear mixed model; interaction: $F_{2,613} = 47.9$, $p < 0.0001$; Fig. 4A; Table S1). The duration and frequency of tidal conditions varied throughout deployment, with ebb and flood periods generally persisting longer than slack tides (Table 1). On average, ebb and flood phases lasted between 3 and 4 hours, whereas slack periods averaged 2–2.5 hours. Daytime conditions accounted for about 60 % of the total deployment time, with ebb, slack, and flood phases occurring in roughly equal proportions. During the day, ebb and flood phases were about twice as long as slack tides, while at night, flood tides were both brief and infrequent, occurring only ~3% of the time. Overall, ebb tides were the most common (41%), followed by slack tides (36%) and flood tides (23%). While tidal conditions were assigned based on current direction, the strength of ebb and flood currents differed, with ebb currents peaking near 100 cm s^{-1} and flood currents around 70 cm s^{-1} (Fig. 4B).

Over the 17-week deployment, dissolved oxygen (DO) and pH were strongly and positively correlated across all habitats (median $r > 0.9$; Fig. S2). Correlation strength did not

differ across most habitats with values generally consistent throughout the kelp forest. The only significant pairwise differences occurred between the canopy habitats and the outside sites (Kruskal–Wallis: $\chi^2 = 23.2$, df = 6, p = 0.001), Table S2). Correlations in the Middle Canopy (median $r \approx 0.97$) and South Canopy ($r \approx 0.98$) were slightly higher than those at the Outside Bottom ($r \approx 0.92$) and Outside Surface ($r \approx 0.95$; Dunn's test, adjusted $p < 0.01$). All other pairwise comparisons were not significantly different ($p > 0.05$), indicating that pH and DO tracked one another closely and consistently across most of the kelp forest. Due to this tight relationship, subsequent analyses focused on DO, with mirrored pH results provided in the Supplementary Material (Figs. S11-12; Tables S3 and S6-7).

Dissolved oxygen fluctuated over time at all locations, including the middle canopy (MC) and outside surface (OS), ranging from ~150 to 250 μmol L^{-1} (Fig.5A). Within the kelp canopy, daily DO values—summarized over 24 h cycles—fluctuated 61 (± SE 21) μmol L^{-1} and single-day fluctuations reaching 123 μmol L^{-1} (n=113). Oxygen concentrations were higher in the canopy than outside, with pronounced daytime peaks (Fig. 5A). On average, DO inside the middle canopy exceeded the outside reference location by 6 μmol L^{-1} (ΔDO = MC – OS; Fig. 5B), with daily maximum differences reaching up to 120 μmol L^{-1} (Fig. S3B). Other canopy comparisons (NC–OS and SC–OS) also showed similar variation in ΔDO over the 17-week deployment (Fig. S3A and S3C). Differences in DO among depth locations followed a vertical gradient, with DO decreasing with depth; the largest difference occurred between the middle canopy and middle bottom (average daytime ΔDO = 1.87 (± SE 10.9) μmol L^{-1}, maximum ~100 μmol L^{-1}), though these depth-related differences were much smaller in magnitude compared to canopy–outside comparisons (Fig. S3D–F). Peaks in ΔDO typically occurred during midday slack tides, when light availability was highest and predicted current speeds were lowest (Fig.

5C). ΔDO approached zero during faster ebb and flood conditions (day or night) and became slightly negative during nighttime slacks.

Spectral analysis revealed underlying frequencies at which the time series of ΔDO between the Middle Canopy and outside fluctuated (MC-OS, Fig. 6). Specifically, peaks in PSD occurred at frequencies corresponding to tidal constituents common to complex estuarine habitats with mixed semidiurnal tides: O1 diurnal lunar (25.8 hr), M2 semidiurnal (12.4 hr), M2 ⅔ overtide (8.3 hr), and M4 overtide (6.2 hr). Less prominent is the peak for Mf fortnightly (14.7d), which is poorly resolved with a 17-week signal. These tidal constituents are strongly represented in the spectrum for predicted current speed. Also present in the MC – OS spectrum is a peak at 24 hr, corresponding to a diel cycle (24h) - the dominant peak in the light spectrum. Overall, the spectrum for the time series of ΔDO between the Middle Canopy and outside reflected the combined influence of predicted current speed and light. A similar pattern is evident in all-time series for habitat comparisons and in the raw time series for each habitat (Fig. S4). The spectra for salinity and temperature are similar to the predicted current speed (Figure S5).

DO also varied spatially across locations within and outside the kelp canopy (Fig. 7A). In canopy locations (Middle, South, and North Canopy), oxygen concentrations showed strong diel cycling, with pronounced increases during midday when light levels were highest. However, both the timing and magnitude of these peaks varied across locations and through time. For example, on some days (e.g., July 15), DO in the Middle Canopy peaked first and reached the highest values, whereas on others (e.g., July 12), the South Canopy peaked earlier and the North Canopy exhibited the largest amplitude in DO (Fig. 7A). In contrast, DO signals recorded at

different depths along the middle mooring (Middle Canopy, Middle Mid-water, and Middle Bottom) were closely aligned in timing but became increasingly dampened with increasing depth (Fig. 7C).

The best-fitting linear mixed-effects model for ΔDO included all fixed factors and their interactions (habitat comparison, diel period, and tidal condition; Table 2, Fig. 8). Across all canopy habitats, ΔDO was generally higher inside the kelp forest during the day (9–11 μmol L^{-1}) than at night (~0 μmol L^{-1}), but the strength of these diel differences varied with tidal phase. During ebb tides (Fig. 8A), daytime ΔDO increased from north to south, with the largest differences observed in the South Canopy (SC–OS), where day values were roughly twice those observed during slack conditions ($p < 0.001$; Table S3). Under slack conditions (Fig. 8B), diel differences persisted but spatial contrasts narrowed, with similar day–night ΔDO across all canopy–outside comparisons (7–8 μmol L^{-1}, $p < 0.001$). During flood tides (Fig. 8C), the pattern reversed, day–night differences decreased from north to south, with the strongest ΔDO in the North Canopy (NC–OS) and no significant diel variation in the Middle or South Canopy ($p > 0.05$; Table S3).

Vertical differences in dissolved oxygen increased with depth, with the largest contrasts occurring between the surface and bottom sensors (MC–MB), where daytime ΔDO exceeded nighttime values by over 4 μmol L^{-1}—the greatest diel difference observed across all depth and tidal comparisons (Fig. 8D–F; Table S4, $p < 0.0001$). Diel variability was strongest during slack and ebb tides and weakest during flood, indicating that vertical oxygen gradients developed primarily under reduced flow. Among depth comparisons, MM–MB exhibited intermediate differences, whereas MC–MM showed the smallest overall magnitudes. Flood periods produced

near-zero or slightly negative ΔDO values across all depths, reflecting weak or reversed vertical oxygen gradients.

As indicated in the FFT analyses, a ~14-day spring-neap cycle in ΔDO was evident in all of the time series for habitat comparisons as well as predicted speed, salinity, and temperature (Fig. S4 & S5). This pattern was more pronounced when high-frequency variation was smoothed with a 2-day rolling mean (Fig. S6, using the MC-OS comparison as an example). Cross-correlation analyses indicated a significant negative correlation between ΔDO and predicted current speed, as expected, but with ΔDO peaks lagging behind current speed minima by 1.3 days. Both salinity and temperature, which are highly correlated, lagged the predicted current speed by 2.4 days. The correlation was positive for salinity and negative for temperature, indicating that warmer, lower-salinity periods typically follow periods of lower mean flow.

Filtering the dataset to include only periods when salinity differences between habitats were ≤ 1 PSU did not substantially alter the mean ΔDO values across tidal and diel conditions (Table S8). Across all canopy–outside comparisons, mean ΔDO values in the salinity-filtered dataset differed by less than ~3 μmol L^{-1} from the full dataset, with similar 95% confidence intervals and distribution ranges. Likewise, across-depth comparisons (MC–MM, MC–MB, MM–MB) showed minimal changes (< 1 μmol L^{-1} on average) following salinity filtering.

Discussion

Kelp-driven changes in seawater chemistry at Turn Rock were strongly constrained by local hydrodynamics, as the timing, speed, and direction of tidal currents modified both the magnitude and the spatial pattern of oxygen enrichment within the kelp canopy. Over the 17-week sampling period, tidal conditions were unequal in duration and, coupled with diel light

cycles, set predictable windows for biogenic enhancement of oxygen by kelp. These cycles limited kelp-driven chemical changes to short periods that rarely persisted beyond the duration of one tidal condition (ebb, slack, or flood). In general, Dissolved Oxygen (DO) differences between the kelp canopy and outside surface waters were consistently greater during the day than at night. Differences in DO were spatially structured, with the biggest increases in DO transiently shifting throughout the canopy to locations adjacent to the main flow direction. Together, these findings show that kelp effects on local seawater chemistry are not static "hotspots" but dynamic, flow-dependent features that vary predictably across space and time. This pattern is consistent with the view that macrophyte canopies create chemical habitats whose magnitude and persistence depend on flow–metabolism interactions and residence time (Noisette et al. 2022; Kosek & Kukliński 2023; Strain et al. 2024) and physical exchange frequently constrains realized buffering in canopy-forming kelp systems (Koweek et al. 2017; Hirsh et al. 2020; Traiger et al. 2022).

The diel (day–night) cycles of DO we observed inside versus outside the kelp canopy are consistent with kelp metabolic activity- increasing during the day due to photosynthesis and decreasing at night due to respiration. The range of inside–outside differences in DO we observed in daytime (9–67 μmol L^{-1}) overlaps partially with those reported from kelp forests on wave-dominated coasts (~ 40–100 μmol L^{-1}; Koweek et al. 2017; Hirsh et al. 2020; Traiger et al. 2022; Murie and Bourdeau 2020). However, the average daytime ΔDO across all inside–outside kelp canopy comparisons at Turn Rock was smaller in magnitude (~5–10 μmol L^{-1}) than in other studies examining inside–outside DO differences (Koweek et al. 2017; Hirsh et al. 2020; Traiger et al. 2022; Murie and Bourdeau 2020), likely due to enhanced mixing and frequent water exchange driven by strong tidal currents. At Turn Rock, tidal phases typically lasted 2–4 hours,

with current speeds reaching up to 100 cm s^{-1} (Table 1), indicating rapid water exchange through the canopy. In contrast, wave-dominated kelp systems often experience slower, oscillatory flow that allows water to remain within the canopy for much of the daylight period, enhancing recirculation and stratification (e.g., Koweek et al. 2017; Hirsh et al. 2020). In tidally mixed systems, diel variability in DO and pH is constrained by frequent tidal flushing.

While many studies document instances of low pH and low DO amelioration by macrophytes (e.g., Ricart et al. 2021, Pfister et al. 2019; Murie & Bourdeau 2020), other empirical and modeling analyses indicate that expectations for broad-scale buffering may be overestimated once hydrodynamic and other constraints are fully accounted for (Koweek et al. 2018; Van Dam et al. 2021; Ricart et al. 2022). Our findings support this latter view for bull kelp forests: high metabolic capacity exists, but the timing, duration, and magnitude of tidal exchange will limit amelioration. This is best illustrated by focusing on the South Canopy (SC) location, where we observed the largest average daytime ΔDO (~20 μmol L^{-1}). This is surprising because we initially hypothesized that the Middle Canopy–Outside (MC–OS) comparison would have stronger differences under slack conditions. These spatial patterns in ΔDO reflects how tidal flow interacts with the kelp canopy and local topography at Turn Rock. During ebb tides, the SC experiences reduced current speeds and partial flow buffering by the kelp and surrounding substrate (demonstrated by the tilt sensor -Fig. 3). Combined with an average 3.6-hour ebb period followed by ~2 hours of daytime slack, the ΔDO results from roughly 6 hours of low-flow residence time, sufficient for kelp photosynthesis to drive elevated daytime DO. In contrast, the MC-OS can be influenced by both the ebb and flood currents, thus only having an average of 2.1 hrs during slack periods for biogenic modification to accumulate. These results help reconcile seemingly contradictory findings from previous kelp forest studies, which reported either strong

within-forest chemical modification (Pfister et al. 2019; Murie & Bourdeau 2020) or little measurable buffering under high current exchange (Traiger et al. 2022). Our results indicate that both outcomes can occur, depending on the hydrodynamic context and residence time in the system.

Within the canopy, DO differences decreased with depth. During the day, DO in the middle canopy was on average 2.4% higher than in the benthos (213 vs. 208 μmol L^{-1}), and diel DO fluctuations between the middle canopy, mid-water, and benthos were small (< 6 μmol L^{-1}). These depth-related differences were an order of magnitude lower than those reported by Murie and Bourdeau (2020) in a wave-exposed bull kelp forest, where canopy DO was 23% higher than the benthos and diel changes exceeded 11 mg L^{-1} (~334 μmol L^{-1}). Across the vertical gradient within the middle mooring, DO differences between the canopy and benthos (MC-MB) rarely exceeded 30 μmol L^{-1} (~1 mg L^{-1}), occurring in only ~2 % of observations, indicating that vertical DO stratification was weak and transient compared to horizontal (inside vs outside the canopy) differences (Fig. S3). The muted vertical differences at Turn Rock likely reflect the strong tidal mixing and shorter water residence times within this tidally dominated kelp forest, which reduce vertical stratification and limit the buildup of photosynthetically produced oxygen in the upper canopy. In contrast, at wave-exposed sites where water exchange is slower and canopy residence time is longer, photosynthetic activity during calm periods can drive much greater DO enrichment and stronger vertical biogeochemical differences (Murie and Bourdeau 2020).

We used a single “outside” reference mooring to represent ambient conditions, which may not have adequately represented “external” conditions at all locations in the canopy throughout the 17-week deployment. For instance, new water masses arriving through upwelling,

downwelling, or freshwater inputs from nearby rivers can generate substantial small-scale variation in temperature and salinity (Figures S7–S10). Although just ~50 m apart, the North Canopy (NC) and Outside Surface (OS) sensors differed by up to 5 PSU and 4 °C (Figure S8). At the same time, salinity and temperature varied up to 6 PSU and 4 °C between the Middle Canopy (MC) and the Middle Bottom (MB) (Figure S9). Figure 9 shows that the Outside Surface (OS) reference sensor did not consistently represent ambient conditions across tidal phases. During ebb tides, ΔDO at the Middle Canopy (MC–OS) was strongly positive during the day (~15 µmol L^{-1}), but in contrast, during flood tides, daytime ΔDO at MC dropped below 3 µmol L^{-1} and diel differences disappeared. This suggests that during flood conditions, the OS sensor sampled water masses that also reached the MC site, reducing the apparent chemical gradient between them. In ebb and slack periods, however, the OS location was more hydrodynamically isolated, better representing external conditions. Thus, the reliability of the outside reference (one of the most common methods used in marine macrophyte refugia studies) varies with tidal flow, emphasizing that inside–outside differences must be interpreted within their hydrodynamic context rather than as fixed indicators of canopy-driven modification (Kosek & Kukliński, 2023; Strain et al., 2024). Future studies interested in the ability of vegetated habitats to alter local chemistry should carefully consider the number and placement of "reference" sensors to sufficiently characterize ambient (non-vegetated) chemistry across different flow conditions.

Spatial heterogeneity in salinity and temperature in and out of the kelp forest indicates that some of the observed differences in DO between canopy and outside waters likely reflect physical, rather than purely biological drivers. For example, variation in salinity and temperature relationships at a fixed location are indicate water masses originating from different sources (e.g. deep, upwelled seawater vs Fraser River discharge). Once those water masses arrive, further DO

variability arises not only from kelp metabolism but also from the inherent physical effects of these properties on oxygen solubility. Teasing which mechanism is driving DO variability and isolating a kelp metabolic effect can be difficult. Salinity and temperature have opposing influences on DO—lower salinity increases oxygen solubility, whereas higher temperature reduces it (Garcia & Gordon 1992; Weiss 1970). In the Salish Sea, these two variables often covary because freshwater input from the Fraser River lowers salinity while raising temperature during summer snowmelt periods (Morrison et al. 2012).

Because salinity and temperature deviations are strongly correlated with current speed, their effects cannot be statistically isolated in this system. By filtering periods when salinity and temperature differ across habitat comparisons, we follow the approach by Van Dam et al. (2021), who demonstrated that even small salinity differences (~0.1 PSU) can generate chemical shifts equivalent to those attributed to seagrass metabolism, underscoring that water-mass mixing alone can mimic biological modification. When periods with $|\Delta\text{Salinity}| < 1$ PSU and associated temperature differences (< 2.5 °C) were isolated, mean ΔDO values differed by only ~3 μmol L^{-1} from the unfiltered dataset (Table S5), suggesting that physical water-mass variability explains part—but not all—of the observed chemical gradients between canopy and outside habitat. Regardless of whether physical effects drive changes in DO, kelps still have an inherent benefit in capturing water.

From a chemical refugia perspective, studies across different kelp forest ecosystems and different kelp species have shown mixed results regarding the ability of kelp forests to mitigate low oxygen conditions and acidification (Hoshijima and Hofmann 2019, Traiger et al. 2022). Critical DO and pH thresholds for kelp forest animals vary significantly by species and life stage. Some animals, like rockfish, are sensitive to moderate drops in oxygen (ΔDO 4.5-6.5 mg L^{-1},

roughly 140–203 μmol L^{-1} - Gibson & Atkinson, 2003, Mattiasen et al. 2020); while more robust species, such as some invertebrates (e.g., urchins), can tolerate much lower levels in oxygen (1 mg L^{-1}, but reduce grazing under 5.5 mg L^{-1}, even under short periods (3-8 days) (Low &Micheli, 2018, Murie and Bourdeau, 2020). Dissolved oxygen (DO) concentrations at Turn Rock never approached hypoxic thresholds (≤ 62.5 μmol L^{-1} or 2 mg L^{-1}; Vaquer-Sunyer & Duarte, 2008) in any of the seven sensor locations. However, the outside surface (OS) sensor recorded DO concentrations below 156 μmol L^{-1} (5 mg L^{-1}) during 38 distinct low-oxygen events, each lasting on average ~2.7 hours and up to 12.5 hours (Fig. 5A). These 38 excursions were probably examples of local community respiration or local upwelling as salinity remained around 31 PSU and temperature around 9-10°C. During these same 38 unique excursions, the kelp canopies (NC, MC, and SC) rarely dropped below 156 μmol L^{-1}, with only one excursion occurring in the SC and NC, lasting only 30 minutes. On average, the three canopies remained ~14-15 μmol L^{-1}, higher than the outside surface.

Although these patterns provide evidence that the bull kelp is capable of elevating DO above levels outside the kelp forest that may be stressful to other organisms, the frequency and duration of these events do not represent strong or persistent refugia like those found in more retentive or wave-sheltered systems (Frieder et al. 2012, Ling et al. 2020, Murie and Bourdeau 2020). Nevertheless, even relatively small differences, such as those observed here, may become ecologically important under future climate change scenarios if progressive ocean acidification or deoxygenation pushes background conditions closer to physiological thresholds, potentially shifting organisms toward or away from critical tipping points (Low & Micheli, 2018). Together with recent reviews (Strain et al. 2024; Kosek & Kukliński 2023) and empirical studies (Koweek et al. 2017; Hirsh et al. 2020; Traiger et al. 2022), we argue for reframing kelp-based mitigation

from the ‘static buffer’ concept to a ‘dynamic exposure’ perspective. This aligns with similar calls from seagrass studies that show that, whereas mitigation benefits can be real, they are contingent on environmental context (Koweek et al. 2018; Van Dam et al. 2021; Ricart et al. 2022).

Bull kelp forests span a broad continuum of hydrodynamic settings, but Turn Rock represents the higher-flow end of that spectrum. In inland seas, bull kelp is most persistent and reaches its greatest canopy biomass in high-flow habitats, as this species thrives under strong tidal exchange and performs poorly in more quiescent, low-flow environments (Coleman and Martone 2024, Mora-Soto et al. 2024, Berry et al. 2021). For kelp mitigation strategies in tidally dominated locations (e.g., inland seas), leveraging timing (daytime slack), site selection (reduced background exchange), and canopy geometry (which enhances retention without excessive drag-related loss) will more likely yield measurable and functional chemical amelioration windows. The magnitude of DO modification observed at Turn Rock was smaller than that reported from larger kelp forests in the Strait of Juan de Fuca (Pfister et al. 2019), where mixed *Nereocystis* and *Macrocystis* forests spanning up to 103 ha exhibited substantially greater chemical gradients. By comparison, the Turn Rock kelp bed (~2.7 ha) was over 48 times smaller, suggesting that canopy size and biomass strongly influence hydrodynamic damping and water residence time. Thus, larger forests are more capable of slowing local flow, retaining metabolically modified water, and thus amplifying biogeochemical gradients.

Despite differences in magnitude, patterns in DO at Turn Rock were consistent with those reported from other bull kelp systems in coastal habitats. For example, Murie & Bourdeau (2020) found that DO was highest at the forest edge relative to the interior, likely due to greater light

availability and reduced self-shading, patterns that were mirrored by our South and North Canopy sensors, which exhibited higher ΔDO than the Middle Canopy. This spatial structure aligns with the physical constraints of bull kelp morphology and flow exposure. Bull kelp is an annual species that thrives in high-flow habitats (Koehl et al. 2008, Springer et al. 2010) and may not persist in quiescent environments where residence times are long enough to cause hypoxia. In such settings, high flow supports kelp health but limits their ability to create long-lived chemical refugia, confining amelioration to short windows during low-exchange periods (Berry et al. 2021).

In this tidally dominated kelp forest, chemical modification is periodic, hydrodynamically constrained, and spatially heterogeneous. The canopy exhibits a strong instantaneous capacity to elevate DO and pH when residence time peaks under daylight, but energetic tidal exchange rapidly dissipates these signals. Collectively, our findings support recent reviews (Noisette et al. 2022; Kosek & Kukliński 2023; Strain et al. 2024) emphasizing that the ability of kelp forests to function as chemical refugia is highly context dependent. Our results also help reconcile contrasting outcomes from other kelp systems (Pfister et al. 2019; Hirsh et al. 2020; Murie & Bourdeau 2020; Traiger et al. 2022) and parallel the ongoing seagrass debate (Koweek et al. 2018; Van Dam et al. 2021; Ricart et al. 2021, 2022): marine macrophytes can create chemical refugia, but only within the physical limits imposed by hydrodynamic exchange and light availability. Accordingly, both ecological interpretation and climate-adaptation planning should focus on when and where metabolic signals are retained, not merely on how much metabolism occurs.

Acknowledgments

We thank the UW Friday Harbor Laboratories' director and staff— Megan Dethier, Jakob Bueche, Peggy Combs, Doug Engel, Pema Kitaeff, Kristy Kull, Eric Loss, and Diana Pieples—for logistical support of this project. We also thank boat drivers and SCUBA divers: Paul Bourdeau, Mary Cortese, Katie Dobkowski, Timothy Dwyer, Eric Finn, Olivia Graham, Isabel Graham, Grace Leuchtenberger, Mike Nishizaki, Carla Narvaez, Xavier Nelson-Rowntree, Ken Sebens, Mo Turner, Marissa Varade, Brooke Weigel, Mason Wiley, and Eleanor Rollins, as well as the Three Seas student divers. We thank Jack Litle, Robin Fales, Grace Leuchtenberger and Alli Cramer for timely feedback and support throughout the project. Dissertation committee members, Jennifer Ruesink, Thomas Daniel, and Alex Gagnon provided thoughtful feedback that improved the manuscript.

Author contributions

KM led the conceptual development of the study, designed the methodology, curated and analyzed the data, produced all graphical visualizations, drafted the original manuscript, addressed co-authors' revisions, and secured project funding. AN contributed to the methodology for seawater chemistry analysis, assisted with data curation and analysis, participated in manuscript review and editing, and assisted with funding acquisition. EC provided additional methodological support, conducted time-series analyses, contributed to manuscript review and editing, and secured project funding. RW supported the project through diving operations and data collection and contributed to manuscript editing.

Funding

This project was supported by the National Science Foundation (GRF to KM, OCE-2050273 to EC, and OCE-2126719 to AN) as well as UW Student Technology Fees and numerous fellowships and scholarships from UW Biology (Friday Harbor Laboratories award, Hoag Award, John S. Edwards Award, Margo & Tom Wyckoff Award) and UW Friday Harbor Laboratories (Patricia L. Dudley Endowment, Frederic H. and Kristin C. Nichols Endowed Graduate Fellowship fund, Emily Carrington Endowed Student Travel Support, Friday Harbor Labs Research Fellowship Endowment, and Brooks and Suzanne Ragen Friday Harbor Laboratories Endowed Scholarship).

References

Banas, N., J. Bricker, G. Carter, F. Gerdes, W. Martin, E. Nelson, and M. Wells. 1999. Flow, stratification, and mixing in San Juan Channel. Coastal and Estuarine Geophysical Fluid Dynamics Oc590b, Friday Harbor Laboratories, University of Washington, Friday Harbor, Washington.

Berry, H. D., Mumford, T. F., Christiaen, B., Dowty, P., Calloway, M., Ferrier, L., ... & VanArendonk, N. R. (2021). Long-term changes in kelp forests in an inner basin of the Salish Sea. *PloS one*, 16(2), e0229703.

Brennan, M. L., D. H. Schoellhamer, J. R. Burau, and S. G. Monismith. 2002. Tidal asymmetry and variability of bed shear stress and sediment bed flux at a site in San Francisco Bay, USA. *Proc. Mar. Sci.* 5: 93–107. Elsevier.

Britton-Simmons, K., J. E. Eckman, and D. O. Duggins. 2008. Effect of tidal currents and tidal stage on estimates of bed size in the kelp Nereocystis luetkeana. *Mar. Ecol. Prog. Ser.* 355: 95–105. doi:10.3354/meps07235

Carrington, E. 2025. Weather Station data from University of Washington, Friday Harbor Laboratories, Friday Harbor, WA, Cantilever Point from 2006 to 2024. *Biol. Chem. Oceanogr. Data Manag.* Office (BCO-DMO), Version 4. doi:10.26008/1912/bco-dmo.491262.4

Coleman, L. J., & Martone, P. T. (2024). Grow with the flow: Is phenotypic plasticity across hydrodynamic gradients common in seaweeds? *J. Phycol*, 60(5), 1058-1067.

Cornwall, C. E., C. D. Hepburn, D. Pritchard, K. I. Currie, C. M. McGraw, K. A. Hunter, and C. L. Hurd. 2012. Carbon-use strategies in macroalgae: Differential responses to lowered pH and implications for ocean acidification. *J. Phycol.* 48: 137–144. doi:10.1111/j.1529-8817.2011.01085.x

Cyronak, T., A. J. Andersson, C. Langdon, R. Albright, N. R. Bates, K. Caldeira, and others. 2018. Taking the metabolic pulse of the world's coral reefs. *PLoS One* 13: e0190872. doi:10.1371/journal.pone.0190872

Duarte, C. M. 2017. Reviews and syntheses: Hidden forests, the role of vegetated coastal habitats in the ocean carbon budget. *Biogeosciences* 14: 301–310. doi:10.5194/bg-14-301-2017

Eger, A. M., E. M. Marzinelli, R. Beas-Luna, C. O. Blain, L. K. Blamey, J. E. Byrnes, and others. 2023. The value of ecosystem services in global marine kelp forests. *Nat. Commun.* 14: 1894. doi:10.1038/s41467-023-37421-4

Filbee-Dexter, K., and T. Wernberg. 2020. Substantial blue carbon in overlooked Australian kelp forests. *Sci. Rep.* 10: 12341. doi:10.1038/s41598-020-69258-7

Filbee-Dexter, K., T. Wernberg, R. Barreiro, M. A. Coleman, T. de Bettignies, C. J. Feehan, and others. 2022. Leveraging the blue economy to transform marine forest restoration. *J. Phycol.* 58: 198–207. doi:10.1111/jpy.13218

Frieder, C. A., S. H. Nam, T. R. Martz, and L. A. Levin. 2012. High temporal and spatial variability of dissolved oxygen and pH in a nearshore California kelp forest. *Biogeosciences* 9: 3917–3930. doi:10.5194/bg-9-3917-2012

Garcia, H. E., and L. I. Gordon. 1992. Oxygen solubility in seawater: Better fitting equations. *Limnol. Oceanogr*. 37: 1307–1312. doi:10.4319/lo.1992.37.6.1307

Gaylord, B., J. H. Rosman, D. C. Reed, J. R. Koseff, J. Fram, S. MacIntyre, and others. 2007. Spatial patterns of flow and their modification within and around a giant kelp forest. *Limnol. Oceanogr.* 52: 1838–1852. doi:10.4319/lo.2007.52.5.1838

Gaylord, B., K. J. Nickols, and L. Jurgens. 2012. Roles of transport and mixing processes in kelp forest ecology. *J. Exp. Biol.* 215: 997–1007. doi:10.1242/jeb.059824

Gibson, R. N., and R. J. A. Atkinson. 2003. Oxygen minimum zone benthos: Adaptation and community response to hypoxia. *Oceanogr. Mar. Biol. Annu. Rev*. 41: 1–45.

Graham, M. H., B. P. Kinlan, L. D. Druehl, L. E. Garske, and S. Banks. 2007. Deep-water kelp refugia as potential hotspots of tropical marine diversity and productivity. P*roc. Natl. Acad. Sci.* U.S.A. 104: 16576–16580. doi:10.1073/pnas.0704778104

Guiry, M. D. 2012. How many species of algae are there? *J. Phycol.* 48: 1057–1063. doi:10.1111/j.1529-8817.2012.01222.x

Gunner, R. M., F. Quintana, M. H. Tonini, M. D. Holton, K. Yoda, M. C. Crofoot, and R. P. Wilson. 2025. Penguins exploit tidal currents for efficient navigation and opportunistic foraging. *PLoS Biol.* 23: e3002981. doi:10.1371/journal.pbio.3002981

Hirsh, H. K., K. J. Nickols, Y. Takeshita, S. B. Traiger, D. A. Mucciarone, S. Monismith, and R. B. Dunbar. 2020. Drivers of biogeochemical variability in a central California kelp forest:

Implications for local amelioration of ocean acidification. *J. Geophys. Res. Oceans* 125: e2020JC016320. doi:10.1029/2020JC016320

Hoshijima, U., and G. E. Hofmann. 2019. Variability of seawater chemistry in a kelp forest environment is linked to in situ transgenerational effects in the purple sea urchin Strongylocentrotus purpuratus. *Front. Mar. Sci.* 6: 62. doi:10.3389/fmars.2019.00062

Hurd, C. L. 2000. Water motion, marine macroalgal physiology, and production. *J. Phycol*. 36: 453–472. doi:10.1046/j.1529-8817.2000.99139.x

Hurd, C. L. 2015. Slow-flow habitats as refugia for coastal calcifiers from ocean acidification. *J. Phycol.* 51: 599–605. doi:10.1111/jpy.12314

Jones, C. G., J. H. Lawton, and M. Shachak. 1997. Positive and negative effects of organisms as physical ecosystem engineers. *Ecology* 78: 1946–1957. doi:10.1890/0012-9658(1997)078[1946:PANEOP]2.0.CO;2

Kapsenberg, L., and G. E. Hofmann. 2016. Ocean pH time-series and drivers of variability along the northern Channel Islands, California, USA. *Limnol. Oceanogr.* 61: 953–968. doi:10.1002/lno.10264

Koehl, M. A. R., W. K. Silk, H. Liang, and L. Mahadevan. 2008. How kelp produce blade shapes suited to different flow regimes: A new wrinkle. *Integr. Comp. Biol*. 48: 834–851. doi:10.1093/icb/icn062

Kosek, K., and P. Kukliński. 2023. Impact of kelp forest on seawater chemistry: A review. *Mar. Pollut. Bull.* 196: 115655. doi:10.1016/j.marpolbul.2023.115655

Koweek, D. A., K. J. Nickols, P. R. Leary, S. Y. Litvin, T. W. Bell, T. Luthin, and others. 2017. A year in the life of a central California kelp forest: Physical and biological insights into biogeochemical variability. *Biogeosciences* 14: 31–44. doi:10.5194/bg-14-31-2017

Krause-Jensen, D., and C. M. Duarte. 2016. Substantial role of macroalgae in marine carbon sequestration. *Nat. Geosci*. 9: 737–742. doi:10.1038/ngeo2790

Ling, S. D., C. E. Cornwall, B. Tilbrook, and C. L. Hurd. 2020. Remnant kelp bed refugia and future phase-shifts under ocean acidification. *PLoS One* 15: e0239136. doi:10.1371/journal.pone.0239136

Low, N. H., and F. Micheli. 2018. Lethal and functional thresholds of hypoxia in two key benthic grazers. *Mar. Ecol. Prog. Ser.* 594: 165–173. doi:10.3354/meps12530

Masteller, C. C., N. J. Finnegan, J. A. Warrick, and I. M. Miller. 2015. Kelp, cobbles, and currents: Biologic reduction of coarse-grain entrainment stress. *Geology* 43: 543–546. doi:10.1130/G36577.1

Mattiasen, E. G., N. S. Kashef, D. M. Stafford, C. A. Logan, S. M. Sogard, E. P. Bjorkstedt, and S. L. Hamilton. 2020. Effects of hypoxia on the behavior and physiology of kelp forest fishes. *Glob. Change Biol*. 26: 3498–3511. doi:10.1111/gcb.15013

Mora-Soto, A., Schroeder, S., Gendall, L., Wachmann, A., Narayan, G., Read, S., ... & Costa, M. (2024). Back to the past: long-term persistence of bull kelp forests in the Strait of Georgia, Salish Sea, Canada. *Frontiers in Marine Science*, 11, 1446380.

Morrison, J., M. G. G. Foreman, and D. Masson. 2012. A method for estimating monthly freshwater discharge affecting British Columbia coastal waters. *Atmos. Ocean* 50: 1–8. doi:10.1080/07055900.2011.637667

Murie, K. A., and P. E. Bourdeau. 2020. Fragmented kelp forest canopies retain their ability to alter local seawater chemistry. *Sci. Rep.* 10: 11939. doi:10.1038/s41598-020-68548-4

Navarrete, S. A., M. Barahona, N. Weidberg, and B. R. Broitman. 2022. Climate change in the coastal ocean: Shifts in pelagic productivity and regionally diverging dynamics of coastal ecosystems. *Proc. R. Soc. B* 289: 20212772. doi:10.1098/rspb.2021.2772

Nederlof, M. A., M. C. Verdegem, A. C. Smaal, and H. M. Jansen. 2022. Nutrient retention efficiencies in integrated multi-trophic aquaculture. *Rev.Aquac*. 14: 1194–1212. doi:10.1111/raq.12664

Noisette, F., C. Pansch, M. Wall, M. Wahl, and C. L. Hurd. 2022. Role of hydrodynamics in shaping chemical habitats and modulating the responses of coastal benthic systems to ocean global change. *Glob. Change Biol.* 28: 3812–3829. doi:10.1111/gcb.16117

NOAA. 2022. Currents data at PUG1746, bin 10 (June 30–July 1, 2022). Center for Operational Oceanographic Products and Services (CO-OPS), National Oceanic and Atmospheric Administration. Available from: https://tidesandcurrents.noaa.gov

Pfister, C. A., and M. A. Altabet. 2019. Enhanced microbial nitrogen transformations in association with macrobiota from the rocky intertidal. *Biogeosciences* 16: 193–206. doi:10.5194/bg-16-193-2019

Poulson, M. E., A. J. McNeil, and R. A. Donahue. 2011. Photosynthetic response of Nereocystis luetkeana (Phaeophyta) to high light. *Phycological Res.* 59: 156–165. doi:10.1111/j.1440-1835.2011.00607.x

Raven, J. A., C. S. Cockell, and C. L. De La Rocha. 2008. The evolution of inorganic carbon concentrating mechanisms in photosynthesis. *Philos. Trans. R. Soc.* B 363: 2641–2650. doi:10.1098/rstb.2008.0020

Ricart, A. M., M. Ward, T. M. Hill, E. Sanford, K. J. Kroeker, Y. Takeshita, and B. Gaylord. 2021. Coast-wide evidence of low pH amelioration by seagrass ecosystems. *Glob. Change Biol.* 27: 2580–2591. doi:10.1111/gcb.15594

Ricart, A. M., D. Krause-Jensen, K. Hancke, N. N. Price, P. Masqué, and C. M. Duarte. 2022. Sinking seaweed in the deep ocean for carbon neutrality is ahead of science and beyond the ethics. *Environ. Res. Lett.* 17: 081003. doi:10.1088/1748-9326/ac7f7f

Rosman, J. H., J. R. Koseff, S. G. Monismith, and J. Grover. 2007. A field investigation into the effects of a kelp forest (Macrocystis pyrifera) on coastal hydrodynamics and transport. *J. Geophys. Res. Oceans* 112: C02016. doi:10.1029/2005JC003430

Smale, D. A., M. T. Burrows, P. Moore, N. O'Connor, and S. J. Hawkins. 2013. Threats and knowledge gaps for ecosystem services provided by kelp forests: A northeast Atlantic perspective. *Ecol. Evol.* 3: 4016–4038. doi:10.1002/ece3.774

Springer, Y. P., C. G. Hays, M. H. Carr, and M. R. Mackey. 2010. Toward ecosystem-based management of marine macroalgae—The bull kelp Nereocystis luetkeana. *Oceanogr. Mar. Biol. Annu. Rev.* 48: 1–42.

Steneck, R. S., M. H. Graham, B. J. Bourque, D. Corbett, J. M. Erlandson, J. A. Estes, and M. J. Tegner. 2002. Kelp forest ecosystems: Biodiversity, stability, resilience, and future. *Environ. Conserv.* 29: 436–459. doi:10.1017/S0376892902000322

Strain, E. M., S. E. Swearer, I. Ambler, R. L. Morris, and K. J. Nickols. 2024. Assessing the role of natural kelp forests in modifying seawater chemistry. *Sci. Rep.* 14: 22386. doi:10.1038/s41598-024-64039-5

Sutherland, D. A., P. MacCready, N. S. Banas, and L. F. Smedstad. 2011. A model study of the Salish Sea estuarine circulation. *J. Phys. Oceanogr*. 41: 1125–1143. doi:10.1175/2011JPO4540.1

Traiger, S. B., B. Cohn, D. Panos, M. Daly, H. K. Hirsh, M. Martone, and K. J. Nickols. 2022. Limited biogeochemical modification of surface waters by kelp forest canopies: Influence of kelp metabolism and site-specific hydrodynamics. *Limnol. Oceanogr*. 67: 392–403. doi:10.1002/lno.11977

Valle-Levinson, A., M. A. Daly, B. Juarez, L. Tenorio-Fernandez, M. Fagundes, C. B. Woodson, and S. G. Monismith. 2022. Influence of kelp forests on flow around headlands. *Sci. Total Environ.* 825: 153952. doi:10.1016/j.scitotenv.2022.153952

Van Dam, B., C. Lopes, M. A. Zeller, M. Ribas-Ribas, H. Wang, and H. Thomas. 2021. Overstated potential for seagrass meadows to mitigate coastal ocean acidification. *Front. Mar. Sci.* 8: 729992. doi:10.3389/fmars.2021.729992

Vaquer-Sunyer, R., and C. M. Duarte. 2008. Thresholds of hypoxia for marine biodiversity. *Proc. Natl. Acad. Sci.* U.S.A. 105: 15452–15457. doi:10.1073/pnas.0803833105

Viehman, T. S., B. G. Reguero, H. S. Lenihan, J. H. Rosman, C. D. Storlazzi, E. A. Goergen, and J. L. Hench. 2023. Coral restoration for coastal resilience: Integrating ecology, hydrodynamics, and engineering at multiple scales. *Ecosphere* 14: e4517. doi:10.1002/ecs2.4517

Weiss, R. F. 1970. The solubility of nitrogen, oxygen, and argon in water and seawater. *Deep-Sea Res. Oceanogr. Abstr.* 17: 721–735. doi:10.1016/0011-7471(70)90037-9

Wünsche, A., M. Becker, R. Fritzsch, J. Kelln, and C. Winter. 2024. The sensitivity of tidal asymmetry descriptors in the Ems estuary. *Ocean Dyn.* 74: 613–627. doi:10.1007/s10236-024-01642-9

Tables and Figures

Table 1. Summary statistics of duration and frequency of tidal conditions at Turn Rock. Tidal conditions represent combinations of current direction/magnitude (ebb, slack, flood) and light availability (day/night). Columns are sample size (n), duration in hours (mean ± SE in minutes), minimum, maximum, and proportion of time spent in each condition during the deployment (June–September 2022).

Tidal Condition	n	Duration (hours)			Proportion of time
		Mean ± SE	Minimum	Maximum	
Ebb Night	115	3.1 (± 6.8)	1.08	6.25	0.21
Ebb Day	114	3.6 (± 7.5)	0.62	6.50	0.20
Slack Night	115	2.3 (± 6.6)	0.50	5.50	0.16
Slack Day	115	2.1 (± 4.5)	0.25	5.38	0.20
Flood Night	46	1.5 (± 8.8)	0.25	4.00	0.03
Flood Day	114	4.4 (± 8.6)	0.50	6.50	0.20

Table 2. Summary of best-fitting linear mixed-effects models (LMMs) of dissolved oxygen differences (ΔDO) across (A) canopy–outside and (B) within-depth comparisons. Fixed effects included habitat comparison, diel period (day/night), and tidal condition (ebb, slack, flood), with deployment number included as a random intercept to account for repeated measures. Num DF: numerator degrees of freedom, Den DF: denominator degrees of freedom, z.ratio (z-statistic).

A) Canopy vs outside comparisons						
Fixed Effects	Sums of squares	Mean of Squares	Num DF	Den DF	F-value	P-value
habitat comparison	2331	1165	2	32750	8.9	0.0001
diel comparison	221793	221793	1	32751	1688.6	<0.0001
tidal condition	218821	109410	2	32750	833.0	<0.0001
habitat comparison × diel comparison	77	38	2	32750	0.3	0.75
habitat comparison × tidal condition	125872	31468	4	32750	239.6	<0.0001
diel comparison × tidal condition	20557	10279	2	32750	78.3	<0.0001
habitat comparison × diel comparison × tidal condition	86351	21588	4	32750	164.4	<0.0001
		Random Effect		Variance		Std.Dev
		Deployment number (intercept)		44.0		6.6
		Residuals		131.4		11.5
B) Within depth comparisons						
Fixed Effects	Sums of squares	Mean of Squares	Num DF	Den DF	F-value	P-value
habitat comparison	36	18	2	32750	0.4	0.69
diel comparison	36618	36618	1	32757	748.7	<0.0001
tidal condition	31681	15841	2	32753	323.9	<0.0001
habitat comparison × diel comparison	8573	4286	2	32750	87.6	<0.0001
habitat comparison × tidal condition	3914	979	4	32750	20.0	<0.0001
diel comparison × tidal condition	4499	2249	2	32754	46.0	<0.0001
habitat comparison × diel comparison × tidal condition	873	218	4	32750	4.5	0.001
		Random Effect		Variance		Std.Dev
		Deployment number (intercept)		0.8		0.9
		Residuals		48.9		7.0

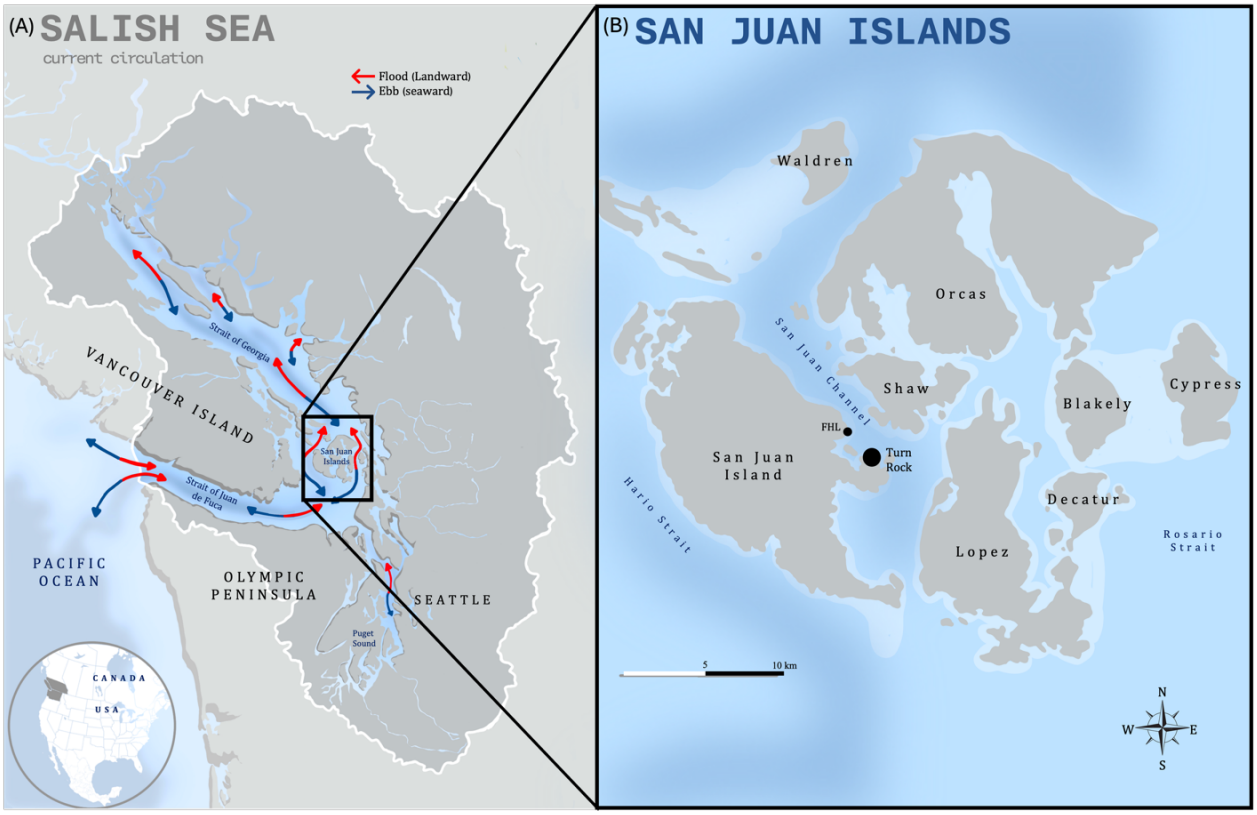

Figure 1. Map of the Salish Sea and San Juan Islands showing regional current circulation and study site location. Panel (A) illustrates dominant current patterns during ebb (red arrows; landward flow) and flood (blue arrows; seaward flow) conditions throughout the Salish Sea, including the Strait of Georgia, Strait of Juan de Fuca, and Puget Sound. Panel (B) is an inset map of the San Juan Islands, Washington, USA, highlighting Turn Rock (black circle) in the San Juan Channel, where the study took place, and Friday Harbor Laboratories (FHL), where the FHL weather station is located.

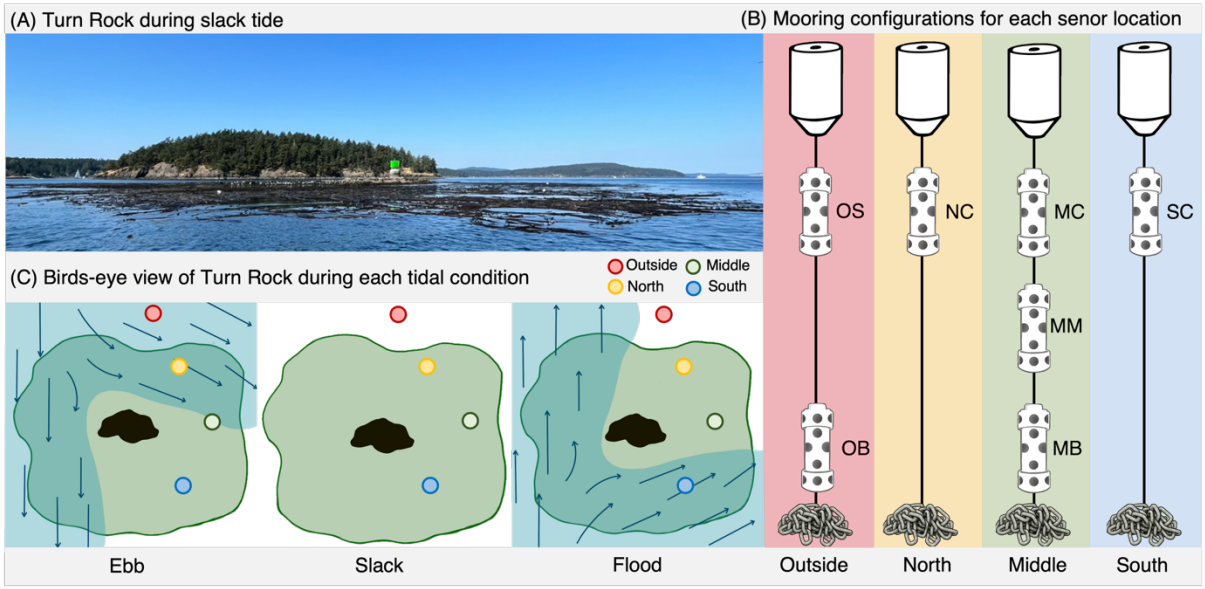

Figure 2. Deployment of chemical sensors in a bull kelp (*Nereocystis luetkeana*) forest at Turn Rock in the San Juan Islands, WA. (A) Photo of surface kelp canopy surrounding Turn Rock during slack tide in 2022. Image was taken from a boat on the east side of Turn Rock (green channel marker), looking WNW with Turn Island in the background. (B) Schematic of mooring configurations used to secure the seven sensor arrays (Outside Surface – OS, Outside Bottom – OB, North Canopy- NC, Middle Canopy- MC, Middle Midwater- MM, Middle Bottom- MB, South Canopy- SC. Each sensor array contained instruments to measure dissolved oxygen (DO), pH, conductivity, and temperature. Each mooring line was anchored to the seafloor by large chain bundles and held taught by large surface buoys. (C) Conceptual birds-eye view of observed currents at Turn Rock during ebb, slack, and flood tidal conditions. Tidally-driven flow (blue arrows) interacts with Turn Rock topography and dictates when bull kelp experiences low flow and remains floating at the surface. Circles indicate mooring locations: Outside-red, North-yellow, Middle-green, and South-blue.

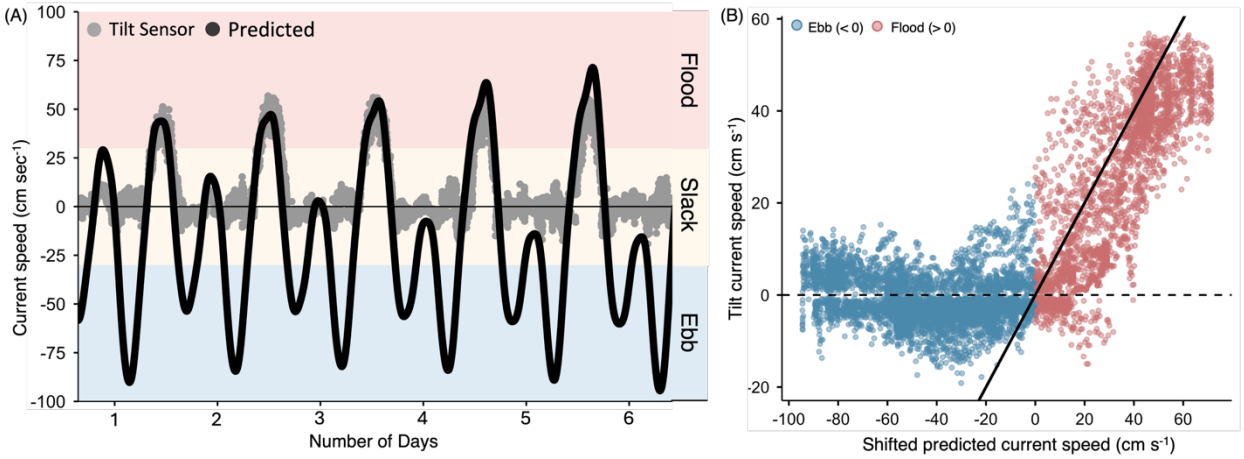

Figure 3. Comparison of predicted and observed tidal currents at Turn Rock July 21- 27, 2022. (A) Time series of predicted current (black, from NOAA predicted current shifted forward by 30 minutes, see main text for details) and measured current using a Lowell tilt sensor (grey) deployed at the south end of Turn Rock. Background shading indicates current regimes: flood (>30 cm s^{-1}, red), slack (≤30 cm s^{-1}, yellow), and ebb (<–30 cm s^{-1}, blue). (B) Scatter plot of observed versus predicted current speed, colored by tidal current direction; the black line represents the 1:1 line.

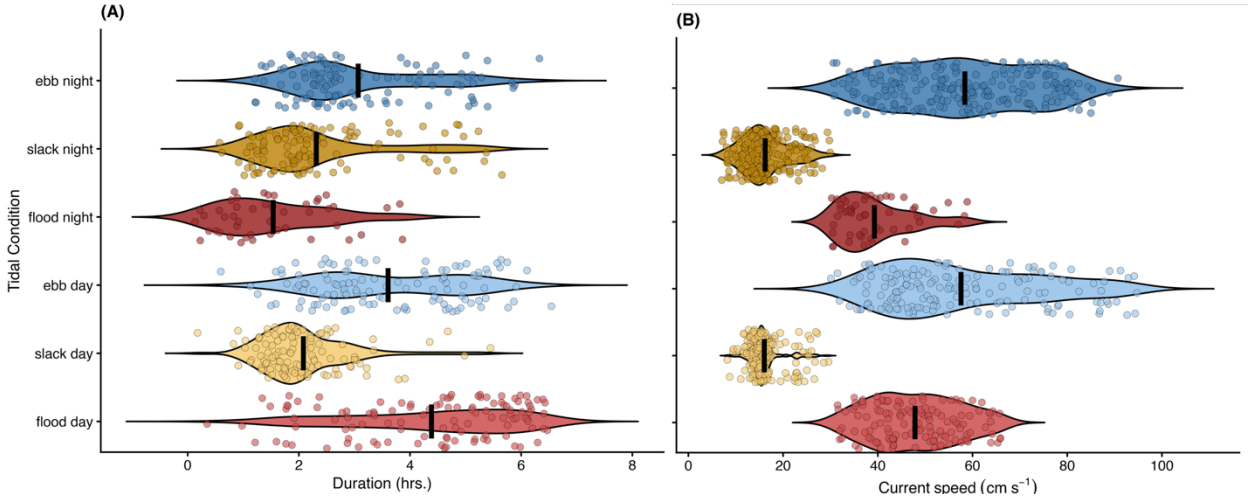

Figure 4. Duration of tidal conditions and associated current speeds at Turn Rock, separated by tidal category (ebb, slack, flood) and diurnal period (day/night). Violin plots show the distribution across the full 17-week deployment of (A) duration (hours) for each tidal–diurnal period and (B) current speeds (cm s^{-1}). Black bars indicate the mean. Sample sizes for each tidal condition are reported in Table 1.

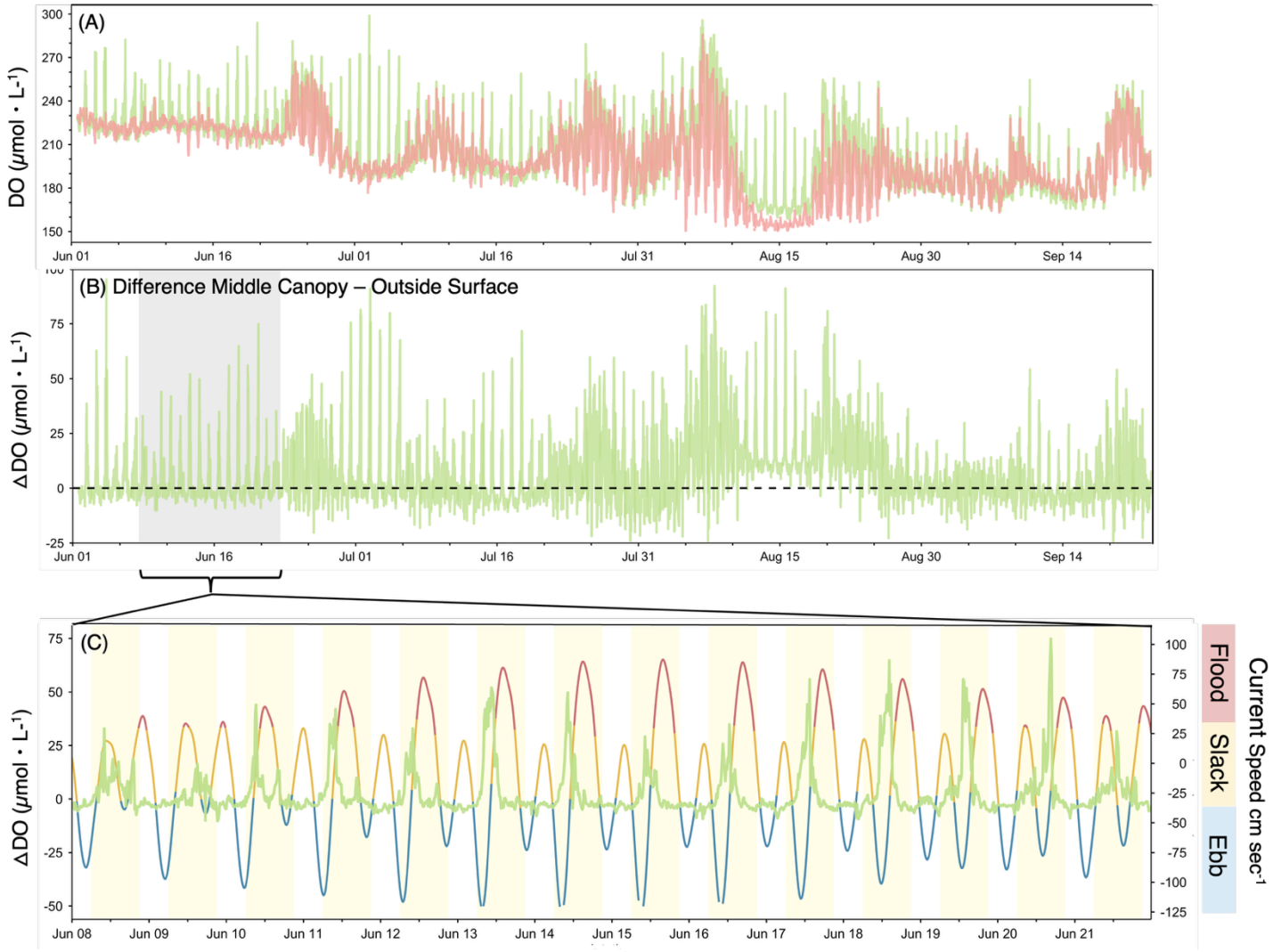

Figure 5. Representative time series illustrating the derivation of ΔDO and its relation to environmental fluctuations (current speed and light). (A) Dissolved oxygen (DO; µmol L^{-1}) measured in the middle canopy (MC, green) and outside surface (OS, red) from June to September 2022. (B) The difference in DO (ΔDO) is calculated as MC-OS. (C) A zoomed-in segment from June 8-21 (grey block in B), showing ΔDO (left axis, green) and predicted current speed (right axis) colored by tidal condition (flood-red, slack-dark yellow, and ebb-blue). Light-yellow vertical blocks indicate daytime periods.

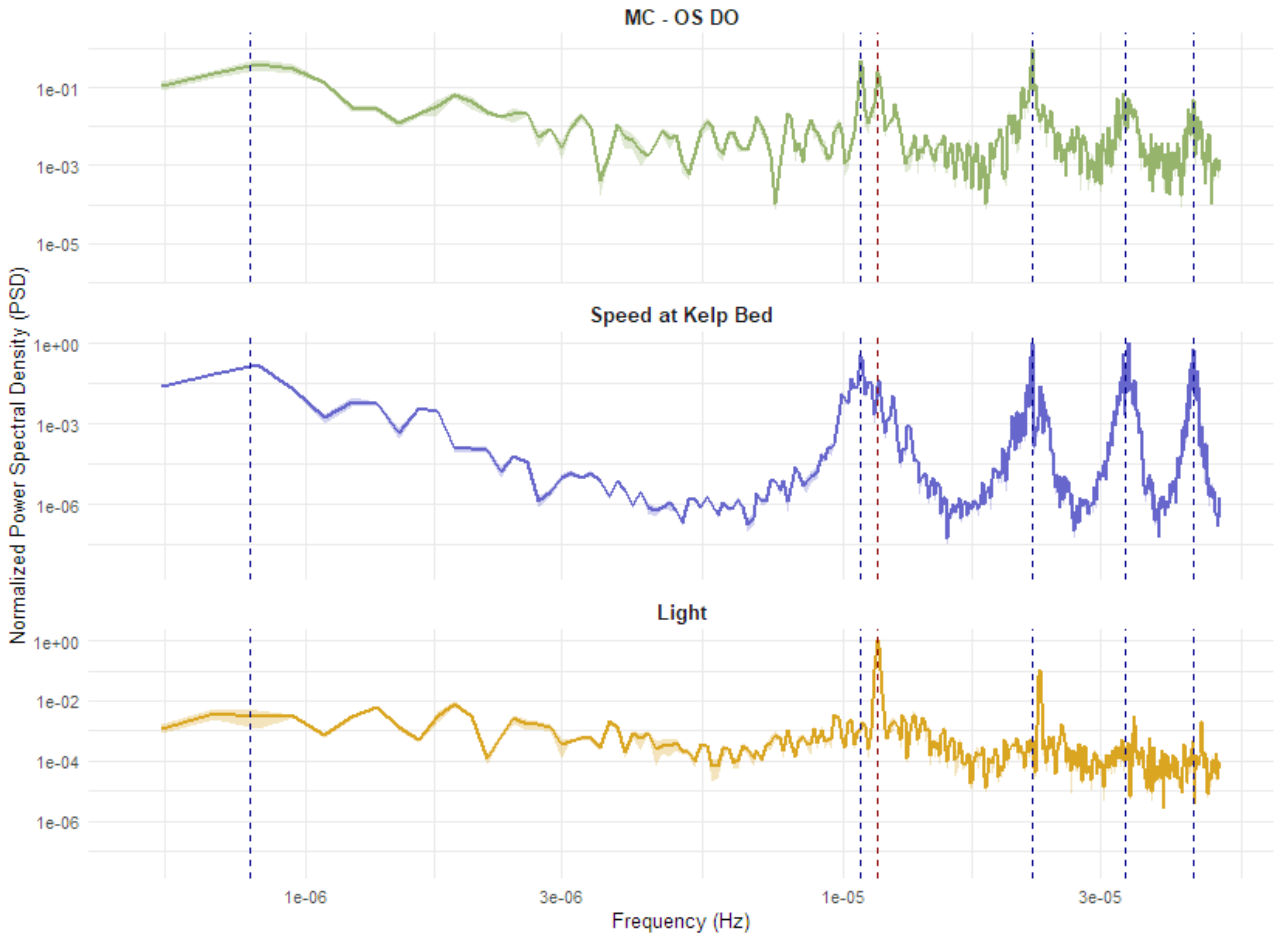

Figure 6. Time series analyses (Welch-averaged FFT) of kelp canopy DO, predicted current speed and light. A. DO difference between the middle canopy and outside surface (MS-OS DO). B. Predicted current speed. C. PAR at the surface. FFT mean amplitude was normalized to power spectrum density (PSD) for each time series; ribbons are ± 1 SE. Vertical dashed lines indicate frequencies associated with major tidal (blue) and solar (red) oscillations, in the following order: tidal Mf fortnightly 14.7d, tidal O1 diurnal lunar 25.8 hr, solar diel 24h, tidal M2 semidiurnal 12.4 hr, tidal M2 ⅔ overtide 8.3 hr, tidal M4 overtide 6.2 hr).

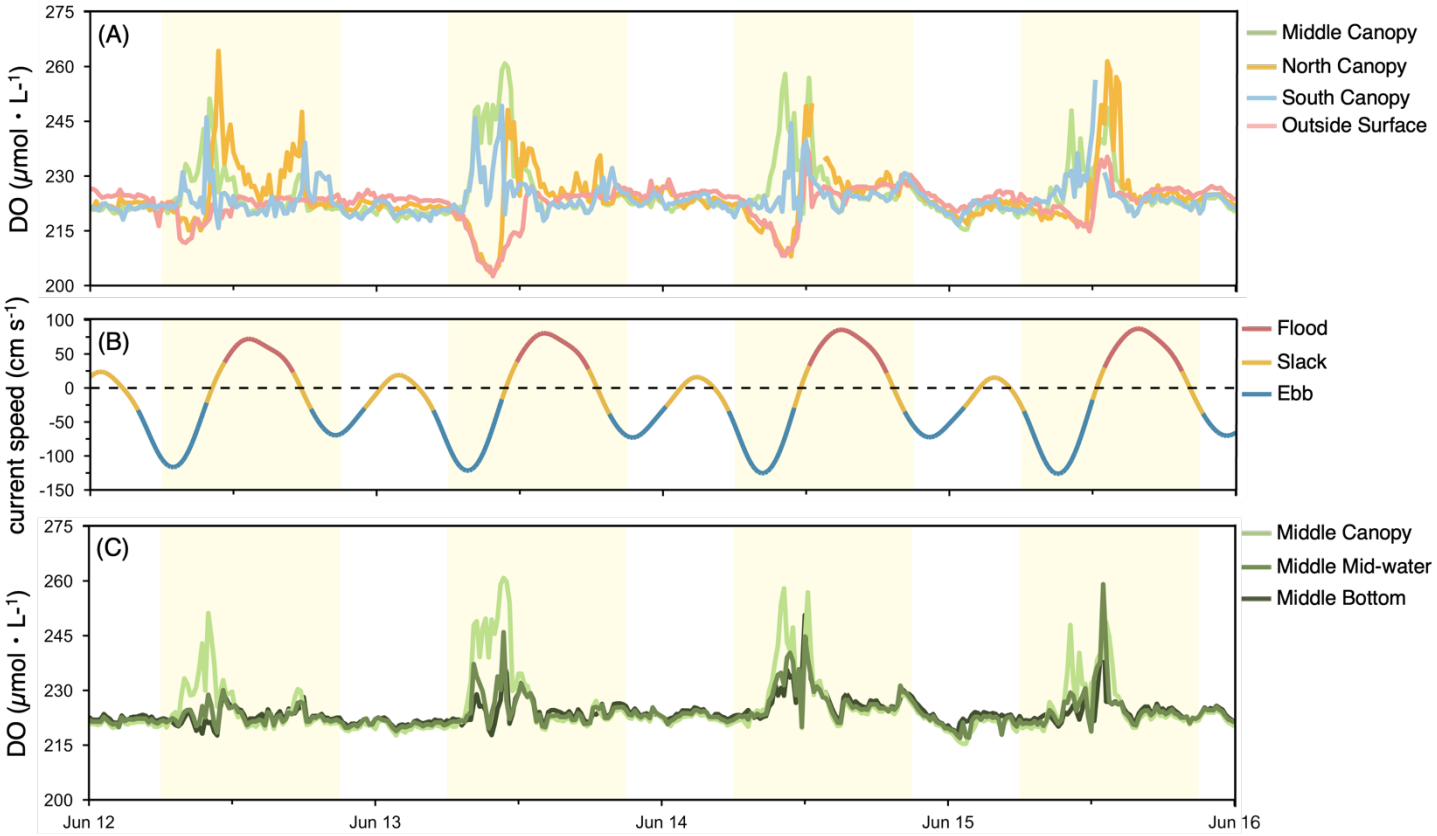

Figure 7. Representative data illustrating spatial variation in DO and its relation to environmental fluctuations (current speed and light) at Turn Rock (June 12–16, 2022). (A) DO concentrations (µmol L^{-1}) in locations within and outside the kelp canopy (Middle Canopy- light green, North Canopy- yellow, South Canopy-blue, Outside Surface- light red) showing variation in timing of peak DO across habitat locations. (B) Predicted current speeds (cm s^{-1}) colored by tidal phase (flood, slack, ebb). (C) DO concentrations (µmol L^{-1}) of three locations measured at the Middle Mooring (Middle Bottom- dark green, Middle Mid-water- green, and Middle Canopy- light green) showing differences in magnitude of DO through time across depths. Yellow shading marks daytime hours.

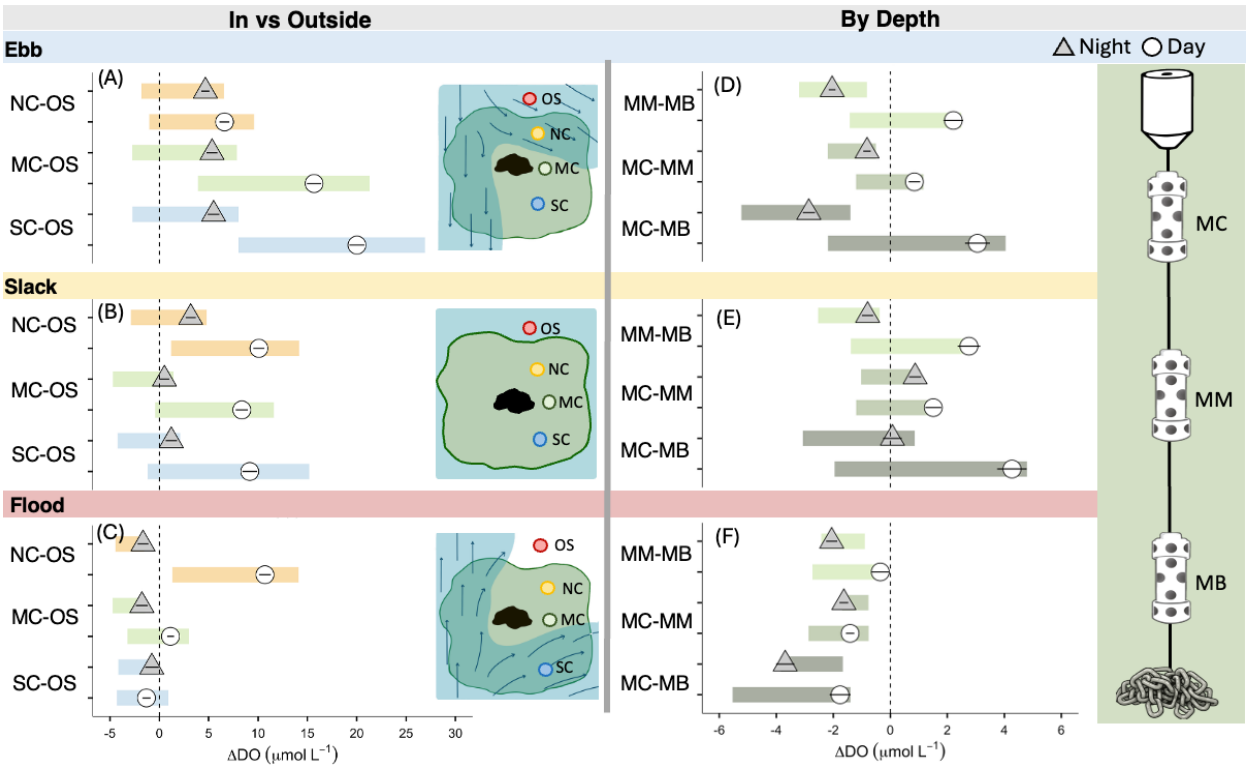

Figure 8. Summary of differences in dissolved oxygen (ΔDO) between paired sensor locations across diel and tidal conditions. ΔDO between sensors placed inside and outside the kelp canopy (A–C) and among depths on the middle mooring (D–F) are plotted separately for ebb (A, D), slack (B, E), and flood (C, F) tidal conditions. Symbols denote mean ΔDO during nighttime (grey triangles) and daytime (white circles) periods across a 17-week study, with black lines showing ± 95% confidence intervals around the mean. Shaded bars represent the 30–70th percentile range. Inset graphics excerpted from Figure 1 illustrate (A–C) a conceptual birds-eye view of currents and surface sensors at Turn Rock during each tidal phase (Outside = red, North = yellow, Middle = green, South = blue) and (D–F) the middle mooring with sensor positions at different depths (Middle Canopy = MC, Middle Mid-water = MM, Middle Bottom = MB).

Supplemental Material

Table S1. Summary of a linear model of the effects of tidal-light condition: (ebb day, ebb night, slack day, slack night, flood day, flood night), *Num DF* = numerator degrees of freedom. B) Post hoc pairwise comparisons (Tukey-adjusted) for significant effects across tidal-light conditions. Estimates represent mean differences in hours between conditions; positive values indicate that the first condition in the comparison lasted longer than the second.

(A) Type III Anova Table	Sums of squares	Means of squares	Num DF	F-value	*P*-value
Tidal-light Condition	587.05	117.41	5	56.64	<0.0001
(B) Post Hoc Pairwise Comparison					
Comparisons	Estimate	SE	DF	t-ratio	*P*-value
ebb day - slack day	1.21	0.14	613	8.46	<.0001
ebb day - flood day	-0.84	0.17	613	-4.98	<.0001
ebb day - ebb night	0.50	0.15	613	3.36	0.01
ebb day - slack night	1.21	0.15	613	8.15	<.0001
ebb day - flood night	1.80	0.23	613	7.85	<.0001
slack day - flood day	-2.05	0.15	613	-13.37	<.0001
slack day - ebb night	-0.71	0.13	613	-5.34	<.0001
slack day - slack night	0.00	0.13	613	0.03	1.00
slack day - flood night	0.59	0.22	613	2.70	0.08
flood day - ebb night	1.34	0.16	613	8.40	<.0001

Table S2. **Summary of Kruskal–Wallis test and post hoc Dunn's pairwise comparisons assessing differences in weekly correlation strength (r) between pH and DO across kelp forest habitats.** Dunn test p-values were corrected using the Benjamini-Hochberg method. Significant differences (adjusted $P < 0.05$) are bolded.

Kruskal-Wallis	Chi-square	df	P-value
	23.2	6	**0.001**
Dunn's Pairwise Comparisons			
Habitat comparisons		Z-scores	Adjusted P-value
South Canopy- Outside Surface		**-3.03**	**0.013**
Middle Canopy- Outside Surface		**3.29**	**0.007**
North Canopy- Outside Surface		1.76	0.167
Middle Canopy- North Canopy		1.53	0.220
Middle Canopy- South Canopy		0.26	0.836
North Canopy- South Canopy		-1.27	0.284
Middle Canopy- Middle Mid-water		1.34	0.272
Middle Bottom – Middle Mid-water		-0.50	0.765
Middle Bottom - Middle Canopy		-1.83	0.155
Outside Bottom - Outside Surface		-0.40	0.802
Middle Bottom - Outside Bottom		1.85	0.167

Table S3. Summary of best-fitting linear mixed-effects models (LMMs) of pH differences (ΔpH) across (A) canopy–outside and (B) within-depth comparisons. Fixed effects included habitat comparison, diel period (day/night), and tidal condition (ebb, slack, flood), with deployment number included as a random intercept to account for repeated measures. Num DF: numerator degrees of freedom, Den DF: denominator degrees of freedom, z.ratio (z-statistic).

A) Canopy vs outside comparisons						
Fixed Effects	Sums of squares	Mean of Squares	Num DF	Den DF	F-value	P-value
habitat comparison	0.01	0.01	2	32750	4.08	0.02
diel comparison	1.82	1.82	1	32751	1340.99	<0.0001
tidal condition	1.29	0.65	2	32750	475.55	<0.0001
habitat comparison × diel comparison	0.00	0.00	2	32750	0.30	0.74
habitat comparison × tidal condition	0.91	0.23	4	32750	167.21	<0.0001
diel comparison × tidal condition	0.16	0.08	2	32750	59.14	<0.0001
habitat comparison × diel comparison × tidal condition	0.73	0.18	4	32750	135.40	<0.0001
		Random Effect		Variance		Std.Dev
		Deployment number (intercept)		0.0003		0.02
		Residuals		0.001		0.04
B) Within depth comparisons						
Fixed Effects	Sums of squares	Mean of Squares	Num DF	Den DF	F-value	P-value
habitat comparison	0.02	0.01	2	32750	13.63	<0.0001
diel comparison	0.37	0.37	1	32757	598.29	<0.0001
tidal condition	0.30	0.15	2	32753	242.31	<0.0001
habitat comparison × diel comparison	0.09	0.04	2	32750	69.06	<0.0001
habitat comparison × tidal condition	0.05	0.01	4	32750	18.53	<0.0001
diel comparison × tidal condition	0.05	0.02	2	32754	36.79	<0.0001
habitat comparison × diel comparison × tidal condition	0.02	0.004	4	32750	6.41	<0.0001
		Random Effect		Variance		Std.Dev
		Deployment number (intercept)		0.000004		0.002
		Residuals		0.001		0.025

Table S4: Model selection and pairwise comparisons for within-canopy versus outside habitats. (A) AIC results comparing mixed-effects models describing variation in ΔDO (μmol L^{-1}) across tidal (ebb, slack, flood) and diel (day, night) conditions for each habitat comparison. ΔAIC values, degrees of freedom (df), and model weights are shown relative to the top model. (B) Tukey-adjusted pairwise comparisons of ΔDO across tidal and diel conditions for each habitat pairing. SE is the standard error; z-ratio is the test statistic.

(A) In canopy versus outside - AIC Model selection

Model Description	ΔAIC	df	Model weight
Full Model	0	20	1
All two-way interactions	643.2	16	<0.001
Habitat comparison × tidal + diel	1007.3	12	<0.001
Diel × tidal + habitat comparison	2752.0	10	<0.001
Additive model	2891.6	8	<0.001
Habitat comparison × diel + tidal	2893.3	10	<0.001
Diel only	5676.4	4	<0.001
Tidal only	5905.8	5	<0.001
Habitat comparison only	7230.8	5	<0.001
Deployment number only	7250.8	3	<0.001

B) In canopy versus outside - Pairwise Comparisons

Comparison	estimate	SE	z.ratio	P-value
MC-OS day ebb vs MC_OS day slack	7.38	0.35	21.19	<0.0001
MC-OS day ebb vs MC_OS night ebb	10.64	0.34	30.94	<0.0001
MC-OS day ebb vs NC_OS day ebb	9.08	0.35	25.82	<0.0001
MC-OS day flood vs MC_OS day slack	-7.53	0.34	-21.68	<0.0001
MC-OS-day flood vs MC-OS night flood	1.60	0.70	2.27	0.70
MC-OS day flood vs SC-OS-day flood	2.44	0.35	6.97	<0.0001
MC-OS day slack vs MC-OS night slack	8.04	0.36	22.08	<0.0001
NC-OS day slack vs NC-OS night slack	7.10	0.36	19.50	<0.0001
NC-OS day ebb vs NC-OS day slack	-3.42	0.35	-9.82	<0.0001
NC-OS day ebb vs NC-OS night ebb	2.24	0.34	6.51	<0.0001
NC-OS day flood vs NC-OS day slack	0.31	0.35	0.90	1.00
NC-OS day flood vs NC-OS night flood	11.06	0.70	15.72	<0.0001
NC-OS-day flood vs SC-OS day flood	12.01	0.35	34.34	<0.0001
NC-OS day slack vs NC-OS night flood	10.86	0.70	15.46	<0.0001
SC-OS day ebb vs SC-OS day slack	10.91	0.35	31.31	<0.0001
SC-OS day ebb vs SC-OS night ebb	14.82	0.34	43.11	<0.0001
SC-OS day flood vs SC-OS day slack	-10.78	0.35	-31.03	<0.0001
SC-OS day flood vs SC-OS night flood	-1.84	0.70	-2.62	0.44
SC-OS day slack vs SC-OS night slack	8.16	0.36	22.41	<0.0001

Table S5. Model selection and pairwise comparisons for within-depth habitat comparisons. (A) AIC model selection results comparing mixed-effects models that describe variation in ΔDO (μmol L^{-1}) across tidal (ebb, slack, flood) and diel (day, night) conditions for each habitat comparison. ΔAIC values, degrees of freedom (df), and model weights are shown relative to the top model. (B) Tukey-adjusted pairwise comparisons from the best model highlight significant differences in ΔDO across tidal and diel conditions for each habitat pairing. SE is the standard error, *z*-ratio is the test statistic.

(A) Within Depth - AIC Model selection			
Model Description	ΔAIC	df	Model weight
Full Model	0	20	0.99
All two-way interactions	9.9	16	0.007
habitat comparison × diel + tidal	260.6	10	<0.001
habitat comparison × tidal + diel	436.6	12	<0.001
diel × tidal + habitat comparison	460.8	10	<0.001
Additive model	547.3	8	<0.001
diel only	1870.2	4	<0.001
Tidal only	1979.7	5	<0.001
Habitat comparison only	2744.0	5	<0.001
Deployment number only	2748.8	3	<0.001

B) Within Depth - Pairwise Comparisons				
Comparison	estimate	SE	z.ratio	P-value
MM-MB day ebb - MM-MB night ebb	3.73	0.21	17.79	<0.0001
MC-MM day ebb - MC-MM night ebb	4.28	0.21	20.41	<0.0001
MC-MB day ebb - MC-MB night ebb	5.94	0.21	28.34	<0.0001
MM-MB day slack - MM-MB night slack	0.63	0.22	2.84	0.29
MC-MM day slack - MC-MM night slack	3.54	0.22	16.00	<0.0001
MC-MB day slack - MC-MB night slack	4.18	0.22	18.82	<0.0001
MM-MB day flood - MM-MB night flood	0.55	0.43	1.28	1.00
MC-MM day flood - MC-MM night flood	2.04	0.43	4.76	0.0003
MC-MB day flood - MC-MB night flood	2.25	0.43	5.25	<0.0001

Table S6: Model selection and pairwise comparisons for within-canopy versus outside habitats. (A) AIC results comparing mixed-effects models describing variation in ΔpH across tidal (ebb, slack, flood) and diel (day, night) conditions for each habitat comparison. ΔAIC values, degrees of freedom (df), and model weights are shown relative to the top model. (B) Tukey-adjusted pairwise comparisons of ΔDO across tidal and diel conditions for each habitat pairing. SE is the standard error; z-ratio is the test statistic.

(A) In canopy versus outside - AIC Model selection

Model Description	ΔAIC	df	Model weight
Full Model	0	20	1
All two-way interactions	529.4	16	<0.001
Habitat comparison × tidal + diel	819.8	12	<0.001
Diel × tidal + habitat comparison	2005.8	10	<0.001
Habitat comparison × diel + tidal	2111.4	10	<0.001
Additive model	2112.8	8	<0.001
Diel only	3810.7	4	<0.001
Tidal only	4485.4	5	<0.001
Deployment number only	5213.3	3	<0.001
Habitat comparison only	5214.5	5	<0.001

B) In canopy versus outside - Pairwise Comparisons

Comparison	estimate	SE	z.ratio	P-value
MC-OS day ebb vs MC_OS day slack	0.03	0.001	25.91	< 0.001
MC-OS day ebb vs MC_OS night ebb	0.03	0.001	26.29	< 0.001
MC-OS day ebb vs NC_OS day ebb	0.02	0.001	17.9	< 0.001
MC-OS day flood vs MC_OS day slack	-0.01	0.001	-10.01	< 0.001
MC-OS-day flood vs MC-OS night flood	0.01	0.001	5.28	< 0.001
MC-OS day flood vs SC-OS-day flood	0.04	0.001	38.28	< 0.001
MC-OS day slack vs MC-OS night slack	0.03	0.001	28.79	< 0.001
NC-OS day slack vs NC-OS night slack	0.02	0.001	16.08	< 0.001
NC-OS day ebb vs NC-OS day slack	0.02	0.001	18.28	< 0.001
NC-OS day ebb vs NC-OS night ebb	0.02	0.001	18.81	< 0.001
NC-OS day flood vs NC-OS day slack	0.03	0.002	14.52	< 0.001
NC-OS day flood vs NC-OS night flood	0	0.002	-2.05	= 0.84
NC-OS-day flood vs SC-OS day flood	0.01	0.002	2.96	= 0.22
NC-OS day slack vs NC-OS night flood	0.03	0.001	26.42	< 0.001
SC-OS day ebb vs SC-OS day slack	0.01	0.001	4.77	< 0.001
SC-OS day ebb vs SC-OS night ebb	0.03	0.001	25.91	< 0.001
SC-OS day flood vs SC-OS day slack	0.03	0.001	26.29	< 0.001
SC-OS day flood vs SC-OS night flood	0.02	0.001	17.9	< 0.001
SC-OS day slack vs SC-OS night slack	-0.01	0.001	-10.01	< 0.001

Table S7. Model selection and pairwise comparisons for within-depth habitat comparisons. (A) AIC model selection results comparing mixed-effects models that describe variation in ΔpH across tidal (ebb, slack, flood) and diel (day, night) conditions for each habitat comparison. ΔAIC values, degrees of freedom (df), and model weights are shown relative to the top model. (B) Tukey-adjusted pairwise comparisons from the best model highlight significant differences in ΔpH across tidal and diel conditions for each habitat pairing. SE is the standard error, *z*-ratio is the test statistic.

(A) Within Depth - AIC Model selection			
Model Description	ΔAIC	df	Model weight
Full Model	0	20	1.00
All two-way interactions	17.7	16	<0.001
habitat comparison × diel + tidal	212.2	10	<0.001
habitat comparison × tidal + diel	375.8	12	<0.001
diel × tidal + habitat comparison	378.4	10	<0.001
Additive model	447.1	8	<0.001
diel only	1440.7	4	<0.001
Tidal only	1609.7	5	<0.001
Habitat comparison only	2043.9	5	<0.001
Deployment number only	2134	3	<0.001

B) Within Depth - Pairwise Comparisons				
Comparison	estimate	SE	z.ratio	P-value
MM-MB day ebb - MM-MB night ebb	-0.0001	0.0008	-0.16	1.00
MC-MM day ebb - MC-MM night ebb	0.014	0.0008	19.10	<0.001
MC-MB day ebb - MC-MB night ebb	0.019	0.0008	25.33	<0.001
MM-MB day slack - MM-MB night slack	0.004	0.0008	5.84	<0.001
MC-MM day slack - MC-MM night slack	0.011	0.0008	13.68	<0.001
MC-MB day slack - MC-MB night slack	0.012	0.0008	14.94	<0.001
MM-MB day flood - MM-MB night flood	0.001	0.0008	1.19	1.00
MC-MM day flood - MC-MM night flood	0.005	0.0015	3.40	0.07
MC-MB day flood - MC-MB night flood	0.009	0.0015	6.11	<0.001

Table S8. Analysis of the sensitivity of tidal and diel effects on differences in dissolved oxygen (ΔDO) between location comparisons analysis to transient salinity gradients. The "All data" columns reflect the metrics presented in Figure 9 (mean ΔDO (μmol L^{-1}), 95% confidence intervals (CI), and 30–70th percentile ranges), where the entire time series is included. The 'Filtered for ΔSalinity" columns reflect the same metrics when the time series is filtered to exclude periods with large physical differences among habitat comparisons, when |ΔSalinity| ≤ 1.0 PSU, and are shown in Figure S10. The "Summary" columns indicate how filtering affected the mean value and proportion of data excluded for each combination of location, tidal period and diel period. (A) Comparisons between canopy and outside locations (NC–OS, MC–OS, SC–OS) and (B) comparisons among depths within the middle mooring (MC–MM, MC–MB, MM–MB).

(A) In Canopy vs Outside Comparisons												
			All data				Filtered for ΔSalinity				Summary	
Location Comparison	Tidal Condition	Diel period	mean	95% CI (lower, upper)	Distribution Percentile (30–70)	n	mean	95% CI (lower, upper)	Distribution Percentile (30–70)	n	Difference in means: all data – filtered (% changed in mean)	Proportion of data filtered
NC – OS	ebb	night	4.7	(4.3, 5.1)	(-1.8, 6.5)	2338	3.8	(3.4, 4.2)	(-1.9, 5.7)	2245	0.9 (19.1)	0.04
		day	6.6	(6.1, 7.1)	(-1.0, 9.6)	2126	4.5	(4.1, 4.9)	(-1.3, 7.1)	1938	2.1 (31.8)	0.09
MC – OS		night	5.3	(4.8, 5.9)	(-2.8, 7.9)	2338	2.7	(2.3, 3.1)	(-2.8, 4.5)	2131	2.6 (49.1)	0.09
		day	15.7	(15.0, 16.4)	(3.9, 21.)	2126	12.8	(12.0, 13.5)	(2.6, 16.1)	1811	2.9 (18.5)	0.15
SC – OS		night	5.5	(4.9, 6.1)	(-2.7, 8.0)	2338	2.0	(1.7, 2.5)	(-3.0, 4.1)	2091	3.4 (63.6)	0.11
		day	20.0	(19.2, 20.8)	(8.0, 26.9)	2126	17.3	(16.5, 18.1)	(6.7, 22.4)	1818	2.7 (13.5)	0.14
NC – OS	slack	night	3.2	(2.7, 3.7)	(-2.9, 4.8)	1802	2.0	(1.5, 2.4)	(-3.0, 3.8)	1695	1.2 (37.5)	0.06
		day	10.1	(9.5, 10.7)	(1.2, 14.2)	2207	9.5	(8.9, 10.0)	(1.0, 13.6)	2130	0.6 (5.9)	0.03
MC – OS		night	0.5	(0.01, 1.0)	(-4.7, 1.4)	1802	-0.6	(-1.0, -0.2)	(-4.9, 0.3)	1730	1.1 (220.0)	0.04
		day	8.4	(7.7, 9.0)	(-0.4, 11.6)	2207	7.7	(7.1, 8.3)	(-0.7, 10.8)	2094	0.6 (8.3)	0.05
SC – OS		night	1.2	(0.6, 1.8)	(-4.2, 2.1)	1802	-0.3	(-0.7, 0.2)	(-4.3, 0.7)	1714	1.5 (125.0)	0.05
		day	9.2	(8.4, 9.9)	(-1.2, 15.2)	2207	9.2	(8.5, 9.9)	(-0.9, 14.5)	2052	-0.02 (0)	0.07
NC – OS	flood	night	-1.7	(-2.2, -1.1)	(-4.5, -1.5)	304	-1.7	(-2.2, -1.1)	(-4.5, -1.5)	304	0.0 (0)	0.00
		day	10.7	(10.1, 11.3)	(1.3, 14.1)	2149	9.8	(9.2, 10.4)	(1.2, 13.2)	2075	0.9 (8.4)	0.03
MC – OS		night	-1.8	(-2.4, -1.2)	(-4.7, -1.5)	304	-1.8	(-2.4, -1.3)	(-4.7, -1.5)	304	0.0 (0)	0.00

		day	1.1	(0.8, 1.5)	(-3.2, 3.0)	2149	1.0	(0.7, 1.4)	(-3.2, 2.9)	2100	0.1 (9.1)	0.02
SC – OS		night	-0.8	(-1.4, -0.1)	(-4.2, -0.4)	304	-0.8	(-1.4, -0.1)	(-4.2, -0.4)	304	0.0 (0)	0.00
		day	-1.3	(-1.7, -0.9)	(-4.3, 0.9)	2149	-0.3	(-0.7, 0.02)	(-3.9, 1.2)	2049	-1.0 (76.9)	0.05
(B) Within Depth Comparisons												
MC – MM	ebb	night	-2.04	(-2.2, -1.9)	(-3.2, -0.8)	2338	-2.2	(-2.3, -2.1)	(-3.2, -0.9)	2302	0.1 (-7.8)	0.02
		day	2.21	(1.9, 2.6)	(-1.4, 2.5)	2126	2.2	(1.8, 2.5)	(-1.4, 2.5)	2097	0.1 (0.5)	0.01
MC – MB		night	-2.86	(-3.1, -2.6)	(-5.2, -1.4)	2338	-3.3	(-3.5, -3.2)	(-5.3, -1.4)	2236	0.5 (-15.4)	0.04
		day	3.06	(2.6, 3.5)	(-2.2, 4.0)	2126	2.7	(2.3, 3.2)	(-2.3, 3.6)	2013	0.3 (11.8)	0.05
MM – MB		night	-0.82	(-1.0, -0.7)	(-2.2, -0.5)	2338	-1.0	(-1.1, -0.9)	(-2.2, -0.5)	2295	0.2 (-22.0)	0.02
		day	0.84	(0.6, 1.1)	(-1.2, 1.2)	2126	0.7	(0.5, 0.9)	(-1.2, 1.0)	2074	0.2 (16.7)	0.02
MC – MM	slack	night	-0.80	(-1.0, -0.6)	(-2.5, -0.4)	1802	-1.1	(-1.3, -0.9)	(-2.6, -0.5)	1744	0.3 (-37.5)	0.03
		day	2.76	(2.4, 3.2)	(-1.4, 2.8)	2207	2.4	(2.0, 2.7)	(-1.4, 2.5)	2166	0.4 (13.0)	0.02
MC – MB		night	0.07	(-0.3, 0.4)	(-3.1, 0.9)	1802	-1.0	(-1.3, -0.8)	(-3.3, -0.1)	1643	1.1 (1528.6)	0.09
		day	4.27	(3.8, 4.8)	(-2.0, 4.8)	2207	3.0	(2.5, 3.4)	(-2.1, 3.8)	2066	1.3 (29.7)	0.06
MM – MB		night	0.87	(0.7, 1.1)	(-1.0, 1.1)	1802	0.5	(0.3, 0.7)	(-1.1, 0.7)	1749	0.4 (42.5)	0.03
		day	1.51	(1.2, 1.8)	(-1.2, 1.4)	2207	0.9	(0.6, 1.1)	(-1.3, 1.2)	2127	0.7 (40.5)	0.04
MC – MM	flood	night	-2.06	(-2.3, -1.9)	(-2.4, -0.9)	304	-2.1	(-2.3, -1.9)	(-2.4, -0.9)	304	0.0 (-1.9)	0.00
		day	-0.35	(-0.7, -0.1)	(-2.7, -0.5)	2149	-1.3	(-1.5, -1.1)	(-2.7, -0.6)	2078	0.9 (-271.4)	0.03
MC – MB		night	-3.69	(-4.0, -3.4)	(-3.9, -1.7)	304	-3.7	(-4.1, -3.4)	(-3.9, -1.7)	304	0.0 (-0.3)	0.00
		day	-1.76	(-2.1, -1.4)	(-5.5, -1.4)	2149	-3.0	(-3.2, -2.7)	(-5.7, -1.5)	2066	1.2 (-70.5)	0.04
MM – MB		night	-1.63	(-1.8, -1.5)	(-1.7, -0.8)	304	-1.6	(-1.8, -1.5)	(-1.7, -0.6)	304	0.00 (1.8)	0.00
		day	-1.41	(-1.6, -1.3)	(-2.9, -0.8)	2149	-1.6	(-1.7, -1.5)	(-2.9, -0.8)	2131	0.2 (-13.5)	0.01

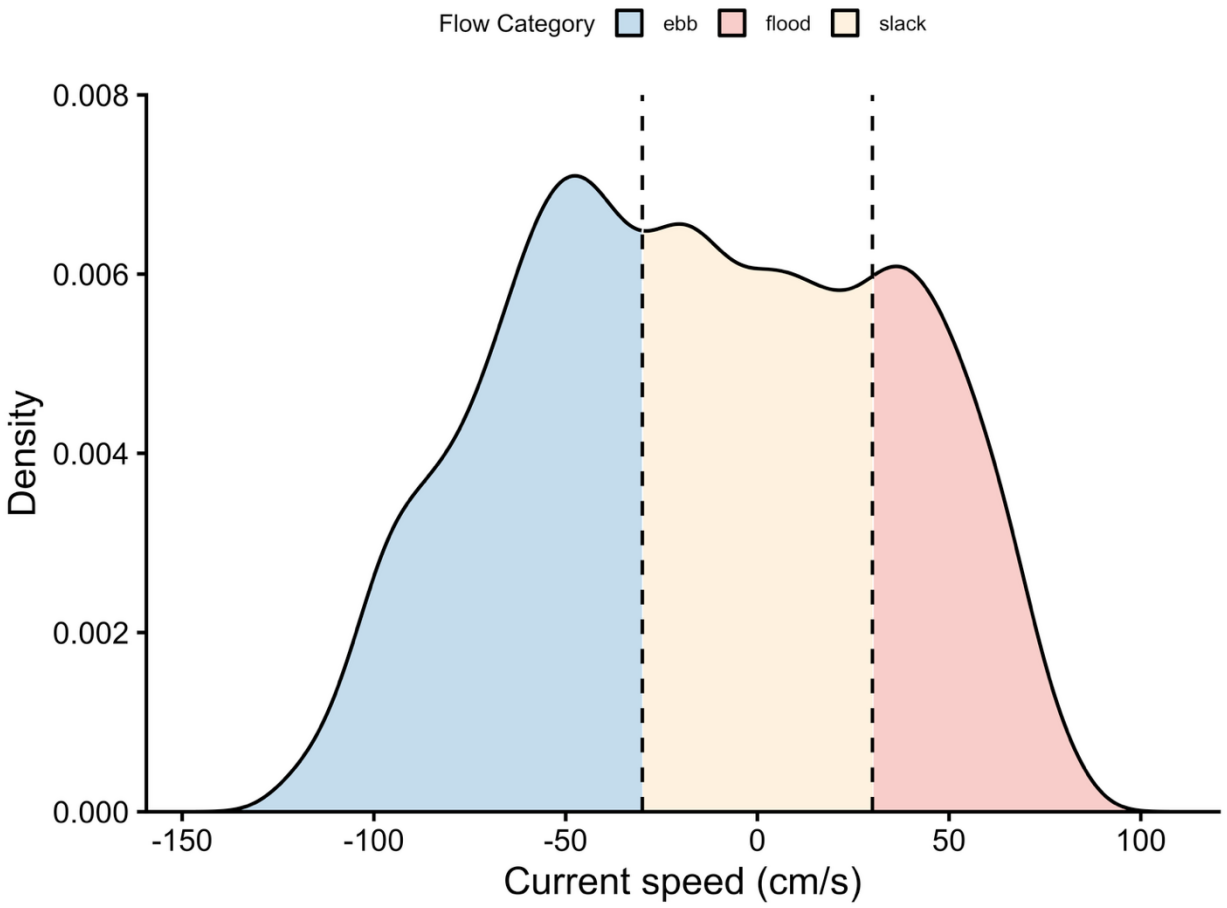

Figure S1. **Distribution of predicted current speeds during the 17-week deployment at Turn Rock.** Tidal conditions (ebb, slack, and flood) are shown with colors based on a slack threshold of ±30 cm s^{-1} (vertical black dashed lines). Negative speeds represent ebb (blue, outgoing flow), positive speeds represent flood (red, incoming flow), and values near zero indicate slack (gold) periods.

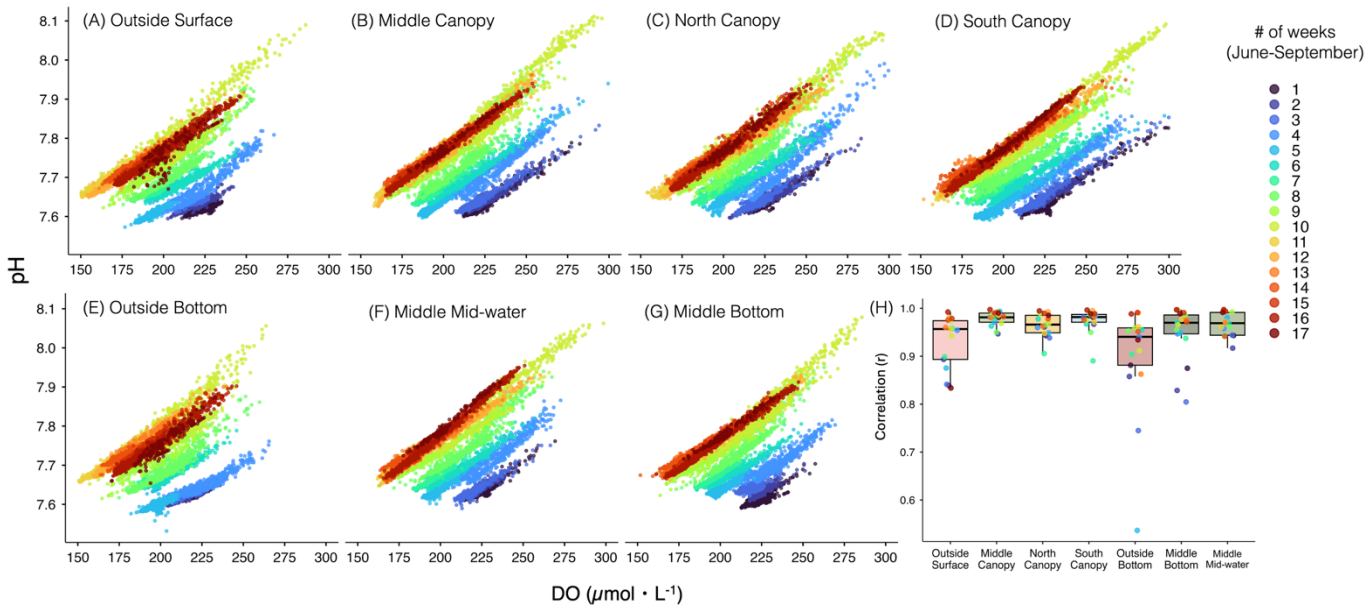

Figure S2. Weekly relationships between DO and pH across sensor locations from June to September 2022. Panels (A–G) display 15-minute interval observations of pH and ΔDO for each week, color-coded from cooler (early June–July) to warmer (August–September) tones. H) Summary of the correlation between pH and DO by habitat. Each circle represents the correlation coefficient (r) at the specified location for a given week (1-17), see inset for color coding. The horizontal black lines mark the median, boxes show the interquartile range (IQR; 25th–75th percentiles), while whiskers extend to data points within 1.5 × IQR. See Fig. S2 for underlying data.

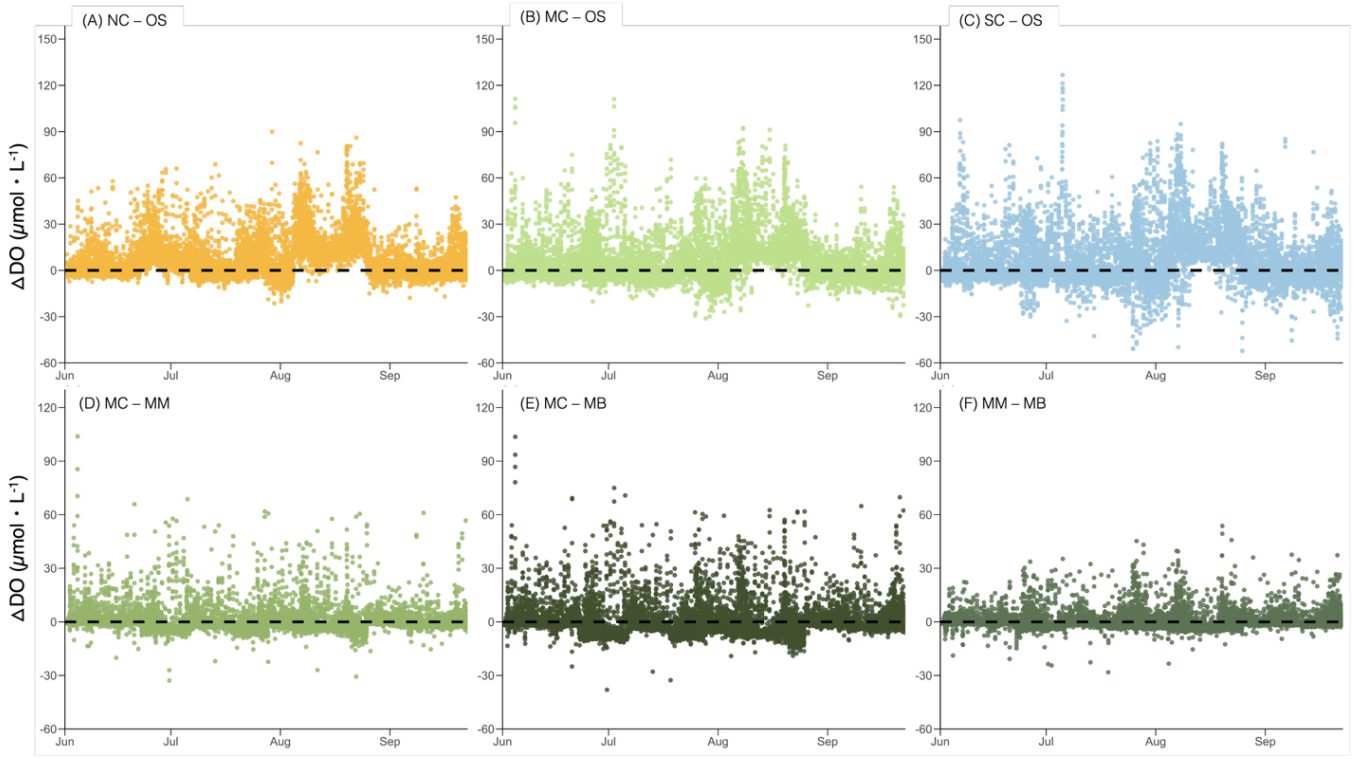

Figure S3. Time series of DO differences (ΔDO µmol L⁻¹) between select sensor locations from June to September 2022. (A–C) Inside versus outside of kelp bed deviations of three canopy sensors from a reference sensor outside the bed: (A) North Canopy – Outside Surface (NC – OS, yellow), (B) Middle Canopy – Outside Surface (MC – OS, medium green), and (C) South Canopy – Outside Surface (SC – OS, blue. (D–F) With depth comparisons all among the Middle Mooring sensor locations: (D) Middle Canopy – Middle Mid-water (MC – MM) light green, (E) Middle Canopy – Middle Bottom (MC – MB), dark green, and (F) Middle Mid-water – Middle Bottom (MM – MB), medium green. Positive values indicate higher DO in the first location listed relative to the second.

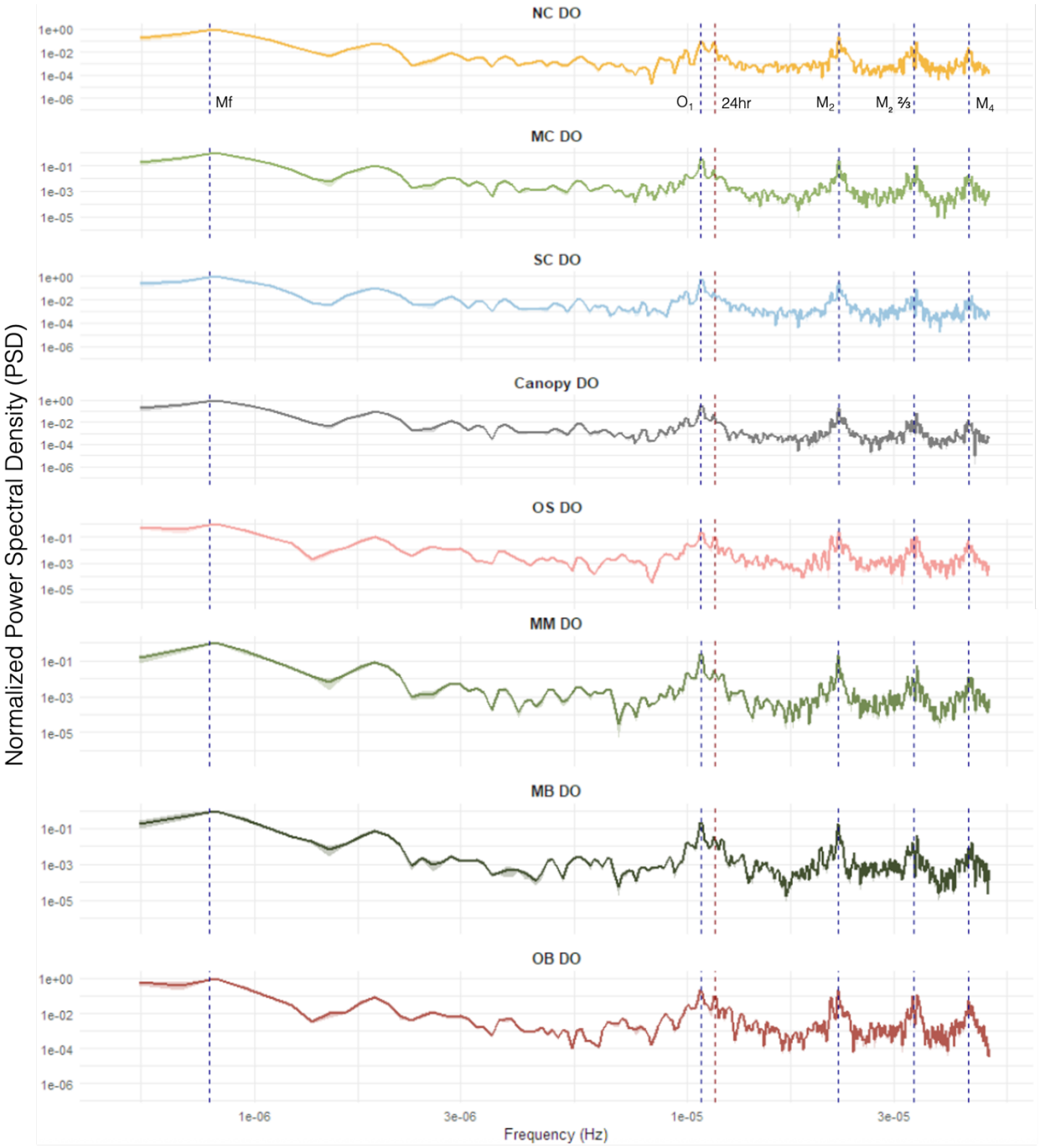

Figure S4. Time series analyses (Welch-averaged FFT) of dissolved oxygen (DO) variability across canopy and outside habitats. Power spectra are shown for the North Canopy (NC), Middle Canopy (MC), South Canopy (SC), mean Canopy (average of NC, MC, and SC), and Outside Surface (OS) Middle-Midwater (MM), Middle Bottom (MB), Outside Bottom (MB). FFT mean amplitude was normalized to power spectral density (PSD) for each time series. Vertical dashed lines indicate frequencies associated with major tidal (blue) and solar (red) oscillations, in the following order: tidal Mf fortnightly 14.7 d, tidal O_1 diurnal lunar 25.8 h, solar diel 24 h, tidal M_2 semidiurnal 12.4 h, tidal M_2 ⅔ overtide 8.3 h, and tidal M_4 overtide 6.2 h.

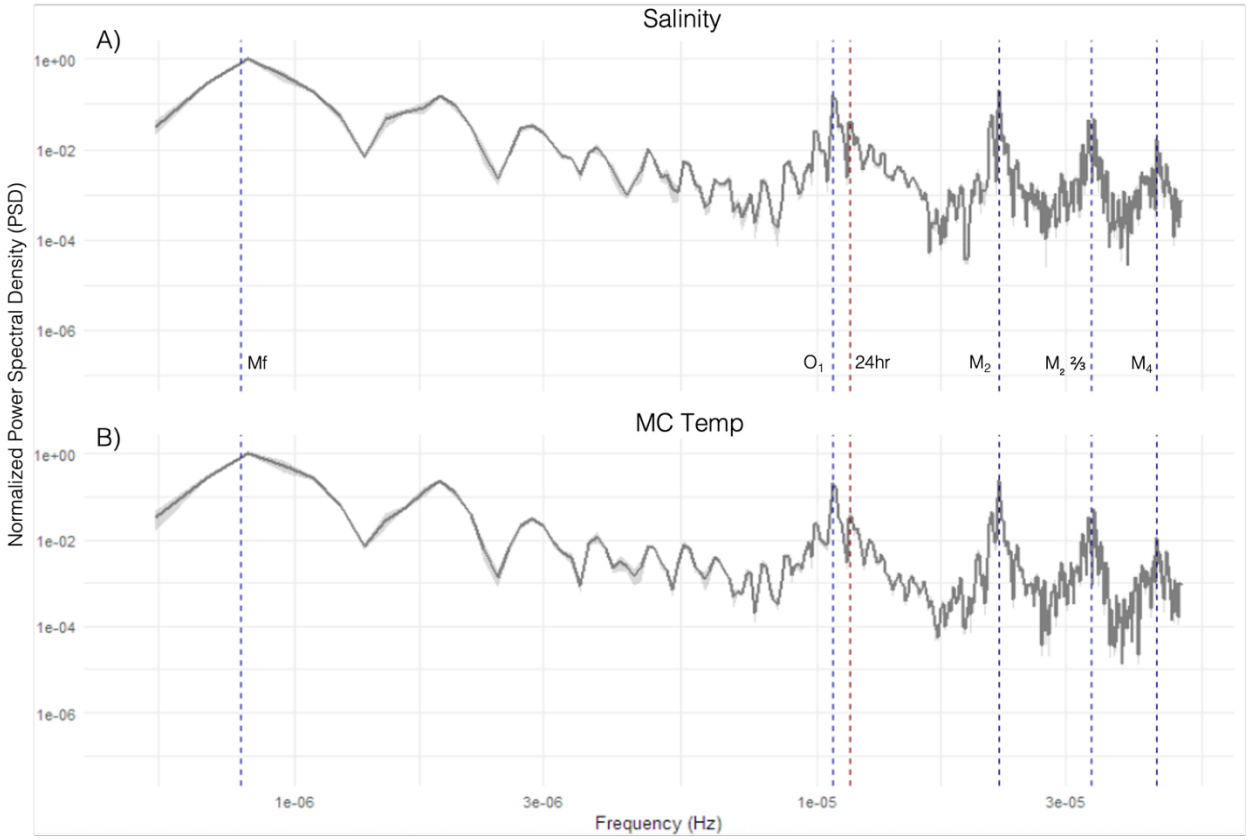

Figure S5. Time-series analyses (Welch-averaged FFT) of salinity (A) and temperature (B) variability at Turn Rock. FFT mean amplitudes were normalized to power spectral density (PSD) for each time series. Vertical dashed lines indicate frequencies associated with major tidal (blue) and solar (red) oscillations, shown in the following order: tidal **Mf** (fortnightly, 14.7 d), tidal **O_1** (diurnal lunar, 25.8 h), solar diel (24 h), tidal **M_2** (semidiurnal, 12.4 h), tidal M_2 ⅔ overtide (8.3 h), and tidal **M_4** (6.2 h).

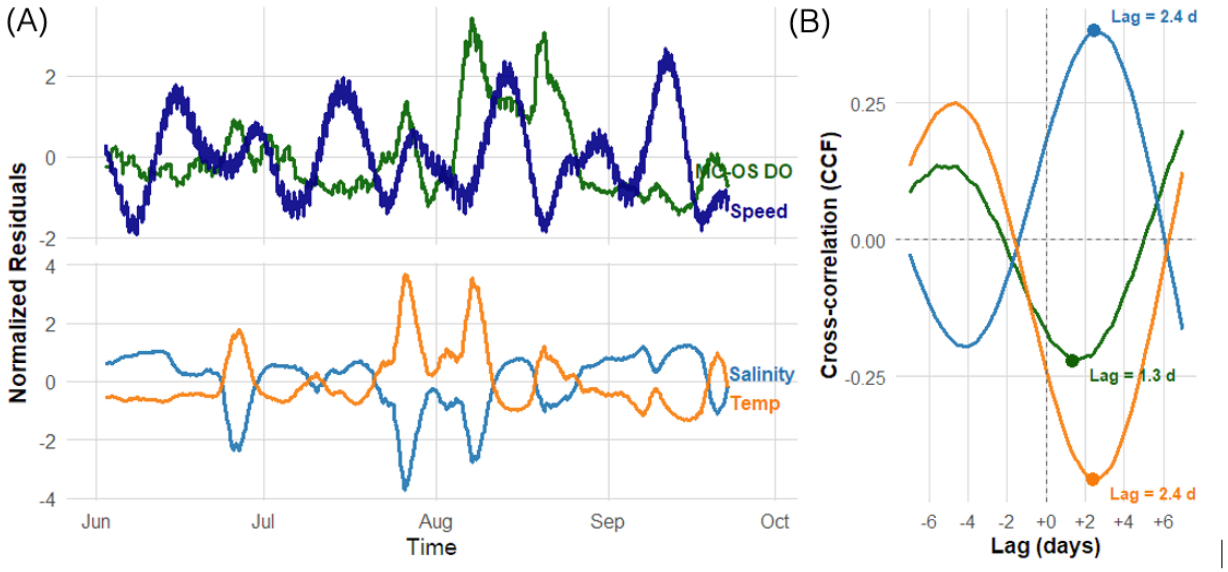

Figure S6. Cross-Correlation (CCF) analysis of select time series, all smoothed with a 2-day rolling average to highlight low-frequency (> ~1 day) variation. (A) Normalized residuals of smoothed detrended time series: (Left Top) MC-OS DO and current speed in green and dark blue, respectively. Note that the current speed is the absolute value of the predicted current, so does not distinguish between ebb and flow. (Left Bottom) Salinity (light blue) and temperature (orange). (B) Cross-correlation for three time series (MC-OS DO, salinity, temperature) lagged by +7 days relative to current speed. The lag (in days) corresponding to the peak absolute correlation is indicated for each time series. For example, the CCF peaks in MC-OS DO lag minima in current speed by 1.3 days. Salinity and temperature, which are inversely correlated, lag current speed by 2.4 days.

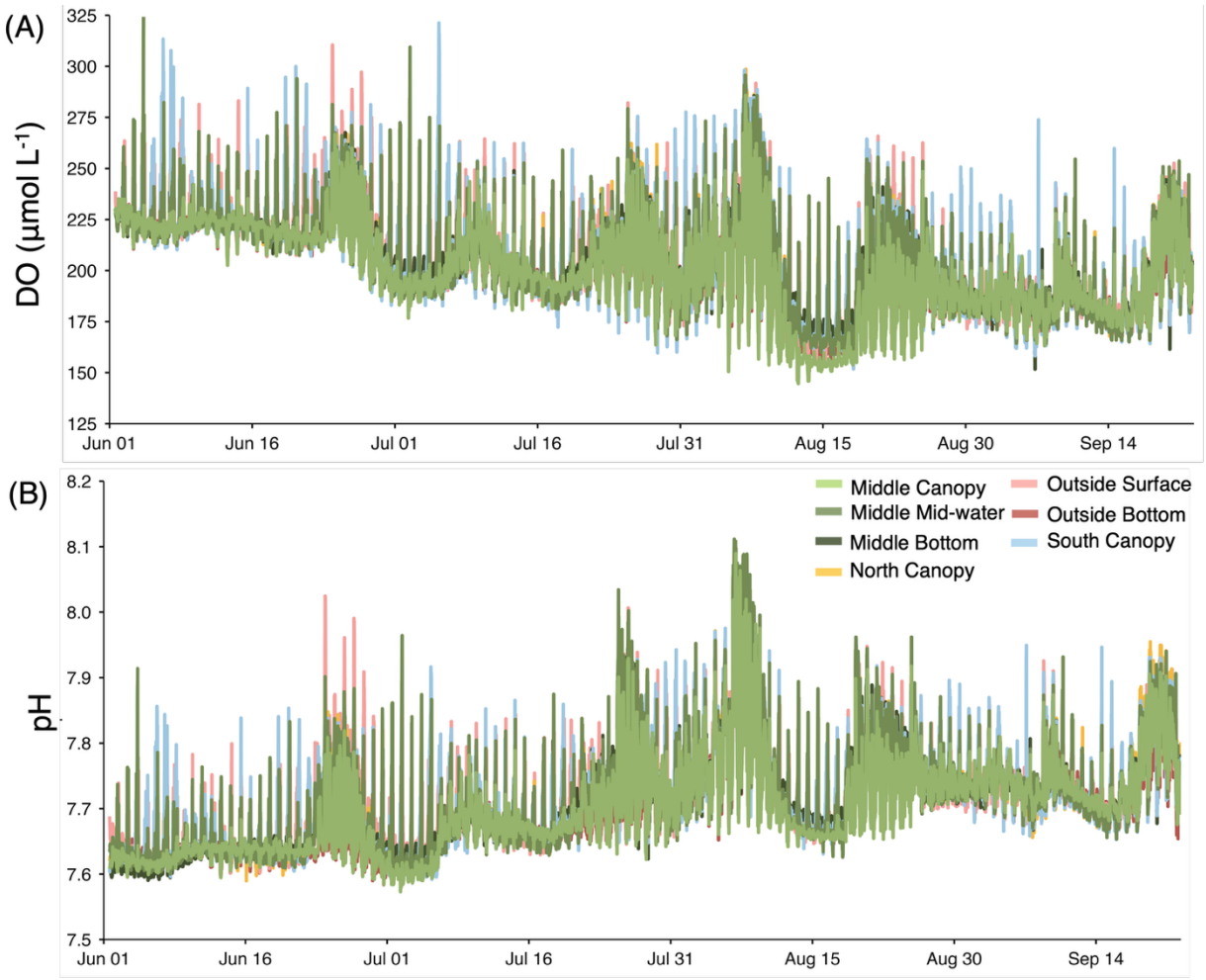

Figure S7. Time series of (A) DO (µmol L⁻¹) and (B) pH measured across multiple sensor locations inside and outside the kelp forest at Turn Rock from June to September 2022. Colored lines represent individual sensor locations: Outside Surface (light red), Middle Canopy (light green), Outside Bottom (dark red), North Canopy (yellow), Middle Midwater (medium green), Middle Bottom (dark green), and South Canopy (blue).

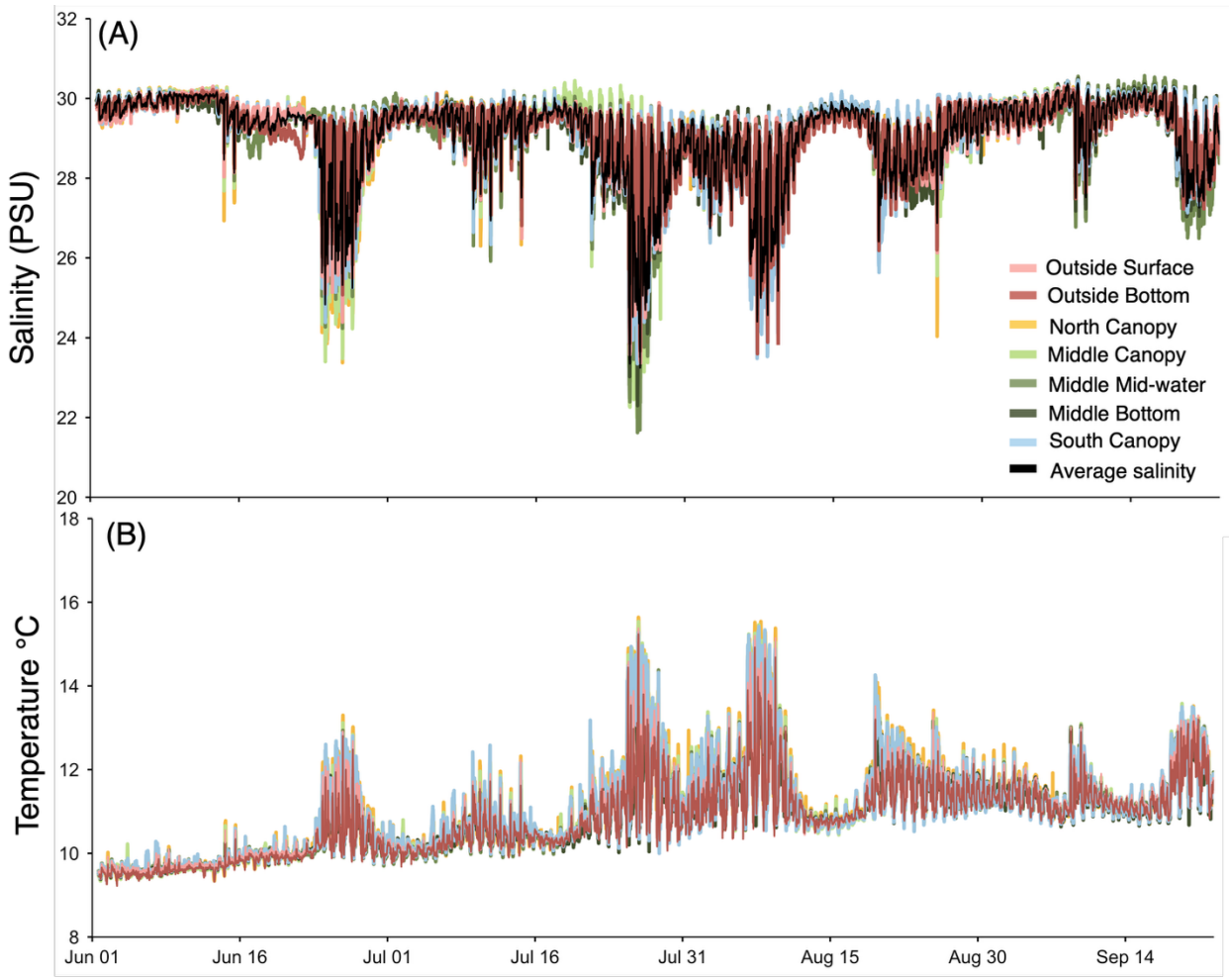

Figure S8 . Time series of (A) salinity (PSU) and (B) temperature (°C) measured across multiple sensor locations inside and outside the kelp forest at Turn Rock from June to September 2022. Colored lines represent individual sensor locations: Outside Surface (light red), Outside Bottom (dark red), North Canopy (yellow), Middle Canopy (light green), Middle Midwater (medium green), Middle Bottom (dark green), and South Canopy (blue). The thick black line indicates the mean salinity averaged across all sensors at each time point.

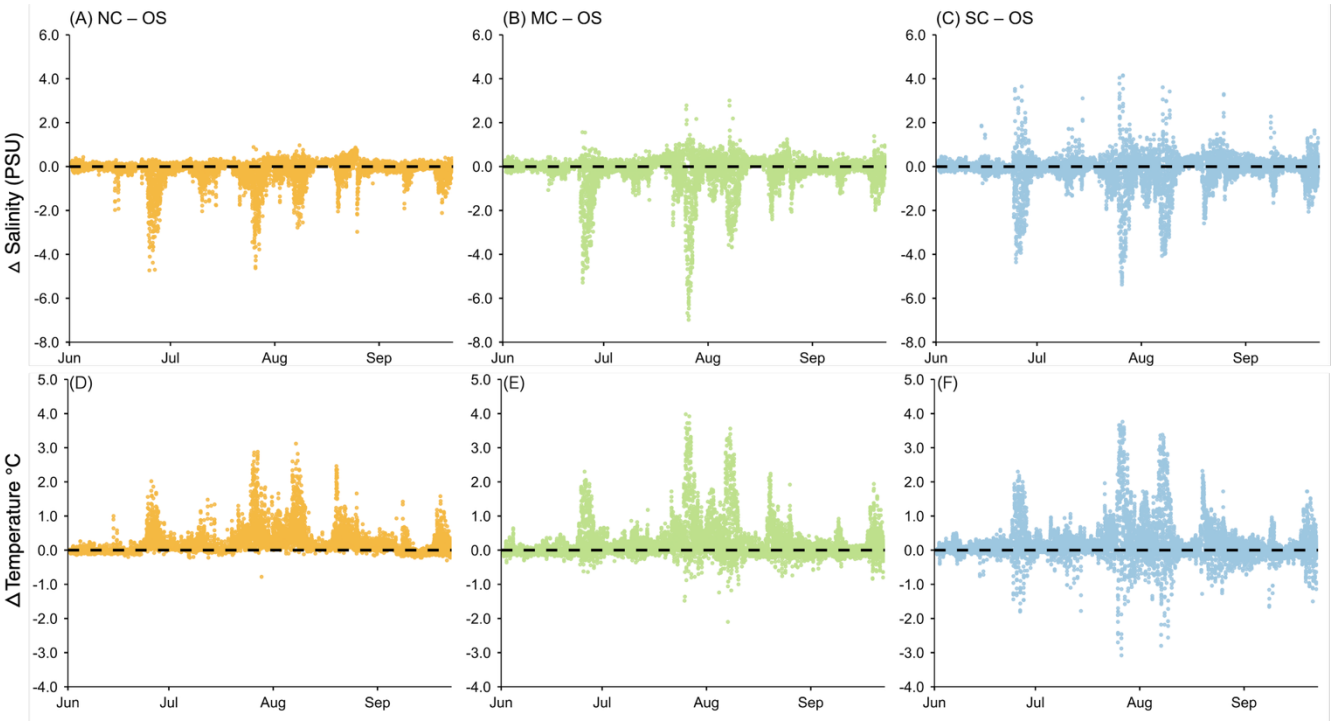

Figure S9. Time series of salinity and temperature differences (ΔSalinity, PSU; ΔTemperature, °C) between canopy and outside surface habitats from June to September 2022. (A–C) Canopy–outside salinity differences: (A) North Canopy – Outside Surface (NC – OS; yellow), (B) Middle Canopy – Outside Surface (MC – OS; medium green), and (C) South Canopy – Outside Surface (SC – OS; blue). (D–F) Corresponding canopy–outside temperature differences for the same habitat pairs. Positive values indicate higher salinity or temperature in the first location listed relative to the second; dashed lines denote zero difference.

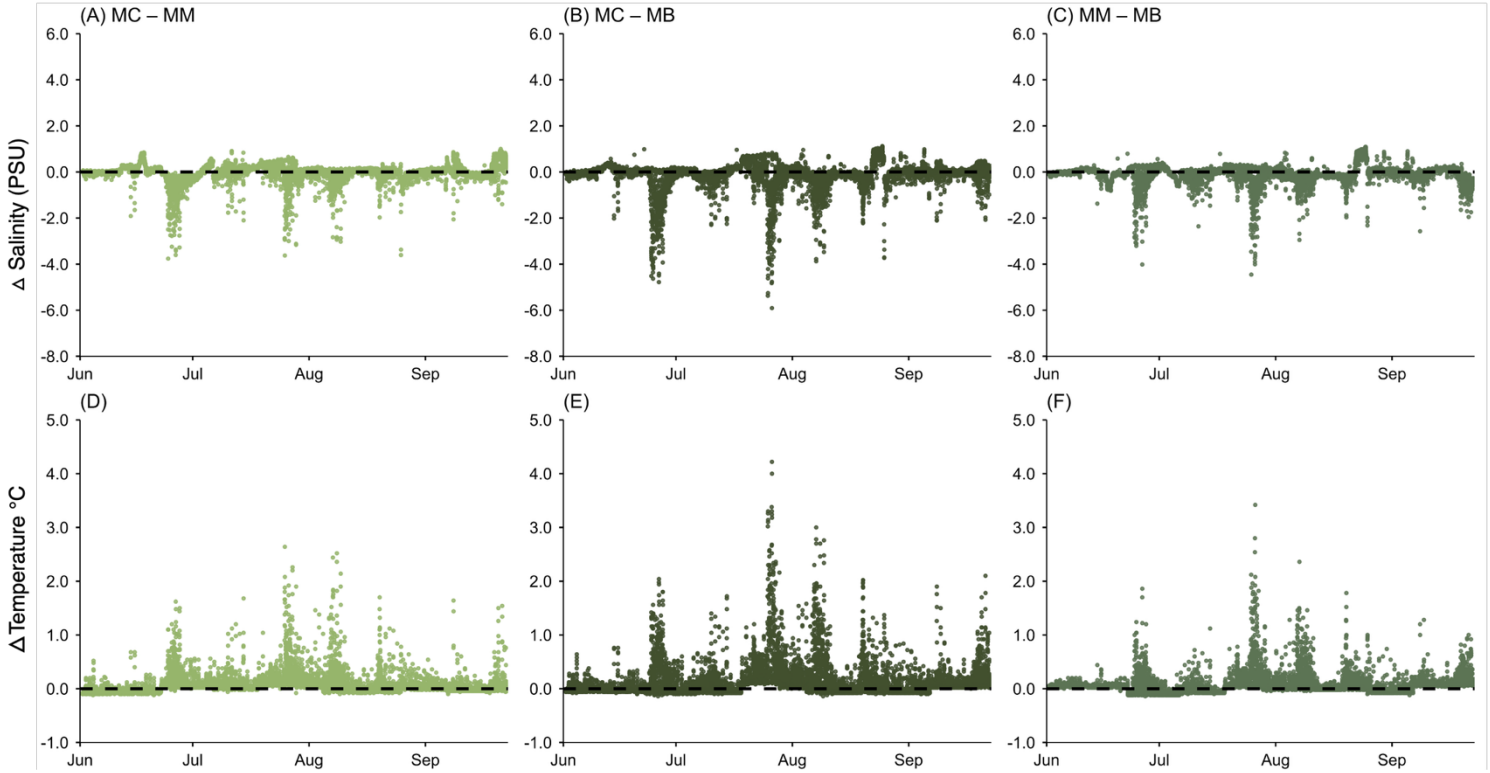

Figure S10. Time series of salinity and temperature differences (ΔSalinity, PSU; ΔTemperature, °C) among depth positions within the kelp canopy from June to September 2022. (A–C) Within-depth salinity differences: (A) Middle Canopy – Middle Mid-water (MC – MM; light green), (B) Middle Canopy – Middle Bottom (MC – MB; dark green), and (C) Middle Mid-water – Middle Bottom (MM – MB; medium green). (D–F) Corresponding temperature differences for the same depth comparisons. Positive values indicate higher salinity or temperature in the shallower (first-listed) habitat relative to the deeper one; dashed lines denote zero difference.

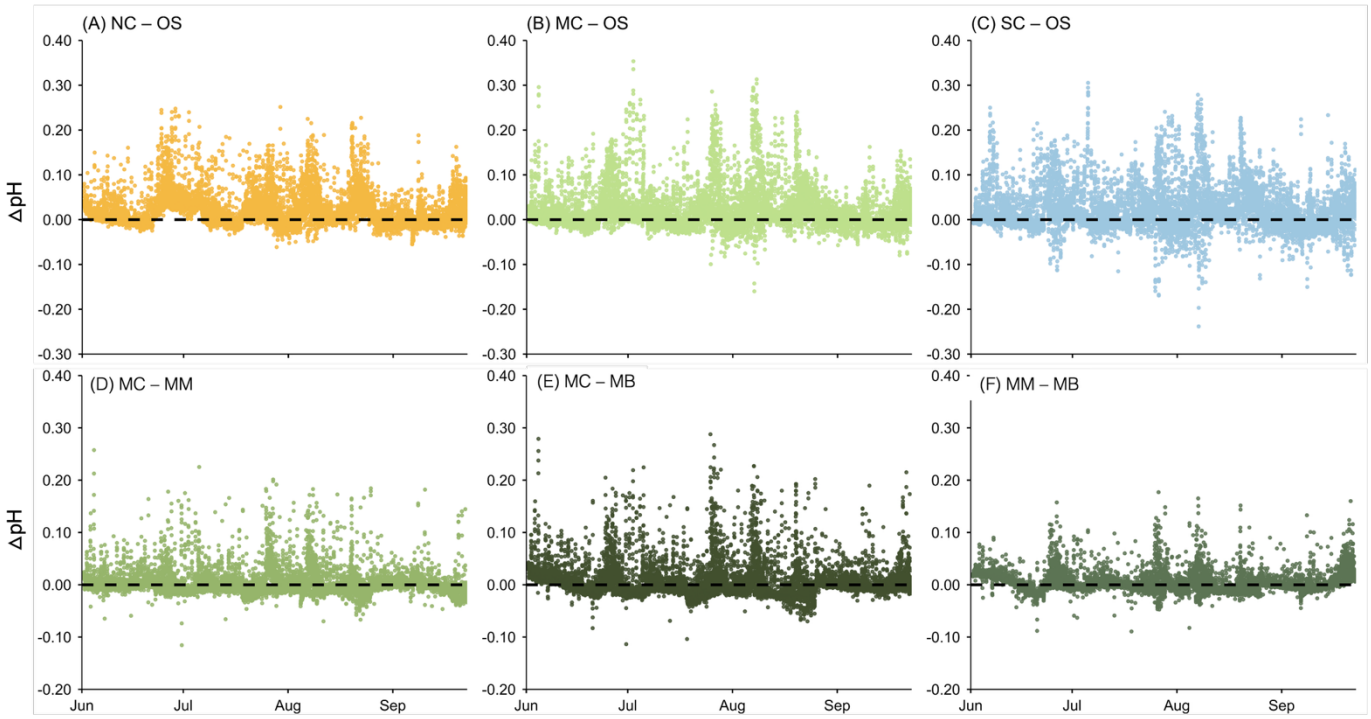

Figure S11. Time series of pH differences between select sensor locations from June to September 2022. (A–C) Inside versus outside of kelp bed deviations of three canopy sensors from a reference sensor outside the bed: (A) North Canopy – Outside Surface (NC – OS, yellow), (B) Middle Canopy – Outside Surface (MC – OS, medium green), and (C) South Canopy – Outside Surface (SC – OS, blue. (D–F) With depth comparisons all among the Middle Mooring sensor locations: (D) Middle Canopy – Middle Mid-water (MC – MM) light green, (E) Middle Canopy – Middle Bottom (MC – MB), dark green, and (F) Middle Mid-water – Middle Bottom (MM – MB), medium green. Positive values indicate higher pH in the first location listed relative to the second.

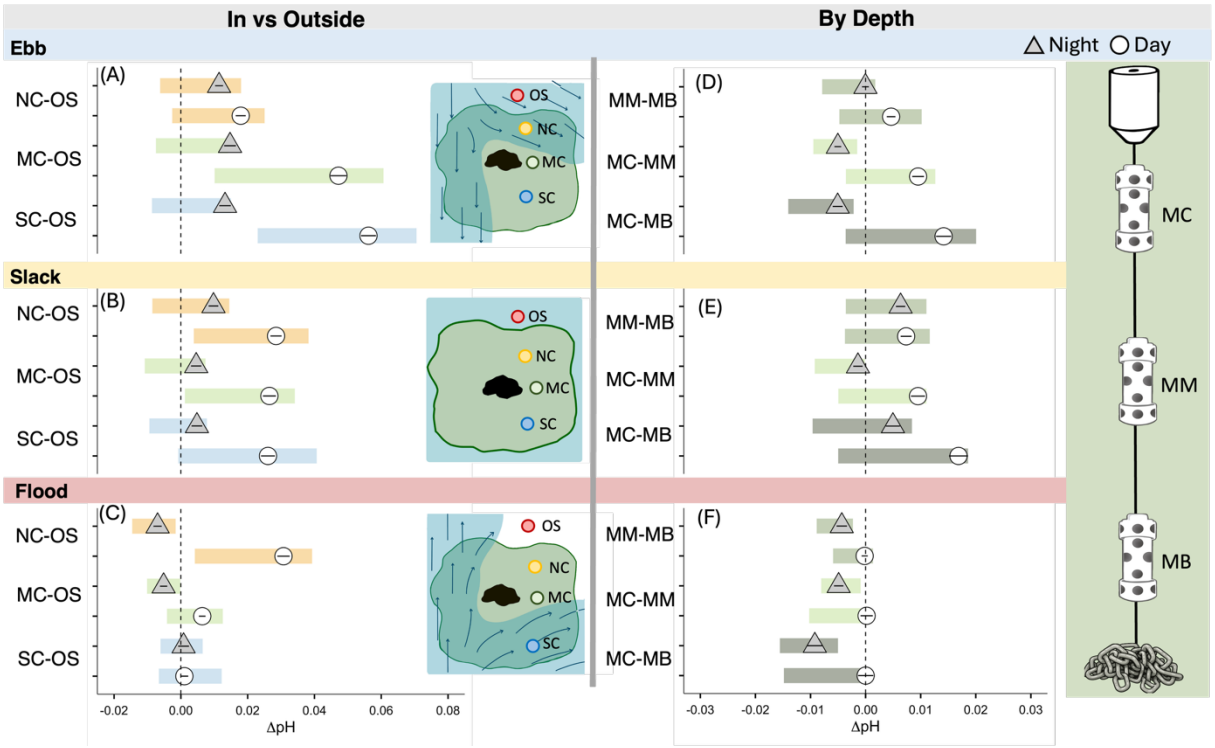

Figure S12. Summary of differences in pH (ΔpH) between paired sensor locations across diel and tidal conditions. ΔpH between sensors placed inside and outside the kelp canopy (A–C) and among depths on the middle mooring (D–F) are plotted separately for ebb (A, D), slack (B, E), and flood (C, F) tidal conditions. Symbols denote mean ΔDO during nighttime (grey triangles) and daytime (white circles) periods across a 17-week study, with black lines showing ± 95% confidence intervals around the mean. Shaded bars represent the 30–70th percentile range.. Inset graphics excerpted from Figure 1 illustrate (A–C) a conceptual birds-eye view of currents and surface sensors at Turn Rock during each tidal phase (Outside = red, North = yellow, Middle = green, South = blue) and (D–F) the middle mooring with sensor positions at different depths (Middle Canopy = MC, Middle Mid-water = MM, Middle Bottom = MB).

Supplementary Text

Sensor calibration details

All sensors were submerged for 2-3 days in each of two flow-through seawater reservoirs; one kept at a pH of 7.7 ± 0.04 and the other at a pH of 7.2 ± 0.03, using a Honeywell UDA2182 pH controller that dosed CO2 to maintain the desired pH levels. We used a HQ4300 Portable Multi-Meter (Hach) to measure pH, conductivity, temperature, salinity, and dissolved oxygen in the reservoirs.

We used discrete bottle samples from the laboratory reservoirs to convert the pH sensors to the total scale (Easley & Byrne, 2012). We measured spectrophotometric pH using a high-precision spectrophotometer (Ocean Optics Model USB 2000+) and unpurified m-cresol purple dye (Clayton & Byrne, 1993) at 25°C in a temperature-controlled water bath (Thermo Scientific NesLab RTE 17). This process resulted in a relationship between sensor mV and total scale pH twice per deployment. We validated our calibration for each pH sensor with internally prepared TRIS buffer; this revealed that the average deviation from actual pH was ±0.005 pH units. Total alkalinity (TA) for the discrete samples was determined by open cell titration on an auto-titrator (Mettler Toledo, DL15). We calibrated the acid concentration by analyzing Certified Reference Material (C.R.M.) from A. Dickson's laboratory (Batch# 127, 162, and 202), before each titration session (Dickson, A. G. 2010). Mean standard deviation of duplicate measurements during the study period was 9.17×10-5 (sd ± 2.15×10-5) mol kg^{-1} (n= 4 duplicates, per date samples were measured). We used the carbonate system software package (CO_2SYS), Version 2.1 for Microsoft Excel (Pierrot & Wallace, 2006), to calculate in situ pH values based on measured TA and in situ salinity and temperature measurements from the Hach meter in the calibration reservoirs.

Following bottle sample calibration for measurements taken in the lab, we cross-calibrated the sensors. For each deployment, co-located pH loggers in the laboratory reservoirs were compared to a designated reference sensor with linear regressions. This two-step approach, bottle-derived calibration of a single sensor followed by cross-sensor adjustment, ensured consistency among sensors while preserving real temporal variation in pH across each deployment.

We calibrated conductivity loggers by converting raw conductivity (µS/cm) and temperature to salinity using the swSCTp() function in oce R package (Dickson, A. G. 2010), and validated against discrete bottle samples taken before and after deployments in reservoir tanks. To correct for inter-sensor offsets, we used co-located deployments in lab reservoirs as described above for pH sensors to produce cross-calibrated salinity values for each deployment. Small offsets persisted after cross calibration but were minimal and their timing is consistent with tidally driven differences in water masses across sites (Mean offset = 1.05, sd= ± 0.6 PSU, n=8). We calculated a single salinity time series by averaging spline-smoothed time series collected at each sensor location. This allowed us to capture the underlying temporal trend in salinity at the site without assuming a constant mean (Fig. S8). We used this average salinity time series to correct the other loggers (e.g., for DO normalization) to minimize the risk that differences across sensor locations reflected calibration offsets rather than true spatial variability in salinity.

We calibrated the dissolved oxygen sensors according to the manufacturer's guidelines, using a one-point calibration at 100% saturation in air before and after deployments. We corrected dissolved oxygen (DO) concentrations for changes in salinity after deployment by first calculating temperature-specific percent saturation at 0 ppt and then recalculating DO in $\mu mol \cdot L^{-1}$ using the average cross-calibrated salinity, as calculated with the marelac R package (Garcia & Gordon, 1992; Dickson, 2010).

Once sensors were calibrated, we identified and corrected outliers in DO, pH, salinity, and temperature time series using an automated rolling regression approach that compared short-term (±50-point) relationships between paired variables (e.g., DO and pH, salinity and temperature) for each sensor location (OS, OB, MC, MM, MB, NC, SC). Data points that deviated beyond a set residual threshold from local regression fits were flagged as outliers. Flagged values were then reviewed and replaced using one of several interpolation methods, depending on context and best visual fit. Interpolations included linear interpolation (approx.) or regression-based estimates from correlated variables (lm predictions). This approach retained high-frequency structure while removing sensor noise and drift, ensuring internal consistency across all environmental variables prior to subsequent analyses.

Flow-induced gradients in seawater chemistry in mussel aggregations are not modulated by gaping behavior

Kindall Murie[1,2*], Luke P. Miller[3], Emily Carrington[1,2*]

[1]University of Washington, Department of Biology, Seattle, WA, United States

[2]University of Washington, Friday Harbor Laboratories, Friday Harbor, WA, United States

[3]Department of Biology, San Diego State University, 5500 Campanile Drive, San Diego, CA 92182, USA

Abstract

Ecosystem engineers reshape their local environments in ways that can have far-reaching ecological effects, yet the benefits or costs of these modifications depend on how biological traits interact with surrounding physical conditions. Mussels, as habitat-forming species, modify their surrounding chemical environment through respiration and calcification, altering both the water above and the interstitial spaces within aggregations. The extent of these chemical modifications is strongly dependent on flow: high flow flushes the interstitial spaces with bulk seawater, whereas low flow allows dissolved oxygen (DO) driven down by mussels' respiration to develop chemical gradients. Whether mussel behaviors, such as gaping and pumping, can further regulate these gradients remains unclear. We conducted laboratory flume experiments with three *Mytilus* species (*M. trossulus*, *M. galloprovincialis*, and *M. californianus*) to evaluate how flow speed and gaping behavior interact to influence interstitial seawater chemistry. Across all species, interstitial DO declined exponentially with flow, reflecting limited exchange with ambient seawater at speeds below ~5 cm s^{-1}. Apparent species-level differences in DO drawdown were largely explained by biomass density; once normalized by this functional trait, species showed similar oxygen depletion dependencies on flow. All species maintained high levels of gaping

(>90% time open) regardless of flow speed or DO conditions, with only subtle interspecific differences in mean gape distance and time spent open. Mussels also showed no evidence of synchrony in valve activity across individuals. Together, these results indicate that flow regime and mussel biomass density, rather than gaping behavior, dictate the magnitude of interstitial chemical gradients in mussel aggregations. This highlights the dominant role of physical hydrodynamics in shaping the engineering effects of mussel beds on seawater chemistry.

Introduction

Structure-forming species in marine environments often reduce water flow, trap particles, and alter light availability—reducing it through shading or increasing it through particle removal. These physical changes influence population and community dynamics, but the same organisms can also modify water chemistry through biological activity. Ecosystem engineers such as kelp, corals, and mussels transform relatively featureless habitats into complex three-dimensional structures that provide shelter and resources for diverse species (Jones 1994; Wernberg et al. 2024). Often, ecosystem engineers in marine ecosystems form dense aggregations that shape population and community dynamics by altering the physical environment at both macro- and micro-scales (Dayton 1972; Duarte 2017; Jones 1994; Ellison et al. 2005; Ellison 2019). At macro-scales, kelp forests and coral reefs can buffer waves and alter light regimes (Gaylord et al. 2007; Villanoy et al. 2012); at micro-scales, mussel beds trap sediment and alter nutrient dynamics (Christensen et al. 2003). While such physical modifications are well understood (Jones & Gutiérrez 2007), the chemical alterations these species produce are still not fully understood and remain an active area of research.

Recent anthropogenically-driven modifications to the chemical environment of marine ecosystems –specifically ocean acidification and deoxygenation– have motivated increased investigation into the ability of ecosystem engineers to modify their local chemical environment, and particularly their potential to ameliorate chemical stress. The capacity for ecosystem engineers to modify their surrounding chemical environment stems from their often dense and metabolically active biomass; biomass-dependent processes such as respiration, photosynthesis, and calcification can drive significant diel and seasonal fluctuations in dissolved oxygen (DO), pH, and nutrient levels (Waldbusser & Salisbury 2014; Lowe et al. 2019).

For example, autotrophic organisms like kelps and seagrasses can increase dissolved oxygen (DO) and pH levels during the day, creating spatial and temporal refuges for other organisms compared to ambient conditions, but these roles reverse when respiration dominates at night (Freider et al. 2012; Pfister et al. 2019; Hirsh et al. 2020; Murie & Bourdeau 2020). Heterotrophic species such as oysters and mussels can also decrease DO and pH levels through respiration, potentially intensifying hypoxic conditions (Nixon et al. 1971; Gutiérrez et al. 2003; George et al. 2019; Tomasetti et al. 2023).

To better understand the role of an ecosystem engineer in shaping its community—both physically and chemically—it is essential to consider how external environmental factors, such as flow, mediate its influence on the surrounding environment (Stachowicz 2001; Bruno et al. 2003; Wahl et al. 2018). In marine systems, flow regime is known to play a critical role by regulating water residence time and, consequently, the accumulation or dispersion of biologically modified water. For instance, in kelp forests, high-flow conditions can rapidly transport water away, limiting the buildup of metabolic byproducts, while low-flow conditions allow photosynthetically driven increases in dissolved oxygen (DO) and pH to accumulate locally

(Gaylord et al. 2012; Traiger et al. 2021). These patterns suggest that the capacity of ecosystem engineers to modify their environment depends not only on their biological activity but also on the hydrodynamic context in which they occur. Furthermore, because biogenic structure modifies the overlying flow regime (Reidenbach et al. 2010), the consequences for water chemistry in dense aggregations of ecosystem engineers must consider both their physical structure and their biological activity.

This study explores the physio-chemical conditions under which an ecosystem engineer facilitates or inhibits other organisms using a model system, Mytilid mussels (Carrington et al. 2015, Van der Schatte Olivier et al. 2020). Mytilids are prominent marine ecosystem engineers that dominate temperate rocky reefs worldwide as superior competitors for space (Suchanek 1978, Seed & Suchanek 1992, Lafferty & Suchanek 2016, Menge et al. 2008). Physically, mussels form dense aggregations (beds) that ameliorate harsh flow conditions and create intricate microhabitats within the interstitial spaces between individuals. This 'interstitial zone' can support upwards of 300 species (Suchanek 1979). Chemically, mussels can alter the water in and around the aggregation through respiration and calcification. During respiration, they consume oxygen (O_2) and release carbon dioxide (CO_2), leading to local decreases in dissolved oxygen (DO) and pH. For instance, George et al. (2019) found substantially lower DO and pH conditions within mussel aggregations relative to ambient conditions that persisted for up to five days during summer months. As mussels deposit calcium carbonate ($CaCO_3$) to build their shells, there can also be a reduction in total alkalinity (TA) and further decreases in pH by increasing CO_2 levels (Ninokawa et al. 2024). The extent to which harsh chemical conditions develop in the interstitial zone depends on how the physical structure of the mussel aggregation interacts with

external flow to regulate mixing between the interstitial spaces and the ambient environment (Nixon et al. 1971; Ninokawa et al. 2020; George et al. 2019).

Understanding how flow interacts with the biogenic structure of a mussel bed is key to explaining how chemical gradients develop within mussel aggregations (Fig 1). Horizontal flow encountering a bed is rerouted above the bed and speeds up, while flow within the bed is dampened to 0.1%–10% of the free-stream velocity (Carrington et al. 2008). This region of reduced flow within the bed represents a momentum boundary layer. Moreover, the interaction of the flow over rough mussel surfaces drives turbulent mixing between the interstitial zone and ambient water, resulting in a concentration boundary layer (Reidenbach et al. 2010). Laboratory experiments of Ninokawa et al. (2020) found flow speeds below 5 $cm \cdot s^{-1}$ create substantial concentration gradients within an aggregation of California mussels (*Mytilus californianus*), from ambient conditions. In this manner, seemingly benign, calm coastal conditions can be deadly; the combination of low flow for an ambient fluid with 'normal' DO and pH can cause a mussel aggregation to drive down interstitial, microscale DO and pH to levels that can harm itself as well as associated species. One aim of this study is to evaluate if there is interspecies variation in the flow threshold at which the role of a mussel aggregation in its community switches from facilitation (ameliorating a harsh flow environment) to inhibition (creating a harsh chemical environment).

Beyond the physical structure of a mussel aggregation, mussel behavior —particularly gaping and generating currents—may also shape how external flow creates chemical gradients within the interstitial zone. Mussels gape (relax adductor muscles to allow valves to passively separate) to enable a range of physiological processes, including feeding, broadcasting gametes, exchanging gasses (respiration) and releasing metabolites (e.g., ammonium). During feeding,

mussels draw water through an incurrent pseudo-siphon, pass it over ctenidia to remove particles, and expel it through an excurrent pseudo-siphon, enhancing mixing between interstitial and ambient waters (Fig 1B; Ward & Targett 1989; Howard & Cuffey 2006; Van Duren et al. 2006; Nishizaki & Ackerman 2017). Their efficient filter-feeding capabilities (up to 2.5 liters of water per hour) could promote mixing and homogenize chemical gradients particularly under low flow conditions (Riisgård et al. 2014; Crimaldi et al. 2007; Frechette 2012; Nishizaki & Ackerman 2017).

Valve gaping modulates current generation; maximum feeding occurs when mussels are fully open, while reduced gape limits flow through narrower interfilament canals (Jørgensen et al. 1988). It remains unclear, however, whether mussels adjust their gaping and pumping behavior in response to local physical and chemical conditions—either to enhance water exchange or to reduce exposure to unfavorable chemistry or physical conditions. For example, aggregated mussels in low-flow conditions may initiate pumping to improve their local chemical environment, effectively "stirring themselves out of trouble." In contrast, high-flow conditions may cause mussels to close ("clam up") and cease pumping and gas exchange altogether. Therefore, a second aim of this study is to evaluate how behavioral feedbacks shape water chemistry gradients within mussel aggregations across flow conditions, including reciprocal interactions between gaping, chemistry, and flow. Specifically, we measure gaping behavior using magnetic sensors that distinguish narrow openings, which restrict siphon extension, from wider gapes that support efficient pumping (Jou et al. 2013, Miller & Dowd 2017).

Gaping behavior has been quantified in various ways (Miller 2022), including percent of maximum gape (Miller & Dowd 2017; Bertolini et al. 2021), time spent open or closed (Dowd &

Somero 2013), frequency of gaping events (Kelleghan et al. 2023), and time-series analyses to examine rhythmic patterns (e.g., circadian or diel cycles) or synchrony across individuals (Bertolini et al. 2021; Miller & Dowd 2017; Ballesta-Artero et al. 2017). Each metric has the potential to provide distinct insights into how mussels influence local water chemistry in different flow conditions. For example, percent time spent open gives insight into when mussels exchange gases or metabolites with their environment, whereas gape distance relates to the pumping strength or mixing potential. Moreover, the degree of synchrony among individuals could influence the temporal variation in water chemistry - a high proportion of mussels closing could briefly alter water chemistry if the closures are simultaneous. Therefore, the third aim of this study is to evaluate which gaping metrics—percent time open, gape distance, and degree of synchrony— best reflect gaping behavior in different flow and water chemistry conditions.

We addressed our three aims by conducting a laboratory flume study to investigate the relationship between mussel gaping behavior and interstitial water chemistry (DO) under a range of flow speeds. We used the gape distance between shell valves as a proxy for pumping behavior because the latter is difficult to quantify in moving water and gaping has been shown to be positively correlated with feeding rates and water flow through the incurrent and excurrent pseudo-siphons (Jørgensen et al. 1988). We expect that low flow speeds will limit mixing between the interstitial zone and bulk flow, causing steeper gradients in water chemistry and more hypoxic conditions within the interstitial zone (Fig. 2). At higher flow speeds, interstitial water is more readily exchanged with the bulk flow, and chemical gradients will be weakened. We test three mechanisms by which mussels might adjust their gaping behavior in response to local water chemistry under a range of flow conditions. First, our null hypothesis is that gaping behavior is “static” and remains constant despite flow-mediated changes in water chemistry (no

feedback- Fig 2A). Our other two hypotheses involve compensatory behavior, where mussels sense and respond to unfavorable chemical environments at low flow to dampen the interstitial chemical gradient (Fig 2B). The mechanism for compensation may be driven by either "activation" or "inhibition" (H2a and H2b, respectively; Fig 2B). Activation involves increased gaping and pumping activity, which potentially enhances the mixing of interstitial water with the bulk flow. In contrast, inhibition involves reduced pumping activity as mussels "clam up" and close their valves in response to stressful chemical conditions at low flow speeds, preventing the continued exchange of metabolites. Both compensatory relationships represent feedback loops that allow mussels to modulate DO levels within the interstitial zone and shift the threshold flow speed below which unfavorable chemical conditions can develop.

We studied three congener mytilid mussels (*M. trossulus*, MT; *M. galloprovincialis*, MG; and *M. californianus*, MC) that are common on subtidal and intertidal shores of the Salish Sea and have well-characterized differences in ecology, physiology, and behavior (e.g., Harger 1967, Suchanek 1981, Braby & Somero 2006, Fly & Hilbish 2013, Dowd & Somero 2013). This approach allowed us to assess how differences among mussel species shape the extent and range of their ecological influence on local chemical environments. The first two species are common to shallow inland waters and embayments and are grown commercially, and *M. trossulus* has a higher metabolic rate and lower thermal tolerance (Tomanek & Zuzow 2010; Fly & Hilbish 2013). *M. californianus* is found in higher energy environments and has higher biomass per shell volume than the other two species (Bell & Gosline 2017). However, many physiological differences in mussels depend on season, reproduction cycle, and year (Suárez et al. 2005, Fly & Hilbish 2013). We expect stronger gradients in chemistry within the interstitial zone for species with higher metabolic rates and relative biomass . To reiterate the specific aims developed above,

the aims of this study are to: 1) quantify species-specific modification of DO across a range of water flow speeds; 2) evaluate the relationship between gaping behavior, flow, and interstitial water chemistry; and 3) assess different gaping metrics—percent time open, gape distance, and synchrony— as useful indicators of how mussel gaping behavior influences and responds to local water chemistry under varying flow conditions.

Methods

Overview of experimental plan

We address these aims by quantifying how flow speed affects mussel gaping behavior and water chemistry within the interstitial zone of a mussel aggregation using a large indoor recirculating flume (Rolling Hills Research Corporation, Model 1520 Water Tunnel; Fig. 3) at Friday Harbor Laboratories (FHL) in autumn 2023. We conducted three separate 10-day flow trials, each focusing on one *Mytilus* species at a time. Specific details of the experimental setup, measurement of DO and mussel gaping for each trial, and statistical analysis corresponding to each aim are described in the following sections. All statistical analyses were performed in R (version 4.5.2; R Core Team 2025).

Experimental setup

We sourced *M. trossulus* in late September 2023 and *M. galloprovincialis* in late November 2023 from Penn Cove Shellfish Farm (Coupeville, WA) and Taylor Shellfish Farm (Totten Inlet, WA), respectively. We collected *M. californianus* from the mid-intertidal zone at Cattle Point (San Juan Island, WA, 48.4505, -122.9670) in early November 2023. After removing epibionts, we held the mussels in flow-through seawater tables at 10–12°C to acclimate for 2–3

days before starting a trial in the flume. We selected mussels with undamaged shells of similar length (shell length ~60 mm, n = 500–1000;; Table 1).

For each trial, we assembled a single-species monolayer aggregation on a platform (100 × 36 × 2 cm, L × W × H) constructed from a 1.3 cm plexiglass sheet atop a 0.7 cm egg crate louver and placed it in the working section of the flume (152 × 38 × 51 cm; Fig 3). To prevent water from flowing underneath the platform, we installed a plexiglass ramp (13 × 36 × 2 cm) upstream. We then exposed each aggregation to a low flow (3 $cm \cdot s^{-1}$) overnight, allowing mussels to acclimate and reposition into a continuous layer without large gaps between individuals. During each trial, we subjected the aggregation to ten randomized flow treatments ranging from 1.5 to 30 $cm \cdot s^{-1}$, maintaining each speed for 24 hours to capture circadian rhythms in mussel gaping behavior (Miller & Dowd 2017; Bertolini et al. 2021). Flow moved unidirectionally across the mussel aggregation before recirculating as the flume operated as a semi-closed system, continuously flushing and cooling the 1520 L recirculating volume with ~2 $L \cdot min^{-1}$ of seawater from the FHL supply, which kept temperatures between 10–12°C across trials (Table 1). We placed air stones downstream of the aggregation to ensure ambient oxygen levels remained above 90% saturation throughout each trial. Salinity was monitored daily using a HQ4300 Portable Multi-Meter (HACH, CO-USA) and was steady at 28.5.

At the end of each trial, we counted the mussels in the aggregation and recorded mortality rates. We measured several morphometric parameters for a subset of mussels (all mussels with a gape sensor plus a random sample of 30 mussels, n = 46). Specifically, we measured mussel shell length (l), width (w), and height (h) to the nearest 0.1 mm using calipers, and dry weight (Table 1) of body tissue removed from the shell and dried to a constant weight for 72 hours at 65°C.

Mussel biomass density (g cm^{-2}) was calculated as dry weight per planform area, assuming an elliptical shape (for a vertically oriented mussel) with shell width and height as the major and minor axes, respectively (Bell and Gosline 1997). This functional trait of an individual mussel can be readily scaled up to whole bed biomass density (also in g cm^{-2}), a metric of interest to benthic ecologists, by multiplying by $\pi/4$ (the ratio of the area of an ellipse to its bounding rectangle). We tested for species-level variation in each morphometric parameter using a one-way ANOVA, followed by Tukey's HSD post hoc comparisons.

Aim 1: Species-specific modification of DO across a range of water flow speeds

We measured DO and conductivity at 1-minute intervals during each trial using HOBO loggers ((HOBO U26-001 and U24-002-C, respectively; Onset, MA-USA)) placed within (interstitial zone) and upstream of the mussel aggregation (Fig 3A). Loggers within the interstitial zone were affixed to the center of the plexiglass platform supporting the mussel aggregation, with the sensors collocated within 5 cm of each other. Before each species trial, we calibrated the sensors using the manufacturer's recommended methods and corrected any offset between loggers before analysis.

To characterize interstitial water chemistry for each flow treatment, we first exposed the mussel aggregation to high flow (35 cm s^{-1} for 15 minutes) to flush and equilibrate the interstitial seawater with ambient seawater, then applied a constant flow speed for 24 hrs. For each species trial, we randomized the order of the 24hr flow treatments. We calculated ΔDO (in $mg \cdot L^{-1}$) as the difference between the interstitial DO and ambient seawater for every minute (Fig. 4). We removed the first hour of measurements to allow the signal to achieve equilibrium, then averaged ΔDO for each hour (ΔDO_{eq} , n = 23 per flow treatment) to reduce autocorrection and non-

independence of ΔDO over time. To address aim one, we evaluated the relationship between ΔDO_{eq} and flow speed (U, in cm s^{-1}) for each species using a nonlinear least-squares regression (R package: nls). Specifically, we fit the exponential decay function , where *a* and *b* are tuning parameters. The parameter *a* represents ΔDO_{eq} at a speed of 0, and *b* describes the rate of exponential decay in ΔDO_{eq} with increasing flow speed. We conducted bootstrapping with 1,000 resamples to generate 95% confidence intervals for both *a* and *b* for each species. We then used biomass density to normalize ΔDO_{eq} for comparisons among species by scaling hourly averages of ΔDO_{eq} ($mg \cdot cm^2 \cdot gDW^{-1} \cdot L^{-1}$) for each species and evaluated its dependence on flow speed using the same nonlinear modeling approach.

Aim 2 & 3: Gaping behavior, flow, and interstitial water chemistry using different gaping metrics

We measured mussel gaping behavior using gape sensors composed of magnetic Hall Effect sensors (Allegro Microsystems A1393, Worcester, MA, USA) and a circular magnet (part number 8195-Radial Magnet Inc. Boca Raton FL). We attached the gape sensor to the posterior end of one valve and the circular magnet to the opposite valve using marine epoxy (Splash Zone, KOP-COAT Inc., Rockaway, NJ, USA). We sampled gape sensor output of the distance between the valves every 5 seconds, a sampling rate our preliminary observations determined to be sufficient to characterize gape behavior dynamics. We equipped a total of 16 mussels with gape sensors for each species trial, each spaced more than ten mussel body lengths apart to prevent sensor interference.

The gape sensors were continuously monitored during each trial using a MusselTracker datalogging system (Miller and Dowd 2017) (Fig 3A & B). We bundled and routed the gape sensor wires downstream using the gap between the bottom of the flume and the plexiglass plate,

minimizing disturbances to the bulk flow above the mussel aggregation. At the end of each trial, we calibrated each gape sensor by severing the mussel's adductor muscle and using calipers to set valve gapes from 0 to 20 mm at 1 mm intervals while measuring the sensor's voltage output. We then fit an exponential function to the data to estimate gape (mm) from voltage output for each sensor (resolution of each gape sensor was < 0.1 mm). Gaping behavior was assessed using the following three metrics.

The first interaction we looked at was the effect of flow on the proportion of time spent open for each of the three species. We calculated the hourly average proportion of time valves stayed open (> 0.5 mm) for each mussel in each flow treatment. We then calculated the mean of these hourly values for all mussels (n=16) in the flow treatment. We then used a Generalized Linear Model (R Package: glm) to evaluate the relationship between the proportion of time mussels spent gaping and flow speed for each *Mytilus* species (Brooks et al. 2017). We included flow speed as a continuous fixed factor and species as a categorical fixed factor and applied a gamma distribution with a log link function because our data was positive and right-skewed (Bolker et al. 2009). We identified the best-fit models using Akaike's Information Criterion (AIC) and used log-likelihood ratio tests to evaluate whether including additional fixed effects significantly improved model fit compared to the null model and simpler alternatives.

Second, we quantified the variation in gape distance during a flow treatment, averaging across all mussels (n=16). We used Model II standardized major axis (SMA) regression to evaluate the relationship between hourly averages of gape distance and ΔDO_{eq} with flow speed as a continuous covariate. We log-transformed hourly-averaged gape distance and ΔDO_{eq} to meet the assumptions of normality. We ran separate models for each mussel species and used 95%

confidence intervals around slope estimates to evaluate significance and identify differences across flow speeds.

Third, we quantified the level of synchrony in mussel gaping behavior in two ways: (1) by calculating the proportion of mussels open over time, and (2) by quantifying the degree of coordination in gape distance across individuals using pairwise correlation matrices. For the latter, we computed Pearson correlation coefficients (based on the R stats package) on continuous gape distance time series between all mussel pairs at each flow speed. We then calculated the average absolute pairwise correlation (|r|) for each flow speed treatment and used one-way ANOVA followed by Tukey's HSD post hoc tests to assess the effect of flow speed on synchrony for each species.

Results

Experimental parameters and mussel morphometrics

The monolayered aggregations of each species were similar in area but differed in the total number of mussels due to differences in shell size (Table 1 & Table S1, ANOVA). *M. trossulus* had the smallest shell dimensions on average—roughly 10–30% smaller in length, height, and width compared to the other species—which allowed for nearly double the number of individuals to be packed into the 0.5 m^2 aggregation relative to *M. californianus*, and ~30% more than *M. galloprovincialis*. Despite its smaller shell size, *M. trossulus* had a relatively high dry weight, second only to *M. californianus*, and nearly 50% greater than *M. galloprovincialis*. As a result, mussels used in the *M. trossulus* aggregation had the highest biomass density, nearly twice that of *M. galloprovincialis* and *M. californianus* aggregations. (Table 1, ANOVA: Biomass density: $P < 0.0001$;).

Aim 1: Species-specific modification of DO across a range of water flow speeds

At the start of each flow treatment, mussel respiration rapidly reduces interstitial DO relative to ambient levels, creating a distinct difference that stabilizes over time (ΔDO_{eq}; Fig 4). This difference is most pronounced at low flow speeds and diminishes with increasing flow, becoming minimal or negligible at the highest speeds (Fig5A, Fig 6A, C). The magnitude of interstitial DO depletion depended on species and flow speed and was well characterized by an exponential decay model (Table 2). Among species, *M. trossulus* had the greatest variability or range in ΔDO_{eq} dynamics (SE = 0.12), particularly at low flow speeds. All species had significantly lower interstitial DO_{eq} than ambient seawater at flow speeds below ~5 cm s^{-1}. The estimate for tuning parameter *a* was approximately twice as high as *M. galloprovincialis* and 3.8 times higher than *M. californianus* (Table 2; Fig 6A). These trends should be interpreted cautiously due to overlapping confidence intervals.

However, these species also differed significantly in biomass density (Table 1; Fig 6B), with *M. trossulus* having approximately double the biomass within the experimental beds than *M. galloprovincialis* and *M. californianus*. Normalizing ΔDO_{eq} by biomass density (Fig 6C), species-specific differences were substantially reduced. The two bay mussels, *M. trossulus* and *M. galloprovincialis*, showed nearly identical relationships between biomass-normalized ΔDO_{eq} and flow speed with estimates of the tuning parameter *a* ranging 7-8 mg DO $\cdot$ cm^2 $\cdot$ $g_{DW}{}^{-1}$ $\cdot$ L^{-1}. In contrast, the drawdown capacity for *M. californianus* remained low (*a* = 3 mg DO $\cdot$ cm^2 $\cdot$ $g_{DW}{}^{-1}$ $\cdot$ L^{-1}) but still showed overlapping confidence intervals (not significantly different) across both tuning parameters compared to *M. trossulus* and *M. galloprovincialis* (Table 2).

Aim 2 & 3: Gaping behavior, flow, and interstitial water chemistry using different gaping metrics

All three species remained open for over 90% of the 23-hour observation period, but there were subtle but significant differences in their baseline gaping behavior ($P < 0.0001$; Fig 5B). *M. californianus* gaped the most consistently with 98% of its time spent open, followed by *M. galloprovincialis* (93%), while *M. trossulus* exhibited the least amount of time open at 90%. *M. trossulus* also showed the highest variability among individuals across flow speeds. Incorporating flow speed and its interaction with species into the model did not improve fit (LRT, $P = 0.62$, Table 3), indicating that flow had no detectable influence on the first gaping behavior metric we used (average proportion of time mussels remained open). This lack of flow dependence is evident in figure 5B, where the species-specific dashed lines (model predictions) remain relatively flat across flow speeds. Notably, individual-level variation (indicated by small, shaded triangles) was more pronounced in *M. trossulus*, consistent with its greater standard deviation. Together, these results suggest that while species identity is a strong predictor of gaping activity, mussels maintain high levels of gaping irrespective of flow speed.

Based on the second metric for gape behavior, *M. galloprovincialis* and *M. trossulus* exhibited a similar range of gape distances across flow treatments (~4-7 mm), compared to *M. californianus* (~2-4 mm; Fig 7 A-C). An increase in gaping distance around midnight was evident for *M. trossulus*, and at the outset of each flow treatment for *M. californianus.* Gape distance was most variable for *M. galloprovincialis* and no trends with flow speed or hour of day were evident. To evaluate the three-way interaction of ΔDO_{eq}, gape distance, and flow speed, Model II regressions revealed that the correlation between ΔDO_{eq} and gape distance depended

significantly on flow speed for all three mussel species (Fig 7D–F, Table S2). Most notable are the trends at the lowest flow speed (1.5 cm s^{-1}) where variation in ΔDO_{eq} is highest, and gape distance was positively related to ΔDO for *M. trossulus* and *M. galloprovincialis* but negatively for *M. californianus*. While these slopes are significant, they account for only 17-39% of the observed variation in gape distance. At flow speeds above 1.5 cm s^{-1}, patterns diverged among species, *M. trossulus* showed additional significant positive associations between gape distance and ΔDO at 4.5, 20, 25, and 30 cm s^{-1}, with relatively high explanatory power (e.g., $R^2 = 0.37$ at 4.5 cm s^{-1} and $R^2 = 0.41$ at 25 cm s^{-1}). *M. galloprovincialis* had significant responses only at 15 and 30 cm s^{-1} ($R^2 = 0.41$ and 0.20, respectively), while *M. californianus* showed significant positive slopes at 6 and 12 cm·s^{-1}, with moderate explanatory power ($R^2 = 0.21$ and 0.46, respectively). Many of the slope estimates, while statistically significant, are derived from a very narrow range of ΔDO_{eq} and should be interpreted with caution.

The mean proportion of mussels open was consistently high across all flow speeds and rarely dropped below 100% for *M. galloprovincialis and M. californianus. M. trossulus* had the most numerous events, where a small proportion of the mussels with gape sensors closed (~ 25%-Fig S1). Similarly, pairwise comparisons of gaping distance revealed consistently low synchrony across individuals for all three mussel species (Fig S2). Across all flow speeds, average absolute correlations between individual mussels remained below 0.5, suggesting weak coordination in valve activity. One-way ANOVAs (Table S3) showed that flow speed had a significant effect on mean pairwise correlation for each species (*M. trossulus*: $p = 0.0003$; *M. galloprovincialis* and *M. californianus*: $p < 0.0001$). However, post hoc comparisons revealed that only a subset of speed comparisons exhibited significant differences in correlation values.

There was no consistent pattern in which flow speeds produced significant pairwise differences across the three species (Table S3).

Discussion

These results suggest that apparent species-specific differences in oxygen depletion were largely driven by variation in mussel biomass, and once normalized, the per-unit biomass effect of flow on ΔDO_{eq} was comparable across all three species (Aim 1). The absence of compensatory gaping across flow and low-DO conditions indicates limited behavioral feedback between gaping, chemistry, and flow (Aim 2). Finally, the static nature of gaping behavior implies that different gaping metrics—percent time open, gape distance, and synchrony - explained little of the variation seen in DO under the flow regimes tested (Aim 3).

Across all three *Mytilus* species, two consistent patterns emerged: (1) ΔDOeq (ambient – interstitial) decreased exponentially with increasing flow speed, and (2) gaping behavior remained static across flow conditions, even at low flow speeds when ΔDOeq was highest, showing no evidence of compensatory behavior. Thus, the null hypothesis of static gaping (H1) was supported (Fig. 2A). At low flow speeds (<5 $cm \cdot s^{-1}$), reduced water exchange between the mussel bed and the mainstream limits oxygen replenishment within the bed, allowing mussel metabolic activity to become the dominant driver of oxygen depletion in the interstitial zone. At higher flow speeds, reoxygenated water rapidly replaced oxygen-depleted water within the bed, bringing interstitial DO levels closer to ambient conditions. Initial assessment of ΔDOeq revealed species-specific differences at flow speeds below 5 $cm \cdot s^{-1}$, with *M. trossulus* differing from both *M. galloprovincialis* and *M. californianus*. These patterns align with findings by Ninokawa et al. (2020), who observed strong ambient–interstitial DO differences at flow speeds

below 5 $cm \cdot s^{-1}$ (e.g., ΔDO of ~0.7 mg L^{-1} at 0 $cm \cdot s^{-1}$ in *M. californianus*). Although measured at a different flow speed, our observed ΔDOeq of ~0.5 mg L^{-1} at 1.5 $cm \cdot s^{-1}$ is comparable in magnitude. However, after accounting for differences in mussel biomass density between species, this trend disappeared. The numerical dominance of ecosystem engineers likely increases the spatial extent of their environmental modification (Albertson et al. 2024). In fact, many ecosystem engineers would not be recognized as such without their substantial biomass, which is why many ecosystem engineers are also foundation species (Dayton, 1972). Our study underscores the importance of considering the biomass density as a key functional trait of ecosystem engineers when evaluating their capacity to modify local chemical conditions. By normalizing ΔDO_{eq} by mussel biomass density, we reduced differences in ΔDO_{eq} for the two bay mussel species, *M. trossulus* and *M. galloprovincialis*, which share many similarities in size, shape and physiology. The lower values for *M. californianus* may reflect low metabolic activity at our test temperature. Overall, the lack of significant differences in oxygen drawdown among species suggests a shared capacity for driving flow-mediated changes in interstitial chemistry. Additionally, our findings are one of the few that support previous research indicating a strong correlation between biomass and respiration-driven chemical gradients created by ecosystem engineers (Hendriks et al., 2014; George et al., 2019).

Our study indicates that mussel gaping behavior remains relatively consistent across flow conditions, reinforcing the dominant role of external flow in shaping chemical gradients within monolayer mussel aggregations. While we detected statistically significant differences in the proportion of time spent gaping among species, all three mussels remained open for the vast majority of the time (>90%), and small differences (e.g., MT: 90% vs. MC:98%) are unlikely to meaningfully alter interstitial DO dynamics at the bed scale. This prolonged gaping behavior

aligns with previous findings from aquaculture settings, where mussels were reported to gape continuously over extended periods (~97.5% time open across 10 days; Comeau et al. 2018).

Unlike ΔDO_{eq}, which showed a greater range in ΔDO low flow speeds, the proportion of time gaping did not follow a consistent trend with flow. *M. trossulus* and *M. galloprovincialis* both exhibited higher variation in gaping behavior across flow speeds, suggesting individual-level flexibility, while *M. californianus* remained more uniform, gaping consistently at high levels regardless of flow.

It is possible that the magnitude of ΔDO_{eq} observed for each species was not sufficient to trigger a strong closing response, as all mussel beds in this study were arranged in a monolayer and our experimental design maintained high ambient DO levels. In natural settings, mussel beds often form multiple layers, which can exacerbate chemical gradients—particularly under low-flow conditions that may lead to hypoxia. Under such conditions, mussels may exhibit a more extreme gaping response, functioning like an "on-off switch," where individuals close for prolonged periods to avoid physiologically stressful conditions. Monolayer beds may lack the biomass density necessary to induce sufficiently steep declines in DO to elicit this kind of stress response (Tran et al., 2003; Tran et al., 2004). Prolonged closure is widely recognized as a sign of distress in mussels, commonly observed in response to extreme environmental conditions such as pollutant exposure. Consequently, changes in gaping behavior may be an effective early warning signal in aquaculture and environmental monitoring contexts, where DO levels can be more extreme than in our flume study (Shakespeare et al., 2023; Durier et al., 2022).

In addition to species-specific differences in time spent gaping, we also observed differences in gape distance across species: *M. galloprovincialis* generally maintained the widest gape, followed by *M. trossulus*, with *M. californianus* exhibiting the narrowest. Despite these interspecific differences, gape distance remained relatively stable across all flow speeds and followed no distinct pattern with flow (e.g., we did not see wider gapes at lower flow speeds) (Fig 7A-C). Previous studies have linked gape distance to pumping behavior within a single species of *Mytilus*, with wider openings associated with increased active pumping rates (Jørgensen et al., 1988). However, we did not observe evidence of this relationship in our study. If gape distance were directly related to pumping intensity, we would expect *M. trossulus* and *M. galloprovincialis*—with their wider gapes—to exhibit greater mixing and thus lower ΔDO_{eq} levels. Instead, both species produced the highest ΔDO_{eq} rates. One possible explanation for this discrepancy is that gaping may support two distinct feeding modes: active pumping (which promotes mixing) and passive feeding (in which mussels remain open but rely on ambient flow for particle delivery; Howard & Cuffey, 2006; Van Duren et al., 2006; Nishizaki & Ackerman, 2017). This dual functionality complicates the interpretation of how gaping behavior alone modulates changes in interstitial chemistry. It does not rule out that there is no relationship between gaping distance and pumping, but it is not something we can address with this study.

We observed some significant positive relationships between ΔDO and gape distance, with larger changes in dissolved oxygen corresponding to wider gapes—but only at certain flow speeds (Fig 7 D-F). Interestingly, both bay mussels (*M. trossulus* and *M. galloprovincialis*) showed positive slopes, while *M. californianus* exhibited a significant negative relationship. This may reflect stress-induced valve narrowing in *M. californianus*, a species adapted to high-flow environments, when exposed to unnaturally low flow conditions. However, despite these

statistically significant relationships and interspecific differences, the overall range of ΔDO observed in the experiment was small (~ 0 to <2 mg L^{-1}), particularly at higher flow speeds. This limited variation constrains the biological relevance of the patterns observed.

Minimal changes in DO could also explain the consistency in gaping behavior across individuals. Because mussels were not stressed by the ΔDO or flow speeds, they spent over 90% of their time open, making it difficult to detect synchrony in valve-closing behavior between individuals. Moreover, the ~10% of the time mussels were closed during a given flow treatment was distributed asynchronously; the proportion of mussels open never dropped below 75%. Other studies of mussel gaping behavior have demonstrated that mussels often exhibit synchrony across individuals in response to environmental cycles—especially tidal rhythms in intertidal species (Miller & Dowd, 2017), and effect of light, food, or temperature (Bertolini et al., 2021, Ballesta-Artero et al., 2017). However, Miller & Dowd (2017) also highlight that, even within synchronized patterns, mussels can show persistent inter-individual differences based on past environmental conditions.

It is also important to consider bed architecture when assessing how mussel aggregations modify interstitial chemistry relative to the surrounding water. Mussels frequently self-organize into clumps—"clustering"—by attaching their byssal threads to nearby conspecifics (van de Koppel et al., 2008). Although clustering is usually interpreted as a defense against dislodgement or predation (Bertness & Grosholz, 1985), it may also help prevent hypoxia: water sweeping around a clump can penetrate the bed from several sides rather than solely from above, thereby deepening the mixing layer (δ_e) and enhancing exchange between porewater and the ambient flow. Despite our efforts to maintain a gap-free monolayer, some individuals re-positioned themselves, producing irregular surface topography that likely altered flow–bed interactions.

Notably, clustering occurred only in *M. galloprovincialis* and *M. californianus*; the absence of this behavior in *M. trossulus* may explain why it exhibited slightly higher ΔDOeq values at low speeds.

Our findings contribute to a broader understanding of how ecosystem engineers influence their local environment by demonstrating the interplay between physical flow and organismal behavior in shaping chemical gradients. By demonstrating that mussel gaping behavior remains relatively static across flow conditions, our findings highlight the dominant role of physical flow in shaping interstitial DO dynamics within monolayer mussel beds. This research also underscores the importance of considering biomass density as a key functional trait that, along with flow, mediates the balance between biological activity and physical transport processes. Understanding how environmental factors such as flow speed can shape an engineer's role will be key to predicting how these species influence ecosystem function under changing conditions. Future research should focus on identifying the relative contributions of the factors that make ecosystem engineers effective at modifying their surrounding environment, including the abundance of the engineer and species-specific traits that contribute to the physical structure of the biogenic habitat. By addressing these questions, we can better predict when and where ecosystem engineers will act as facilitators, enhancing habitat complexity and resource availability, or as inhibitors, potentially intensifying stressors in their environment.

Acknowledgements

Lauren Strope and other Miller Lab members provided expert help and guidance in developing the gape sensor system. Thank you, Lara Hsia, Grace Leuchtenberger, Ava Martin, and Eleanor Rollins for assisting with gape sensor construction. Penn Cove Shellfish LLC supplied mussels, and Mike Nishizaki assisted with field collections. The staff at UW Friday Harbor Laboratories offered timely logistical support. Jack Litle, Grace Leuchtenberger, Alli Cramer, Matt Reidenbach and Kelsey O'Donnell gave helpful feedback throughout the research process, and Jennifer Ruesink and Tom Daniel improved the manuscript with their comments.

Author contributions

EC and KM led the conceptual development of the study. KM designed the methodology, curated and analyzed the data, produced all graphical visualizations, drafted the original manuscript, addressed co-authors' revisions, and helped secure project funding. LM assisted with the gape sensor and the construction of mussel-tracking boards and participated in manuscript review and editing. EC provided additional methodological support, contributed to manuscript review and editing, and secured project funding.

Funding

The author(s) declare that financial support was received for the research, authorship, and/or publication of this article. All aspects of the research were supported by the National Science Foundation (OCE-2050273 awarded to EC) and GRF awarded to KM. Funding for chemical sensors and computers was provided by University of Washington Student Technology Fee (STF: 2021-33, awarded to EC and KM). KM received funding for laboratory space, housing, travel, and logistical support from UW Friday Harbor Laboratories via the Frederic H. and Kristin C. Nichols Endowed Graduate Fellowship, Emily Carrington Endowed Student Travel Support Fund, and University of Washington Biology Department awards via Friday Harbor Laboratories Award and Hoag Award. Additional stipend support for KM was awarded to EC from the University of Washington College of Arts and Sciences.

References

Albertson, L. K., Sklar, L. S., Tumolo, B. B., Cross, W. F., Collins, S. F., & Woods, H. A. (2024). The ghosts of ecosystem engineers: Legacy effects of biogenic modifications. *Functional Ecology, 38*(1), 52–72.

Ballesta-Artero, I., Witbaard, R., Carroll, M. L., & van der Meer, J. (2017). Environmental factors regulating gaping activity of the bivalve *Arctica islandica* in Northern Norway. *Marine Biology, 164*, 1–15.

Bell, E. C., & Gosline, J. M. (1997). Strategies for life in flow: Tenacity, morphometry, and probability of dislodgment of two *Mytilus* species. *Marine Ecology Progress Series, 159*, 197–208.

Bertness, M. D., & Grosholz, E. (1985). Population dynamics of the ribbed mussel, *Geukensia demissa*: The costs and benefits of an aggregated distribution. *Oecologia, 67*(2), 192–204.

Bertolini, C., Rubinetti, S., Umgiesser, G., Witbaard, R., Bouma, T. J., Rubino, A., & Pastres, R. (2021). How to cope in heterogeneous coastal environments: Spatio-temporally endogenous circadian rhythm of valve gaping by mussels. *Science of the Total Environment, 768*, 145085.

Braby, C. E., & Somero, G. N. (2006). Ecological gradients and relative abundance of native (*Mytilus trossulus*) and invasive (*Mytilus galloprovincialis*) blue mussels in the California hybrid zone. *Marine Biology, 148*, 1249–1262.

Bolker, B. M., Brooks, M. E., Clark, C. J., Geange, S. W., Poulsen, J. R., Stevens, M. H. H., & White, J. S. S. (2009). Generalized linear mixed models: A practical guide for ecology and evolution. *Trends in Ecology & Evolution, 24*(3), 127–135.

Brooks, M. E., Kristensen, K., Van Benthem, K. J., Magnusson, A., Berg, C. W., Nielsen, A., … & Bolker, B. M. (2017). glmmTMB balances speed and flexibility among packages for zero-inflated generalized linear mixed modeling. *The R Journal, 9*(2), 378–400.

Bruno, J. F., Stachowicz, J. J., & Bertness, M. D. (2003). Inclusion of facilitation into ecological theory. *Trends in Ecology & Evolution, 18*(3), 119–125.

Carrington, E., Moeser, G. M., Thompson, S. B., Coutts, L. C., & Craig, C. A. (2008). Mussel attachment on rocky shores: The effect of flow on byssus production. *Integrative and Comparative Biology, 48*(6), 801–807.

Carrington, E., Waite, J. H., Sara, G., & Sebens, K. P. (2015). Mussels as a model system for integrative ecomechanics. *Annual Review of Marine Science, 7*(1), 443–469.

Christensen, P. B., Glud, R. N., Dalsgaard, T., & Gillespie, P. (2003). Impacts of longline mussel farming on oxygen and nitrogen dynamics and biological communities of coastal sediments. *Aquaculture, 218*(1–4), 567–588.

Crimaldi, J. P., Koseff, J. R., & Monismith, S. G. (2007). Structure of mass and momentum fields over a model aggregation of benthic filter feeders. *Biogeosciences, 4*(3), 269–282.

Dayton, P. K. (1972). Toward an understanding of community resilience and the potential effects of enrichments to the benthos at McMurdo Sound, Antarctica. In *Proceedings of the Colloquium on Conservation Problems in Antarctica* (pp. 81–96).

Duarte, C. M. (2017). Reviews and syntheses: Hidden forests—the role of vegetated coastal habitats in the ocean carbon budget. *Biogeosciences, 14*(2), 301–310.

Durier, G., Nadalini, J. B., Comeau, L. A., Starr, M., Michaud, S., Tran, D., … & Tremblay, R. (2022). Use of valvometry as an alert tool to signal the presence of toxic algae *Alexandrium catenella* by *Mytilus edulis*. *Frontiers in Marine Science, 9*, 987872.

Dowd, W. W., & Somero, G. N. (2013). Behavior and survival of *Mytilus* congeners following episodes of elevated body temperature in air and seawater. *Journal of Experimental Biology, 216*(3), 502–514.

Ellison, A. M., Bank, M. S., Clinton, B. D., Colburn, E. A., Elliott, K., Ford, C. R., … & Webster, J. R. (2005). Loss of foundation species: Consequences for the structure and dynamics of forested ecosystems. *Frontiers in Ecology and the Environment, 3*(9), 479–486.

Ellison, A.M. (2019). Foundation species, non-trophic interactions, and the value of being common. *iScience, 13*, 254–268.

Fly, E. K., & Hilbish, T. J. (2013). Physiological energetics and biogeographic range limits of three congeneric mussel species. *Oecologia, 172*, 35–46.

Fréchette, M. (2012). A model of clearance rate regulation in mussels. *Journal of Sea Research, 73*, 32–40.

Frieder, C. A., Nam, S. H., Martz, T. R., & Levin, L. A. (2012). High temporal and spatial variability of dissolved oxygen and pH in a nearshore California kelp forest. *Biogeosciences, 9*(10), 3917–3930.

Gaylord, B., Rosman, J. H., Reed, D. C., Koseff, J. R., Fram, J., MacIntyre, S., … & Mardian, B. (2007). Spatial patterns of flow and their modification within and around a giant kelp forest. *Limnology and Oceanography, 52*(5), 1838–1852.

Gaylord, B., Nickols, K. J., & Jurgens, L. (2012). Roles of transport and mixing processes in kelp forest ecology. *Journal of Experimental Biology, 215*(6), 997–1007.

George, M. N., Andino, J., Huie, J., & Carrington, E. (2019). Microscale pH and dissolved oxygen fluctuations within mussel aggregations and their implications for mussel attachment and raft aquaculture. *Journal of Shellfish Research, 38*(3), 795–809.

Gutiérrez, J. L., Jones, C. G., Strayer, D. L., & Iribarne, O. O. (2003). Mollusks as ecosystem engineers: The role of shell production in aquatic habitats. *Oikos, 101*(1), 79–90.

Harger, J. R. E. (1967). *Population studies on Mytilus communities* (Doctoral dissertation). University of California, Santa Barbara.

Hendriks, I. E., Olsen, Y. S., Ramajo, L., Basso, L., Steckbauer, A., Moore, T. S., … & Duarte, C. M. (2014). Photosynthetic activity buffers ocean acidification in seagrass meadows. *Biogeosciences, 11*(2), 333–346.

Hirsh, H. K., Nickols, K. J., Takeshita, Y., Traiger, S. B., Mucciarone, D. A., Monismith, S., & Dunbar, R. B. (2020). Drivers of biogeochemical variability in a central California kelp forest. *Journal of Geophysical Research: Oceans, 125*(11), e2020JC016270.

Howard, J. K., & Cuffey, K. M. (2006). The functional role of native freshwater mussels in the fluvial benthic environment. *Freshwater Biology, 51*(3), 460–474.

Jones, C. G., Lawton, J. H., & Shachak, M. (1994). Organisms as ecosystem engineers. *Ecosystem Management* (pp. 130–147). Springer, New York, NY.

Jones, C. G., & Gutiérrez, J. L. (2007). On the purpose, meaning, and usage of the physical ecosystem engineering concept. *Ecosystem Engineers: Plants to Protists* (Vol. 4, pp. 3–20). Elsevier.

Jørgensen, C. B., Larsen, P. S., Møhlenberg, F., & Riisgård, H. U. (1988). The mussel pump: Properties and modelling. *Marine Ecology Progress Series, 205–216.*

Jou, L. J., Lin, S. C., Chen, B. C., Chen, W. Y., & Liao, C. M. (2013). Synthesis and measurement of valve activities by an improved online clam-based behavioral monitoring system. *Computers and Electronics in Agriculture, 90*, 106–118.

Kelleghan, D. B., O'Callaghan, L., Huggard, F., Crowe, T. P., & Brooks, P. R. (2023). Using valve gape analysis to compare sensitivity of native *Mytilus edulis* to invasive *Magallana gigas* when exposed to heavy metal contamination. *Marine Environmental Research, 189*, 106043.

Lafferty, K. D., & Suchanek, T. H. (2016). Revisiting Paine's 1966 sea star removal experiment, the most-cited empirical article in *The American Naturalist*. *The American Naturalist, 188*(4), 365–378.

Lowe, A. T., Bos, J., & Ruesink, J. (2019). Ecosystem metabolism drives pH variability and modulates long-term ocean acidification in the Northeast Pacific coastal ocean. *Scientific Reports, 9*(1), 963.

Menge, B. A., Chan, F., & Lubchenco, J. (2008). Response of a rocky intertidal ecosystem engineer and community dominant to climate change. *Ecology Letters, 11*(2), 151–162.

Miller, L. P., & Dowd, W. W. (2017). Multimodal in situ datalogging quantifies inter-individual variation in thermal experience and persistent origin effects on gaping behavior among intertidal mussels (*Mytilus californianus*). *Journal of Experimental Biology, 220*(22), 4305–4319.

Miller, L. P. (2022). Monitoring bivalve behavior and physiology in the laboratory and field using open-source tools. *Integrative and Comparative Biology, 62*(4), 1096–1110.

Murie, K. A., & Bourdeau, P. E. (2020). Fragmented kelp forest canopies retain their ability to alter local seawater chemistry. *Scientific Reports, 10*(1), 1–13.

Ninokawa, A., Takeshita, Y., Jellison, B. M., Jurgens, L. J., & Gaylord, B. (2020). Biological modification of seawater chemistry by an ecosystem engineer, the California mussel *Mytilus californianus*. *Limnology and Oceanography, 65*(1), 157–172.

Ninokawa, A. T., Saley, A. M., Shalchi, R., & Gaylord, B. (2024). Multiple carbonate system parameters independently govern shell formation in a marine mussel. *Communications Earth & Environment, 5*(1), 273.

Nishizaki, M., & Ackerman, J. D. (2017). Mussels blow rings: Jet behavior affects local mixing. *Limnology and Oceanography, 62*(1), 125–136.

Nixon, S. W., Oviatt, C. A., Rogers, C., & Taylor, K. (1971). Mass and metabolism of a mussel bed. *Oecologia, 8*(1), 21–30.

Pfister, C. A., Altabet, M. A., & Weigel, B. L. (2019). Kelp beds and their local effects on seawater chemistry, productivity, and microbial communities. *Ecology, 100*(10), e02798.

R Core Team. (2025). *R: A language and environment for statistical computing.* R Foundation for Statistical Computing, Vienna, Austria. https://www.R-project.org/

Reidenbach, M. A., Limm, M., Hondzo, M., & Stacey, M. T. (2010). Effects of bed roughness on boundary layer mixing and mass flux across the sediment–water interface. *Water Resources Research, 46*(7).

Riisgård, H. U., Larsen, P. S., & Pleissner, D. (2014). Allometric equations for maximum filtration rate in blue mussels *Mytilus edulis* and importance of condition index. *Helgoland Marine Research, 68*, 193–198.

Seed, R., & Suchanek, T. H. (1992). Population and community ecology of *Mytilus*. In *The Mussel Mytilus: Ecology, Physiology, Genetics and Culture* (Vol. 25, pp. 87–170). Elsevier.

Shakspeare, A., Moore, H., Service, M., Wilson, C., Ahmed, H., Cameron, T. C., & Steinke, M. (2023). Gaping behaviour of blue mussels (*Mytilus edulis*) in relation to freshwater runoff risks. *Aquaculture Reports, 33*, 101719.

Stachowicz, J. J. (2001). Mutualism, facilitation, and the structure of ecological communities. *BioScience, 51*(3), 235–246

Suárez, M. P., Alvarez, C., Molist, P., & San Juan, F. (2005). Particular aspects of the gonadal cycle and seasonal distribution of gametogenic stages of *Mytilus galloprovincialis* cultured in the estuary of Vigo. *Journal of Shellfish Research, 24*(2), 531–540.

Suchanek, T. H. (1978). The ecology of *Mytilus edulis* L. in exposed rocky intertidal communities. *Journal of Experimental Marine Biology and Ecology, 31*(1), 105–120.

Suchanek, T. H. (1979). *The Mytilus californianus* community: Studies on the composition, structure, organization, and dynamics of a mussel bed (Doctoral dissertation). University of Washington.

Suchanek, T. H. (1981). The role of disturbance in the evolution of life history strategies in the intertidal mussels *Mytilus edulis* and *Mytilus californianus*. *Oecologia, 50*(2), 143–152.

Tran, D., Ciret, P., Ciutat, A., Durrieu, G., & Massabuau, J. C. (2003). Estimation of potential and limits of bivalve closure responses for contaminant detection: application to cadmium. *Environmental Toxicology and Chemistry*, *22*(4), 914-920.

Tran, D., Fournier, E., Durrieu, G., & Massabuau, J. C. (2004). Copper detection in the Asiatic clam Corbicula fluminea: optimum valve closure response. *Aquatic Toxicology*, *66*(3), 333-343.

Tomanek, L., & Zuzow, M. J. (2010). The proteomic response of the mussel congeners Mytilus galloprovincialis and M. trossulus to acute heat stress: implications for thermal tolerance limits and metabolic costs of thermal stress. *Journal of Experimental Biology*, 213(20), 3559-3574.

Tomasetti, S. J., Doall, M. H., Hallinan, B. D., Kraemer, J. R., & Gobler, C. J. (2023). Oyster reefs' control of carbonate chemistry—Implications for oyster reef restoration in estuaries subject to coastal ocean acidification. *Global Change Biology, 29*(23), 6572–6590.

Traiger, S. B., Cohn, B., Panos, D., Daly, M., Hirsh, H. K., Martone, M., ... & Nickols, K. J. (2021). Limited biogeochemical modification of surface waters by kelp forest canopies: Influence of kelp metabolism and site-specific hydrodynamics. *Limnology and Oceanography.*

van de Koppel, J., Gascoigne, J. C., Theraulaz, G., Rietkerk, M., Mooij, W. M., & Herman, P. M. (2008). Experimental evidence for spatial self-organization and its emergent effects in mussel bed ecosystems. *Science*, *322*(5902), 739-742.

van der Schatte Olivier, A., Jones, L., Vay, L. L., Christie, M., Wilson, J., & Malham, S. K. (2020). A global review of the ecosystem services provided by bivalve aquaculture. *Reviews in Aquaculture*, *12*(1), 3-25.

Van Duren, L. A., Herman, P. M., Sandee, A. J., & Heip, C. H. (2006). Effects of mussel filtering activity on boundary layer structure. *Journal of Sea Research*, 55(1), 3-14.

Villanoy, C., David, L., Cabrera, O., Atrigenio, M., Siringan, F., Aliño, P., & Villaluz, M. (2012). Coral reef ecosystems protect shore from high-energy waves under climate change scenarios. *Climatic change*, 112, 493-505.

Wahl, M., Schneider Covachã, S., Saderne, V., Hiebenthal, C., Müller, J. D., Pansch, C., Sawall, Y. (2018). Macroalgae may mitigate ocean acidification effects on mussel calcification by increasing pH and its fluctuations. *Limnology and Oceanography*, 63(1), 3-21.

Waldbusser, G. G., & Salisbury, J. E. (2014). Ocean acidification in the coastal zone from an organism's perspective: multiple system parameters, frequency domains, and habitats. *Annual review of marine science*, 6, 221-247.

Wernberg, T., Thomsen, M. S., Baum, J. K., Bishop, M. J., Bruno, J. F., Coleman, M. A., ... & Vanderklift, M. A. (2024). Impacts of climate change on marine foundation species. Annual *Review of Marine Science*, 16, 247-282.

Ward, J. E., & Targett, N. M. (1989). Influence of marine microalgal metabolites on the feeding behavior of the blue mussel *Mytilus edulis*. *Marine Biology*, *101*, 313-321.

Tables and Figures

Table 1. Summary of experimental parameters and mussel morphometrics for each *Mytilus* trial. A) Experimental parameters for each mussel aggregation (bed), total number of mussels per aggregation, and average temperature throughout each species trial. B) Morphometrics of a subset of mussels from the aggregation, N=45-46. Bolded *P-values* represent significant differences among species (ANOVA); superscripts (lower case letters) denote which species were different from each other (see Table S2). SEM=Standard error of the mean.

A) Experimental Parameters	*M.trossulus*	*M.galloprovincialis*	*M.californianus*	
Bed dimensions (L ×W ×H, m)	1.1 × 0.5 × 0.03	1.1 × 0.5 × 0.03	1.1 × 0.5 × 0.03	
Mussels in bed (died)	993 (54)	776 (14)	535 (4)	
Average Temperature (±std. dev)	12.3 (±0.5)	10.0 (±0.2)	10.7 (±0.2)	
B) Mussel Morphometrics (mean (±SEM))				*P*-value
Length (mm)	58.9 (±0.8)^{a}	63.1 (±0.7)^{b}	65.1 (±1.0)^{b}	**<0.0001**
Height (mm)	26.8 (±0.5)^{a}	32.8 (±0.4)^{b}	33.2 (±0.4)^{b}	**<0.0001**
Width (mm)	20.2 (±0.4)^{a}	24.6 (±0.4)^{b}	28.2 (±0.5)^{c}	**<0.0001**
Dry Weight (g)	1.95 (±0.1)^{b}	1.33 (±0.1)^{a}	2.01 (±0.1)^{b}	**<0.0001**
Biomass Density (g·cm^{-2})	0.45 (±0.02)^{c}	0.21 (±0.07)^{a}	0.27 (±0.01)^{b}	**<0.0001**
Total aggregation Biomass (kg)	1.93	1.03	1.08	N/A

Table 2. Summary of nonlinear model fits describing the effects of flow speed on ΔDO_{eq} A) before and B) after normalization by biomass density across three Mytilus species.

A) Before $\Delta DO_{eq} = a \cdot e^{-b \cdot \text{flow speed}}$			
Species	Parameter Estimates (95% CI) a	b	Residual Standard Error
M.trossulus (MT)	3.04 (1.71-5.11)	0.31 (0.18-0.48)	0.12
M.galloprovincialis (MG)	1.67 (0.20-2.71)	0.37 (0.08-0.50)	0.05
M.californianus (MC)	0.80 (0.13-2.41)	0.31 (0.05-0.72)	0.06
B) After $\Delta DO mg \cdot cm^2 \cdot g_{DW}^{-1} \cdot L^{-1} = a \cdot e^{-b \cdot \text{flow speed}}$			
M.trossulus (MT)	6.80 (3.81-11.34)	0.31 (0.18-0.48)	0.27
M.galloprovincialis (MG)	7.93(0.97-12.90)	0.37 (0.08-0.50)	0.25
M.californianus (MC)	3.00 (0.47-12.60)	0.31 (0.05-0.72)	0.20

Table 3. Summary of generalized linear modelling (glm) of the effects of flow on gape behavior (proportion of time spent open) for each *Mytilus* trial. A) Model ranking based on Akaike's information criterion (AIC) and summary statistics. B) Matrix of log-likelihood (Pr > Chi-sq) comparisons of models. See Table S4 for additional details.

A) Model Rank Effect(s)		AIC	Deviance	DF residuals
MIXED MODELS		-1012.9	3.35	457
1 Species only		-1008.5	3.34	454
2 Flow speed × Species		-944	3.93	459
3 Null		-9.43	3.92	458
4 Flow speed only				
B) Model Comparisons (*P*-values)				
RANK MODEL	4	3	2	1
4 Flow speed only	-			
3 Null	0.36	-		
2 Flow speed × Species	**<0.0001**	**<0.0001**	-	
1 Species only	**<0.0001**	**<0.0001**	0.62	-

Figure 1. Schematic of flow and chemical gradients created by a mussel aggregation. A) Approaching water interacts with the aggregation, slowing down within the aggregation (interstitial zone) and speeding up above it, creating a momentum boundary layer. The rough mussel surfaces cause eddies to form leading to mixing between the interstitial zone (red) and the ambient environment (white). The mixing depth, d_e, is where the chemical concentration profile (in red) transitions from ambient conditions to those modified by biological activity within the interstitial zone B) Mussels gape and generate currents for suspension feeding and gas exchange, circulating water internally from the incurrent to excurrent pseudo-siphons. By mixing fluids and metabolites with the surrounding environment, gaping behavior (a proxy for pumping behavior) may help determine chemical gradients in the interstitial zone.

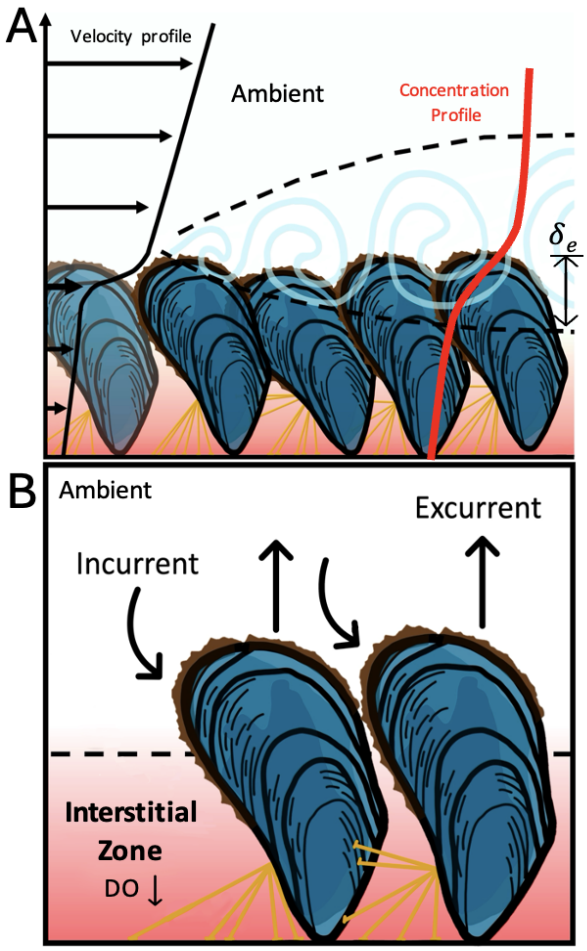

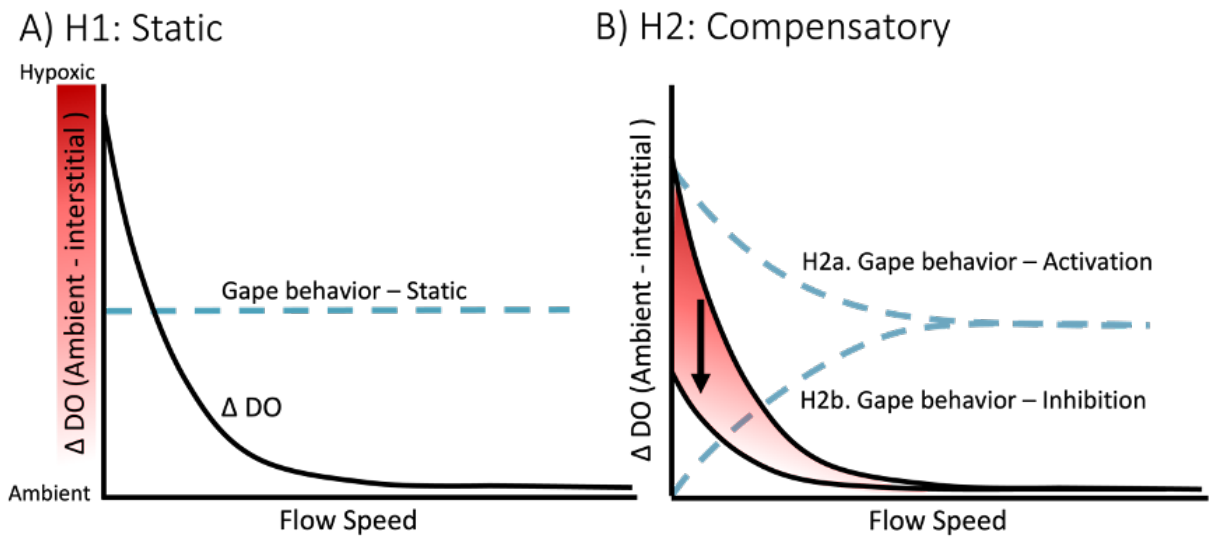

Figure 2. Graphical model illustrating potential mechanisms for mussel behavior to mediate flow-dependent DO gradients in mussel aggregations. When flow speeds are low, mussel respiration depletes oxygen within the interstitial zone, creating a strong hypoxic gradient relative to ambient conditions (ΔDO, black line). Hypothetical mussel gaping behavior (a proxy for pumping behavior) is represented by a blue dotted line. A) The null model (H1) assumes mussel gaping is static and does not ameliorate chemical gradients that develop at low flow speeds. B) The compensatory model (H2) assumes mussels actively adjust their gaping in response to adverse chemical conditions by one of two mechanisms: increased pumping (H2a: activation) or closing (H2b: inhibition) at low flow speeds. Both compensatory mechanisms are behavioral feedbacks that may ameliorate harsh gradients in low flow.

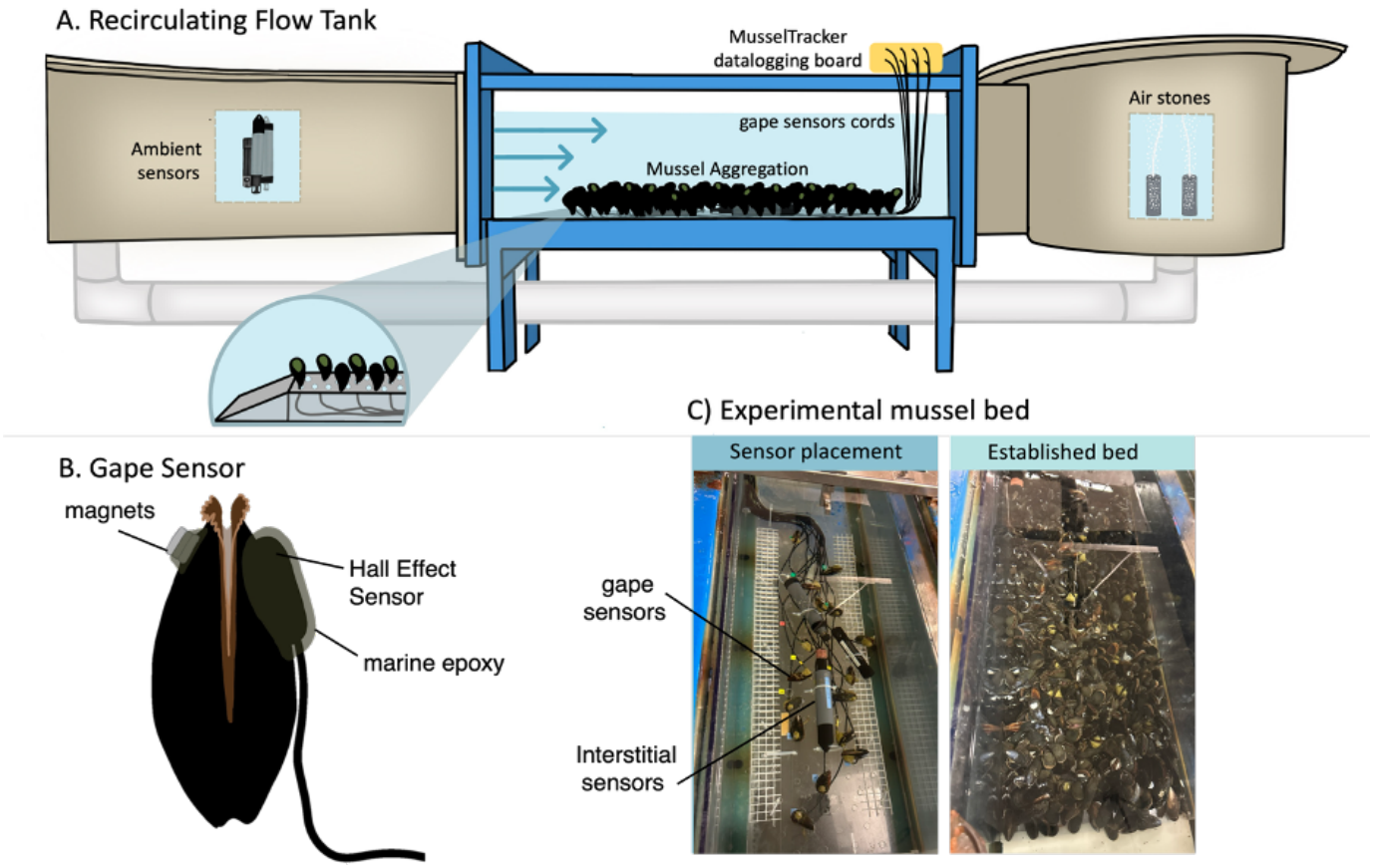

Figure 3. Overview of lab experimental design and instrumentation. A) Schematic of recirculating flow tank and locations of mussel aggregation, gape sensors with logger, and water chemistry sensors (both ambient and in aggregation). B) Each gape sensor is composed of a Hall Effect sensor and magnets fastened to opposite valves of the mussel shell. C) A bird's-eye view of the flow tank working section showing placement of the gape and DO sensors before (left) and after (right) the monolayer bed was filled in.

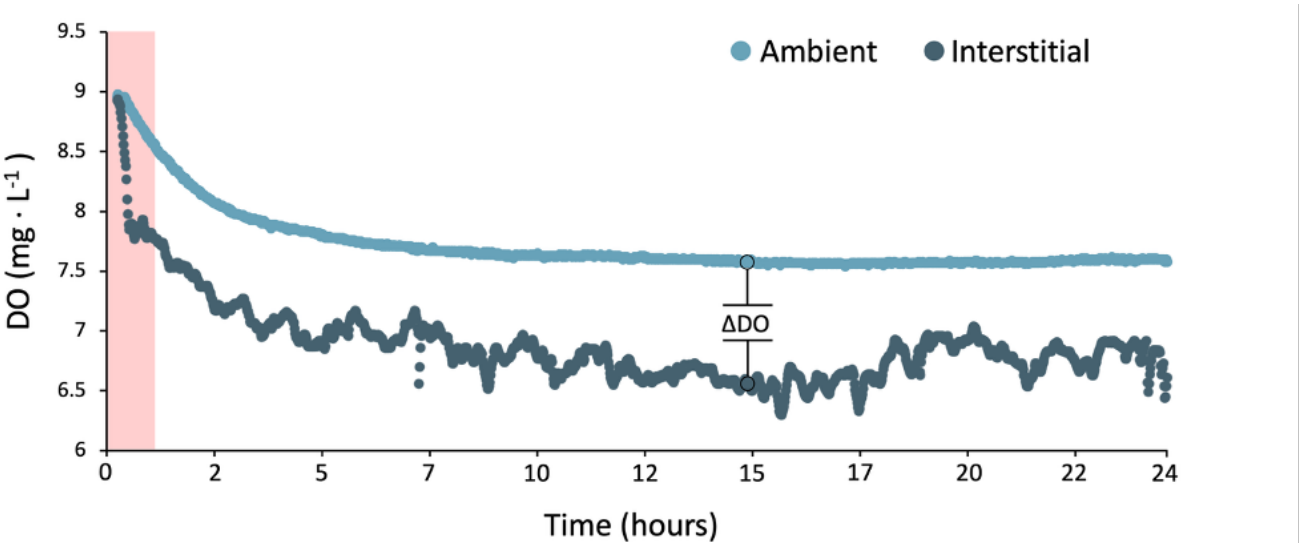

Figure 4. Representative recording of dissolved oxygen (DO) dynamics in a *M. trossulus* aggregation at a flow speed of 4.5 cm s^{-1}. DO concentration ($mg \cdot L^{-1}$) recorded every minute in ambient (light blue) and interstitial (dark blue) water; ΔDO is the difference between these two measurements. The red-shaded region highlights the initial equilibration period; these data were removed from further analysis.

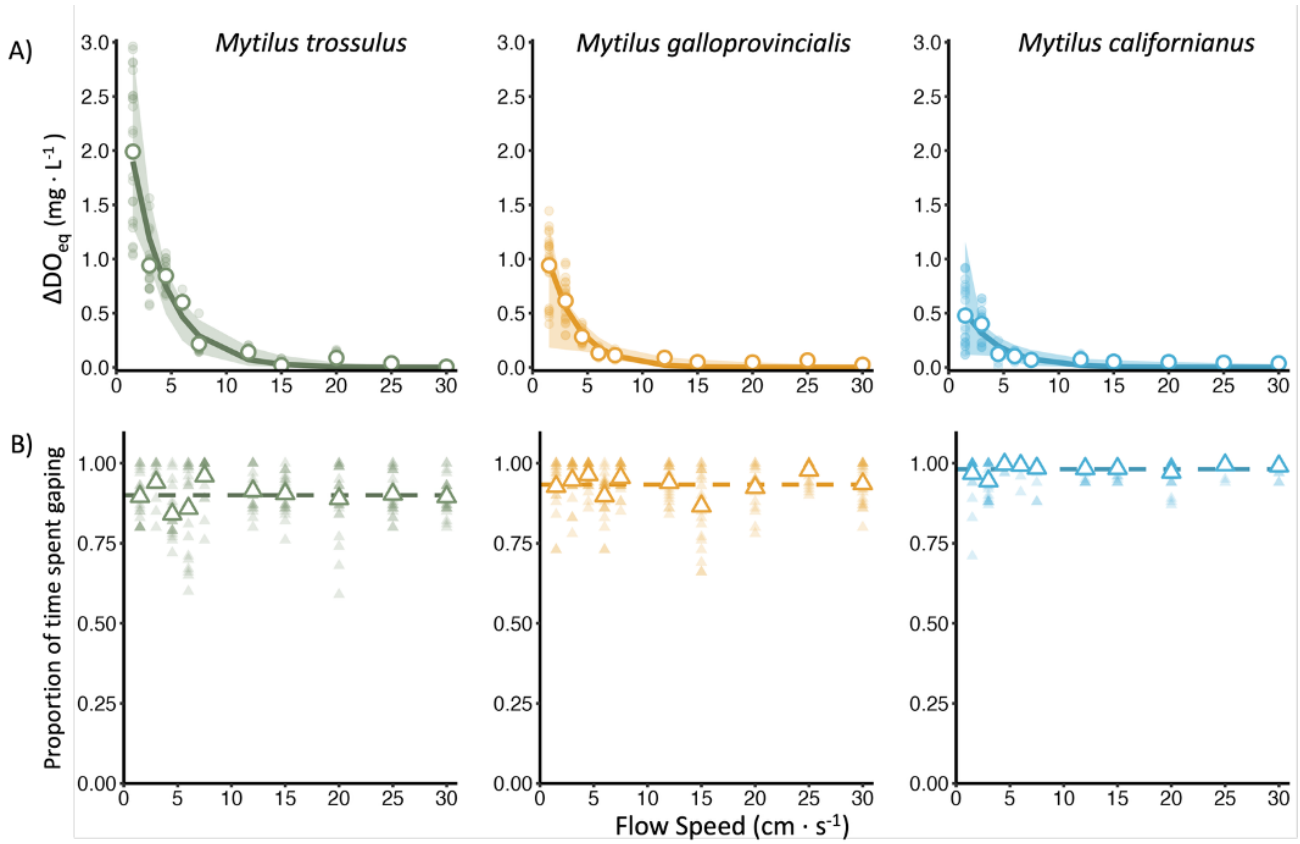

Figure 5. Flow speed effects on dissolved oxygen gradient (ΔDO_{eq}) and gaping behavior for three *Mytilus* species: *M. trossulus* (green), *M. galloprovincialis* (orange), and *M. californianus* (blue). A) White circles represent the mean ΔDO_{eq} values averaged over a 23-hour period at each flow speed, while small, shaded circles show hourly averages (n = 23). Solid lines represent species-specific exponential decay models fitted to the data, and shaded regions indicate the 95% confidence intervals around these model predictions. B) Small, shaded triangles show individual-level average gaping proportions from mussels equipped with gape sensors (n = 16), while large white triangles show the mean proportion of time spent gaping at each flow speed. Dashed lines depict species-specific average gaping responses to flow speed.

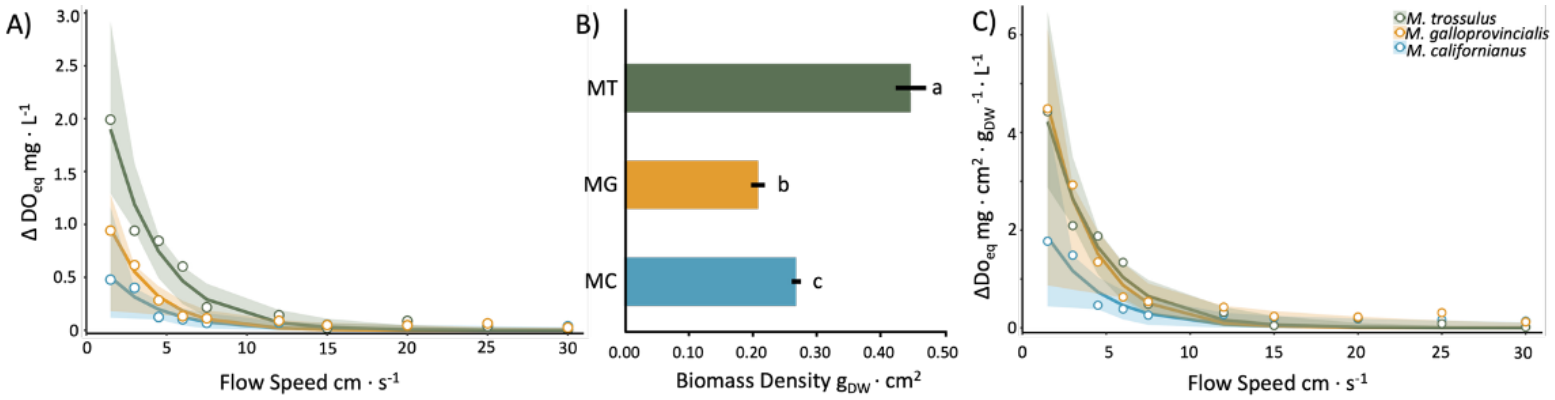

Figure 6. Effects of flow and biomass density on ΔDOeq for three Mytilus species. A) White circles show the average ΔDOeq values over a 23-hour period at each flow speed for M. trossulus (green), M. galloprovincialis (orange), and M. californianus (blue). Solid lines represent species-specific exponential decay models, with shaded regions indicating 95% confidence intervals. B) Bars represent mean biomass density (g DW·cm^{-2} ± SEM) for each species based on 46 mussels per aggregation. Letters denote significant differences among species (Kruskal-Wallis test: Table S2). C) ΔDOeq per biomass density (ΔDOeq mg·cm^2·gDW^{-1}·L^{-1}) as a function of flow speed.

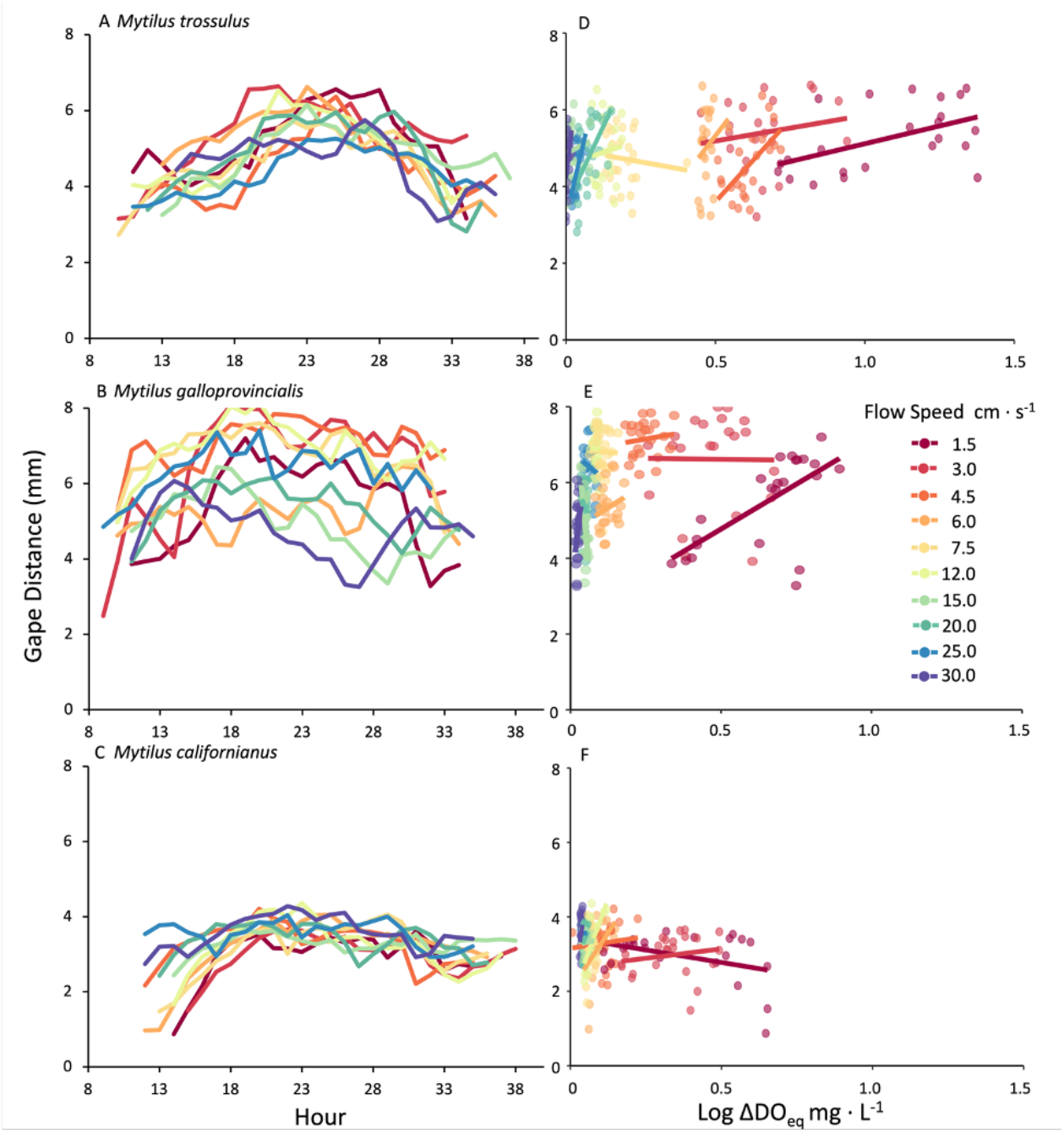

Figure 7. Gaping distance under different flow conditions and its relationship with changes in dissolved oxygen (ΔDO) for three mussel species. Left panels (A–C) show average gape distance (mm) over time for each flow speed trial (colored lines) across 23 hours for Mytilus trossulus (A), M. galloprovincialis (B), and M. californianus (C). Right panels (D–F) show the relationship between log-transformed ΔDO and gape distance for each flow speed. Each point represents the hourly average gape distance (n = 16 mussels) and ΔDOeq during each flow speed treatment (n = 23 hours per treatment).

Supplemental Materials

Table S1. Summary of statistical comparisons of *Mytilus* species morphometrics, including A) shell length, B) height, C) width, D) dry body weight, and E) biomass density. One-way ANOVAs were conducted for length, height, width, and dry body weight, followed by Tukey's post-hoc comparisons for pairwise differences. The terms upper and lower refer to the upper and lower bounds of 95% confidence interval for the difference in means between two species. Biomass density was analyzed using a Kruskal-Wallis test with Wilcoxon rank sum tests for pairwise comparisons. Significant differences ($p < 0.05$) are indicated in bold. *Mytilus trossulus—MT, Mytilus galloprovincialis—MG, and Mytilus californianus* – MC. Df= Degree of freedom, SS= Sums of Square, MS= Mean Squares, F= F-statistic.

A) One-way ANOVA: Length					
	df	SS	MS	F-value	*P*-value
Species	2	899	449.4	13.31	**<0.0001**
Residuals	134	4525	33.8		
Tukey multiple comparisons of means					
Species		difference	95% CI (lower, upper)		adjusted *P*-value
MT-MG		-4.17	-7.05, -1.28		**0.002**
MT-MC		-6.17	-9.06, -3.28		**<0.0001**
MG-MC		-2.00	-4.87,0.87		0.228
B) One-way ANOVA: Height					
	df	SS	MS	F-value	*P*-value
Species	2	1164	582.2	60.1	**<0.0001**
Residuals	134	1287	9.6		
Tukey multiple comparisons of means					
Species		difference	95% CI (lower, upper)		adjusted *P*-value
MT-MG		-5.96	-7.50, -4.43		**<0.0001**
MT-MC		-6.42	-7.96, -4.88		**<0.0001**
MG-MC		-0.45	-1.99, 1.08		0.76

C) One-way ANOVA: Width

	df	SS	MS	F-value	*P*-value
Species	2	1462	730.8	93.47	**<0.0001**
Residuals	134	1048	7.8		
Tukey multiple comparisons of means					
Species		difference	95% CI (lower, upper)		adjusted P-value
MT-MG		-4.36	-5.74, -2.97		**<0.0001**
MT-MC		-8.01	-9.39, -6.62		**<0.0001**
MG-MC		-3.65	-5.03, -2.27		**<0.0001**

D) One-way ANOVA: Dry Body Weight

	df	SS	MS	F-value	*P*-value
Species	2	2.054	1.0272	18.91	**<0.0001**
Residuals	134	7.280	0.0543		
Tukey multiple comparisons of means					
Species		difference	95% CI (lower, upper)		adjusted *P*-value
MT-MG		0.24	0.13, 0.36		**<0.0001**
MT-MC		-0.03	-0.15, 0.09		0.82
MG-MC		-0.27	-0.39, -0.16		**<0.0001**

E) Kruskal-Wallis: Biomass Density

		df	Chi-squared	*P*-value
		2	116.22	**<0.0001**
	Pairwise comparisons using		MT-MG	**<0.0001**
	Wilcoxon rank sum test:		MT-MC	**<0.0001**
			MG-MC	**<0.0001**

Table S2. Summary of Model II (Standard Major Axis) regression evaluating the relationship between gape distance (mm) and log-transformed ΔDOeq across flow speeds for three *Mytilus* species. Each cell shows the regression estimate for elevation (intercept) and slope, along with 95% confidence intervals, R^2 values, and associated P-values. Bolded slopes and R^2 values indicate statistically significant relationships ($P < 0.05$).

Species	*M. trossulus*	*M.galloprovincialis*	*M. californianus*
Likelihood ratio	**185.8**	**228.1**	**190.5**
P-value	**<0.0001**	**<0.0001**	**<0.0001**
Speed 1.5			
Slope Estimate	0.59	1.19	-1.07
95% CI (lower, upper) limits	0.40, 0.86	0.84, 1.69	-1.60, -0.72
R-squared	0.26	0.39	0.17
P-value	0.01	0.002	0.05
Speed 3			
Slope Estimate	1.21	-1.57	1.55
95% CI (lower, upper) limits	0.78, 1.86	-2.44. -1.01	1.00, 2.40
R-squared	0.03	0.0001	0.02
P-value	0.46	0.99	0.54
Speed 4.5			
Slope Estimate	2.46	1.40	3.30
95% CI (lower, upper) limits	1.73, 3.50	0.91, 2.17	2.13, 5.11
R-squared	0.37	0.01	0.005
P-value	0.002	0.58	0.75
Speed 6			
Slope Estimate	8.25	3.53	8.18
95% CI (lower, upper) limits	5.37, 12.68	2.30, 5.42	5.52, 12.11
R-squared	0.05	0.05	0.21
P-value	0.31	0.31	0.03
Speed 7.5			
Slope Estimate	-2.29	-4.31	12.88
95% CI (lower, upper) limits	-3.54, -1.48	-6.68, -2.78	8.34, 19.90
R-squared	0.01	0.0004	0.02
P-value	0.64	0.93	0.50
Speed 12			
Slope Estimate	5.12	11.0	7.66
95% CI (lower, upper) limits	3.30, 7.91	7.11, 17.00	5.52, 10.65
R-squared	0.01	0.02	0.46
P-value	0.65	0.49	0.004
Speed 15			
Slope Estimate	5.18	-22.37	4.30
95% CI (lower, upper) limits	3.35, 8.01	-31.48, -15.90	2.78, 6.65

R-squared	0.02	0.41	0.01
P-value	0.53	0.001	0.62
Speed 20			
Slope Estimate	5.32	-19.56	17.20
95% CI (lower, upper) limits	3.70, 7.63	-30.20, -12.67	11.24, 26.32
R-squared	0.34	0.02	0.07
P-value	0.004	0.47	0.23
Speed 25			
Slope Estimate	9.80	-5.11	15.66
95% CI (lower, upper) limits	6.95, 13.80	-7.87, -3.32	10.09, 24.99
R-squared	0.41	0.04	0.0009
P-value	0.001	0.38	0.89
Speed 30			
Slope Estimate	26.5	28.43	45.62
95% CI (lower, upper) limits	18.1, 39.0	19.16, 24.18	29.83, 69.77
R-squared	0.25	0.20	0.07
P-value	0.02	0.03	0.22

Table S3. Summary of one-way ANOVA and pairwise comparisons testing the effect of flow speed on absolute pairwise correlation between mussel gape sensors for each species: A) *Mytilus trossulus*, B) *M. galloprovincialis*, and C) *M. californianus*. For each pairwise speed comparison, diff indicates the difference in mean correlation, with corresponding 95% confidence intervals (lower, upper). Bolded values indicate pairwise speed comparisons that are significantly different.

A) MT	Df	Sums of Squares	Means of Squares	F-Statistic	*P*-value
Speed	9	0.81	0.09	3.45	**0.0003**
Residuals	1040	26.98	0.03		
Pairwise comparisons	diff	lower	upper		*P*-value
3.0-1.5	0.00	-0.07	0.07		1.00
4.5-1.5	-0.02	-0.10	0.05		0.98
6.0-1.5	-0.03	-0.10	0.04		0.96
7.5-1.5	0.01	-0.06	0.08		1.00
12.0-1.5	-0.05	-0.12	0.02		0.37
15.0-1.5	-0.04	-0.11	0.03		0.63
20.0-1.5	0.03	-0.04	0.10		0.97
25.0-1.5	-0.01	-0.08	0.06		1.00
30.0-1.5	0.04	-0.03	0.11		0.75
4.5-3.0	-0.02	-0.09	0.05		1.00
6.0-3.0	-0.02	-0.10	0.05		0.98
7.5-3.0	0.01	-0.06	0.08		1.00
12.0-3.0	-0.05	-0.12	0.02		0.50
15.0-3.0	-0.04	-0.11	0.03		0.75
20.0-3.0	0.03	-0.04	0.10		0.93
25.0-3.0	-0.01	-0.08	0.06		1.00
30.0-3.0	0.04	-0.03	0.11		0.63
6.0-4.5	0.00	-0.07	0.07		1.00
7.5-4.5	0.03	-0.04	0.10		0.92
12.0-4.5	-0.03	-0.10	0.04		0.97
15.0-4.5	-0.02	-0.09	0.05		1.00
20.0-4.5	0.05	-0.02	0.12		0.38
25.0-4.5	0.01	-0.06	0.08		1.00
30.0-4.5	0.06	-0.01	0.13		0.11
7.5-6.0	0.04	-0.04	0.11		0.85
12.0-6.0	-0.02	-0.09	0.05		0.99
15.0-6.0	-0.02	-0.09	0.06		1.00
20.0-6.0	0.06	-0.01	0.13		0.27
25.0-6.0	0.02	-0.06	0.09		1.00
30.0-6.0	0.07	0.00	0.14		0.07

12.0-7.5	-0.06	-0.13	0.01		0.20
15.0-7.5	-0.05	-0.12	0.02		0.41
20.0-7.5	0.02	-0.05	0.09		1.00
25.0-7.5	-0.02	-0.09	0.05		1.00
30.0-7.5	0.03	-0.04	0.10		0.90
15.0-12.0	0.01	-0.06	0.08		1.00
20.0-12.0	**0.08**	**0.01**	**0.15**		**0.02**
25.0-12.0	0.04	-0.03	0.11		0.78
30.0-12.0	**0.09**	**0.02**	**0.16**		**0.002**
20.0-15.0	**0.07**	**0.00**	**0.14**		**0.05**
25.0-15.0	0.03	-0.04	0.10		0.94
30.0-15.0	**0.08**	**0.01**	**0.15**		**0.01**
25.0-20.0	-0.04	-0.11	0.03		0.73
30.0-20.0	0.01	-0.06	0.08		1.00
30.0-25.0	0.05	-0.02	0.12		0.34
B) MG	Df	Sums of Squares	Means of Squares	F-Statistic	*P*-value
Speed	9	1.83	0.20	11.7	**<0.0001**
Residuals	1040	18.0	0.02		
Pairwise comparisons	diff	lower	upper		*P*-value
3.0-1.5	-0.02	-0.08	0.03		0.96
4.5-1.5	**-0.13**	**-0.19**	**-0.08**		**<0.0001**
6.0-1.5	-0.04	-0.10	0.02		0.52
7.5-1.5	**-0.10**	**-0.15**	**-0.04**		**<0.0001**
12.0-1.5	**-0.09**	**-0.15**	**-0.03**		**<0.0001**
15.0-1.5	-0.02	-0.08	0.04		0.99
20.0-1.5	**-0.06**	**-0.12**	**0.00**		**0.03**
25.0-1.5	**-0.11**	**-0.17**	**-0.05**		**<0.0001**
30.0-1.5	-0.05	-0.11	0.00		0.08
4.5-3.0	**-0.11**	**-0.17**	**-0.05**		**<0.0001**
6.0-3.0	-0.01	-0.07	0.04		1.00
7.5-3.0	-0.07	-0.13	-0.02		**<0.0001**
12.0-3.0	**-0.06**	**-0.12**	**-0.01**		**0.02**
15.0-3.0	0.01	-0.05	0.06		1.00
20.0-3.0	-0.04	-0.10	0.02		0.56
25.0-3.0	**-0.09**	**-0.15**	**-0.03**		**<0.0001**
30.0-3.0	-0.03	-0.09	0.03		0.79
6.0-4.5	**0.10**	**0.04**	**0.15**		**<0.0001**
7.5-4.5	0.04	-0.02	0.09		0.57
12.0-4.5	0.05	-0.01	0.10		0.25
15.0-4.5	**0.12**	**0.06**	**0.17**		**<0.0001**
20.0-4.5	**0.07**	**0.02**	**0.13**		**<0.0001**

25.0-4.5	0.02	-0.04	0.08		0.97
30.0-4.5	**0.08**	**0.02**	**0.14**		**<0.0001**
7.5-6.0	**-0.06**	**-0.12**	**0.00**		**0.04**
12.0-6.0	-0.05	-0.11	0.01		0.17
15.0-6.0	0.02	-0.04	0.08		0.98
20.0-6.0	-0.02	-0.08	0.04		0.97
25.0-6.0	**-0.07**	**-0.13**	**-0.02**		**<0.0001**
30.0-6.0	-0.02	-0.07	0.04		1.00
12.0-7.5	0.01	-0.05	0.07		1.00
15.0-7.5	**0.08**	**0.02**	**0.14**		**<0.0001**
20.0-7.5	0.04	-0.02	0.09		0.62
25.0-7.5	-0.01	-0.07	0.04		1.00
30.0-7.5	0.04	-0.02	0.10		0.38
15.0-12.0	**0.07**	**0.01**	**0.13**		**<0.0001**
20.0-12.0	0.03	-0.03	0.08		0.90
25.0-12.0	-0.02	-0.08	0.03		0.95
30.0-12.0	0.03	-0.02	0.09		0.72
20.0-15.0	-0.04	-0.10	0.01		0.34
25.0-15.0	**-0.09**	**-0.15**	**-0.04**		**<0.0001**
30.0-15.0	-0.04	-0.09	0.02		0.57
25.0-20.0	-0.05	-0.11	0.01		0.14
30.0-20.0	0.01	-0.05	0.06		1.00
30.0-25.0	**0.06**	**0.00**	**0.11**		**0.05**
C) MC	Df	Sums of Squares	Means of Squares	F-Statistic	*P*-value
Speed	9	9.62	1.07	38.44	**<0.0001**
Residuals	1040	33.1	0.03		
Pairwise comparisons	diff	lower	upper		*P*-value
3.0-1.5	**0.15**	**0.08**	**0.22**		**<0.0001**
4.5-1.5	0.05	-0.02	0.12		0.310
6.0-1.5	0.03	-0.04	0.10		0.938
7.5-1.5	**-0.12**	**-0.19**	**-0.05**		**<0.0001**
12.0-1.5	**-0.08**	**-0.15**	**-0.01**		**0.014**
15.0-1.5	**-0.07**	**-0.14**	**0.00**		**0.028**
20.0-1.5	**-0.07**	**-0.14**	**-0.01**		**0.019**
25.0-1.5	**0.15**	**0.08**	**0.22**		**<0.0001**
30.0-1.5	0.02	-0.04	0.09		0.986
4.5-3.0	**-0.10**	**-0.17**	**-0.03**		**<0.0001**
6.0-3.0	**-0.12**	**-0.19**	**-0.05**		**<0.0001**
7.5-3.0	**-0.27**	**-0.34**	**-0.20**		**<0.0001**
12.0-3.0	**-0.23**	**-0.29**	**-0.16**		**<0.0001**
15.0-3.0	**-0.22**	**-0.29**	**-0.15**		**<0.0001**
20.0-3.0	**-0.22**	**-0.29**	**-0.16**		**<0.0001**

25.0-3.0	0.00	-0.06	0.07	1.000
30.0-3.0	**-0.13**	**-0.19**	**-0.06**	**<0.0001**
6.0-4.5	-0.02	-0.09	0.05	0.988
7.5-4.5	**-0.17**	**-0.24**	**-0.10**	**<0.0001**
12.0-4.5	**-0.13**	**-0.20**	**-0.06**	**<0.0001**
15.0-4.5	**-0.12**	**-0.19**	**-0.06**	**<0.0001**
20.0-4.5	**-0.13**	**-0.20**	**-0.06**	**<0.0001**
25.0-4.5	**0.10**	**0.03**	**0.17**	**<0.0001**
30.0-4.5	-0.03	-0.10	0.04	0.945
7.5-6.0	**-0.15**	**-0.22**	**-0.08**	**<0.0001**
12.0-6.0	**-0.11**	**-0.17**	**-0.04**	**<0.0001**
15.0-6.0	**-0.10**	**-0.17**	**-0.03**	**<0.0001**
20.0-6.0	**-0.10**	**-0.17**	**-0.04**	**<0.0001**
25.0-6.0	**0.12**	**0.06**	**0.19**	**<0.0001**
30.0-6.0	-0.01	-0.07	0.06	1.000
12.0-7.5	0.04	-0.03	0.11	0.628
15.0-7.5	0.05	-0.02	0.12	0.474
20.0-7.5	0.04	-0.02	0.11	0.563
25.0-7.5	**0.27**	**0.20**	**0.34**	**<0.0001**
30.0-7.5	**0.14**	**0.07**	**0.21**	**<0.0001**
15.0-12.0	0.00	-0.06	0.07	1.000
20.0-12.0	0.00	-0.07	0.07	1.000
25.0-12.0	**0.23**	**0.16**	**0.30**	**<0.0001**
30.0-12.0	**0.10**	**0.03**	**0.17**	**<0.0001**
20.0-15.0	0.00	-0.07	0.07	1.000
25.0-15.0	**0.22**	**0.16**	**0.29**	**<0.0001**
30.0-15.0	**0.10**	**0.03**	**0.16**	**<0.0001**
25.0-20.0	**0.23**	**0.16**	**0.30**	**<0.0001**
30.0-20.0	**0.10**	**0.03**	**0.17**	**<0.0001**
30.0-25.0	**-0.13**	**-0.20**	**-0.06**	**<0.0001**

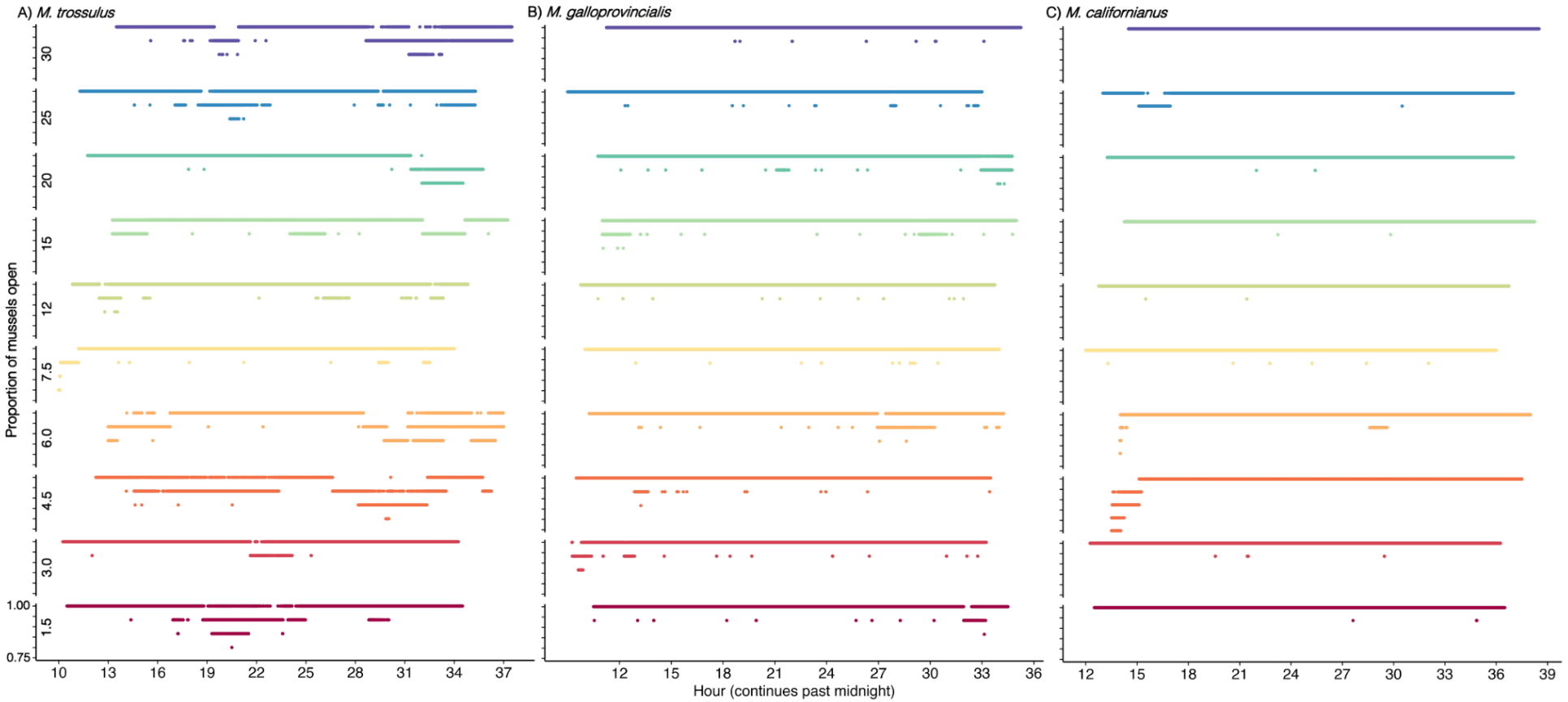

Figure S1. Proportion of mussels with gape sensors that were open across each 24 hr flow speed treatment: A) *Mytilus trossulus* (N=15), B) *M. galloprovincialis* (N=15), and C) *M. californianus* (N=16). Points represent the proportion of mussels open, measured every 5s, for each flow speed (1.5–30 cm s^{-1}) ordered from lowest (bottom) to highest (top). Tick marks along the y-axis denote proportion open at 0.75, 0.80, 0.85, 0.90, 0.95, and 1.00, with labels shown only for the 1.5 cm s^{-1} treatment.

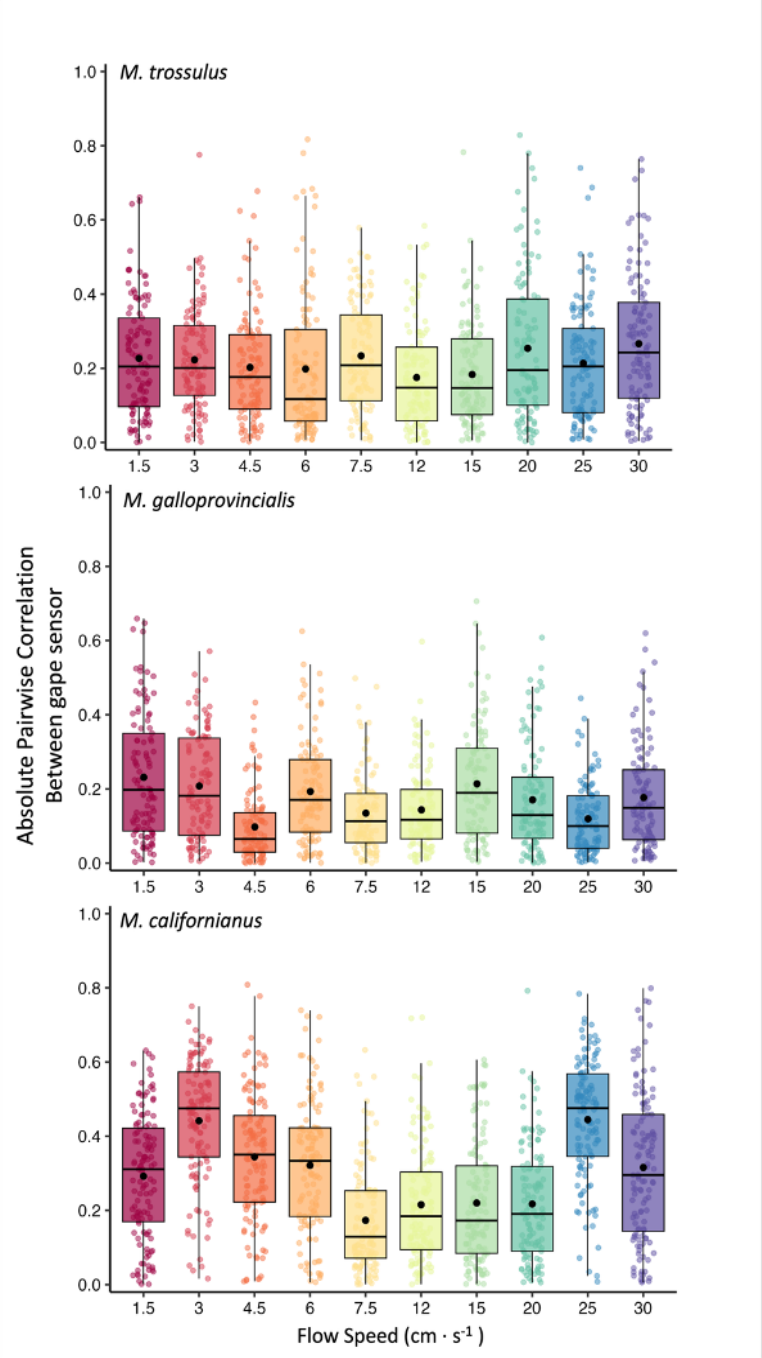

Figure S2. Summary of pairwise correlations (synchrony) of gaping behavior (gape distance-mm) between individuals as a function of flow speed for each mussel species: *Mytilus trossulus* (top), *M. galloprovincialis* (middle) and *M. californianus* (bottom). Each data point is the absolute value of the correlation between two individuals, n = 105-120 unique pairings between 15-16 individuals; each boxplot indicates mean (black dot), median (bar), interquartile range and 95% confidence limits.

Mussel density and flow interact to structure interstitial oxygen and gaping behavior in *Mytilus trossulus* aggregations

Kindall Murie[1,2*], Emily Carrington[1,2*]

[1]University of Washington, Department of Biology, Seattle, WA, United States

[2]University of Washington, Friday Harbor Laboratories, Friday Harbor, WA, United States

Abstract

Mussels are well-known ecosystem engineers that alter both the physical and chemical properties of their surrounding environment. Within aggregations, mussel respiration can drive steep declines in dissolved oxygen (DO), potentially reaching hypoxic levels that negatively affect mussels and associated species. However, flow conditions and aggregation density may interact to shape these chemical modifications, which in turn may alter aspects of mussel behavior. We conducted an eight-day field experiment to test how mussel density within an aggregation influences interstitial DO and gaping behavior under naturally variable flow. Cylindrical aggregations representing three density levels were deployed in the field, each instrumented with DO loggers and Hall-effect gape sensors. DO declined consistently with increasing aggregation density, dropping by more than 4 mg L^{-1}(~ 50%) from ambient in the high-density treatment. Similar to previous laboratory studies, the relationship between DO depletion (ΔDO) and flow speed followed an exponential decay, indicating that oxygen depletion was greatest at low flow speeds (< 4 cm s^{-1}) but had no effect under higher flow conditions. Gaping behavior also varied with density as well as aggregation position: mussels in the interior

of dense aggregations maintained wider gapes and remained open longer than those at the edges, or in low-density aggregations. In contrast, flow speed had little effect on gaping behavior. This study demonstrates that ecosystem engineers, such as mussels, which are often viewed as facilitators that enhance biodiversity, may not always function as such—particularly when high densities and reduced flow create conditions that intensify chemical stress within the habitat.

Introduction

Ecosystem engineers are organisms that modify, maintain, or create habitat through physical or chemical alterations, shaping communities and ecosystem processes (Jones et al., 1994; Ellison et al., 2005; Ellison, 2019). The strength and direction of their influence can be bidirectional and are context-dependent, determined by interactions between environmental conditions and the engineer's traits (e.g., abundance, behavior, size) (Bruno, 2001; Bruno et al., 2003). For example, dense marine macrophyte canopies slow water flow, allowing metabolic processes such as photosynthesis and respiration to generate detectable changes in DO and pH. Under high flow, however, these chemical signals are rapidly flushed and often no longer biologically relevant (Traiger et al., 2021; Chapter 1). In terrestrial systems, ants act as ecosystem engineers, but their net impact on ecological communities depends on both their abundance and behavior. At low colony densities, ants enhance decomposer and herbivore abundance by aerating soils, increasing nutrient turnover, and enriching organic matter through nest-building and waste deposition. At higher densities, however, their predatory behavior dominates, suppressing other arthropods and diminishing these facilitative effects (Sanders & van Veen, 2011; Tomasetti et al., 2023). These examples show how interactions between the engineer, its traits, and/or the surrounding environment can change the way the engineer affects

the local community, where the engineer can go from having positive effects on local species diversity (facilitator) to having no effect, or even shifting to having negative effects (inhibitor).

Few studies have explicitly examined how interactions between an engineer's structural and behavioral traits and its physical and chemical environment determine its capacity to modify the local environment. While the presence or abundance of an ecosystem engineer is often used to predict the magnitude of its environmental impacts, this approach overlooks the potential for feedbacks between behavioral traits (e.g., activity, resource use), structural traits (e.g., density, canopy cover), and the external environment in modulating engineering strength (Stachowicz, 2001). This gap is particularly evident in marine ecosystems, where dynamic environmental gradients (e.g., flow, oxygen, temperature) interact with the structural and behavioral traits of engineers. Our study aims to examine how the hydrodynamic environment and the abundance and behavior of a marine ecosystem engineer shape its capacity to modify its local chemical environment.

Mussels are well-documented ecosystem engineers in coastal marine systems, dominating space on rocky shores, docks, and pilings where they attach to hard substrates and form dense, three-dimensional matrices (Suchanek, 1978, 1979; Seed & Suchanek, 1992; Menge et al., 1976; Menge et al., 2008; Lafferty & Suchanek, 2016). These aggregations provide habitat for diverse assemblages by reducing wave exposure and buffering against thermal and desiccation stress (Arribas et al., 2014; Derksen-Hooijberg et al., 2019). Mussel aggregations also modify local chemistry through respiration and calcification (Nixon et al. 1971; George et al., 2019; Ninokawa et al., 2020. As mussels respire, dissolved oxygen (DO) can decline within the interstitial spaces of the aggregation, at times reaching hypoxic levels (< 2 mg L^{-1}) that may

weaken attachment strength and increase the risk of dislodgement (George et al., 2018, 2019). However, the mechanisms driving these low-oxygen conditions remain unclear, whether they arise primarily from reduced flow, increased aggregation density, or the interaction of both. These chemical changes can also harm other interstitial species, shifting mussels from facilitators to potential inhibitors.

Previous work, including Chapter 2 of this dissertation, quantified how flow speed influences dissolved oxygen (DO) dynamics within the interstitial zone of monolayer mussel aggregations. Oxygen depletion was strongly flow-dependent, with the steepest DO declines at speeds below ~5 cm s^{-1} and diminishing exponentially as flow increased (Chapter 2; Ninokawa et al., 2020). Even at the lowest flow (~1 cm s^{-1}), interstitial DO dropped only 1–2 mg L^{-1} from ambient levels (~8–9 mg L^{-1}), reflecting the high flushing potential and limited biomass of monolayer aggregations, where water circulates freely between individuals, preventing the severe depletion seen in field observations (George et al., 2019). These experiments were conducted under steady, unidirectional flow, which continuously replaces water and limits the time for metabolic modification (Reidenbach et al., 2010). In contrast, natural systems experience variable flow regimes: wave-driven oscillatory flows move water back and forth across aggregations, retaining modified water within aggregations (Koweek et al., 2017; Hirsh et al., 2020; Murie & Bourdeau, 2020), while tidally driven bidirectional currents periodically reverse direction, intermittently flushing and resetting chemical conditions (Chapter 1). Together, these dynamics underscore the need to examine how DO fluctuates within mussel aggregations under naturally variable flow.

Mussels can also actively respond to changing oxygen conditions through behavioral adjustments. They are known to modulate gaping in response to hypoxia and other environmental stressors (e.g., temperature extremes, pollution), often by reducing gaping duration or closing entirely (Shakespeare et al., 2023; Durier et al., 2022; Kong & Sokolova, 2025). During feeding, mussels open their valves and pump water through the mantle cavity, drawing it in through the incurrent siphon and expelling it through the excurrent siphon (Ward & Targett, 1989). This behavior facilitates the exchange of fluids and metabolic byproducts between the mussel and its surroundings (Howard & Cuffey, 2006; Van Duren et al., 2006; Nishizaki & Ackerman 2017) and may help alleviate low-oxygen conditions by promoting mixing between interstitial and overlying water (Riisgård et al., 2014; Crimaldi et al., 2007; Frechette, 2012). However, in Chapter 2, mussels maintained consistently high levels of gaping (>90% time open) even when interstitial DO declined at low flow speeds, suggesting that the modest DO differences observed were not large enough to trigger changes in gaping or pumping behavior. Further research is therefore needed to determine whether stronger oxygen gradients, such as those expected in denser, multilayered aggregations, could elicit behavioral responses.

When exploring how dense mussel aggregations alter local seawater chemistry and, in turn, affect the gaping behavior of mussels within that aggregation, it is also essential to consider a mussel's position in the aggregation. It is well established that mussels experience and respond to distinct microclimates within an aggregation. Mussels positioned along the edge of an aggregation are exposed to greater hydrodynamic and thermal stress, while those in the interior experience more sheltered conditions. For instance, Bell and Gosline (1997) showed that edge mussels produce more byssal threads and exhibit stronger attachment due to increased hydrodynamic loading, whereas interior mussels face lower physical stress. Similarly, Jurgens

and Gaylord (2016, 2018) found that edge mussels were more exposed to thermal extremes and displayed different physiological stress responses than individuals deeper within an aggregation. These positional differences likely extend to dissolved oxygen (DO), with interior mussels experiencing reduced flow and oxygen replenishment compared to those at the edge. Such spatial variation in flow and chemistry may drive differences in gaping behavior, linking aggregation structure and mussel behavior to patterns of chemical modification.

We conducted a field experiment to evaluate how the density of a mussel aggregation modulates local environmental conditions (dissolved oxygen) under natural flow regimes, and whether these environmental changes, in turn, influence how mussels respond behaviorally. Specifically, we first aimed to quantify how dissolved oxygen (DO) in the interstitial zone differs from ambient conditions across mussel aggregations of varying densities as a function of flow speed. Second, we assessed whether gaping behavior varied as a function of mussel density, flow speed, and/or DO concentration. Third, we evaluated whether a mussel's position within the aggregation affects its gaping behavior and response to changes in DO. We predicted that higher mussel densities and lower flow speeds would lead to greater DO drawdown within the aggregation due to increased metabolic demand and reduced water exchange. We also predicted that interior mussels in high-density aggregations, those most isolated from ambient flow, would have one of two potential responses: 1) remain closed more frequently to shelter from intensified chemical stress; or 2) remain open more often to draw in ambient waters to ameliorate chemical stress or to capture more food.

Methods

Experimental overview

We evaluated how mussel aggregation density of the bay mussel (*Mytilus trossulus*) interacts with mussel behavior to affect local seawater chemistry under natural flow conditions by conducting a 21-day experiment off the floating dock of the University of Washington's Friday Harbor Laboratories (San Juan Island, WA). Due to a disturbance on the dock at FHL on June 19th that altered the flow conditions during the experiment, we chose to analyze data from the dates preceding the disturbance, resulting in an 8-day experiment from June 10 to 18, 2024. We constructed cylindrical mussel aggregations inside Vexar mesh caging (mesh size 13mm x 13mm), sealing the top and bottom with plexiglass sheets (Figure 1). We established an aggregation density treatment with three levels based on cylinder diameter measured in mussel shell lengths. Mussels were collected from Penn Cove, Washington, with an average shell length of approximately 6 cm.

The three density levels were: low–2L (two shell lengths wide, 312 mussels), medium–4L (four shell lengths wide, 1,082 mussels), and high–6L (six shell lengths wide, 3,047 mussels; Table 1). The three treatment diameters also allowed us to test for the effect of different mussel positions within each aggregation. In low-2L, mussels formed a single layer, with all individuals occupying the edge of the aggregation. Mussels in medium-4L, occupied both edge and middle positions in the aggregation. In high-6L, mussels occupied three distinct positions within the aggregation: edge, middle, and interior. For our experiment, which were collected from Penn Cove Shellfish Farm (Coupeville, WA) two days before the experiment and transported back to Friday Harbor Laboratories (San Juan Island, WA). We removed any epibionts from the valves before placing them in the density cylinder before the start of the experiment. We randomly

selected mussels for each density cylinder and arranged them so that the anterior (umbo) side of each mussel faced the middle of the cylinder (Figure 1C).

Each density treatment was kept submerged at a constant depth of 1.5 m below the water surface. To control for positional effects, the bags were rotated roughly ever 4-5 days through the experiment so that each one occupied a different location on the dock at least once. We measured flow magnitude and direction at 1 Hz using a TCM-1 tilt current meter (Lowell Instruments LLC. MA, USA) placed midway along the dock between all density treatments.

Chemistry sensors

We embedded a HOBO dissolved oxygen (resolution: ± 0.2 mg L^{-1}, U26-001, Onset, MA, USA) logger in the core of each mussel aggregation treatment, affixing it inside a protective PVC tube with large holes that allowed flow to reach the sensor (Fig 1). We measured ambient conditions by placing a DO sensor within an empty vexar cylinder with the same diameter as the low-2L density cylinder, 2m away from the other density cylinders with mussels. The ambient cylinder also housed a conductivity sensor (U24-002-C, Onset, MA, USA), necessary for adjusting raw DO values for changes in salinity. Dissolved oxygen and conductivity sensors logged data continuously at 1-minute intervals throughout the study. While rotating each density cylinder, we also randomly swapped and rotated all DO sensors within each density cylinder. We calibrated the sensors using the manufacturer's recommended methods and corrected any sensor offset prior to analyses. We excluded the first hour of each following a deployment or repositioning to ensure DO values were stable and representative of each treatment

Measuring gaping behavior and MusselTracker system

We tracked mussel gaping behavior using Allegro A1393 magnetic Hall Effect sensors (Allegro MicroSystems, Worcester, MA, USA) connected to a MusselTracker datalogging system (Miller and Dowd 2017) (Figure 1B). The Hall Effect sensor (hereafter referred to as the 'Hall sensor') can detect the strength and direction of a magnetic field produced by a permanent magnet, and the resulting voltage (mV) can be calibrated to a known distance (mm). Four individual mussels per available aggregation position (edge, middle, interior) within each density level were randomly selected for instrumentation (low-2L: n = 4 [edge only], medium-4L: n = 8 [edge and middle], high-6L: n = 12 [edge, middle, interior]). Each gape sensor was attached to the mussel on the posterior end of one valve of the shell using marine epoxy (Splash Zone, KOP-COAT Inc., Rockaway, NJ, USA), while the magnet (6.35mm x 1.59mm) was placed on the other valve (Figure 1C). We attached sensors and magnets to mussels a day prior to the start of the experiment, allowing the epoxy to set completely. We sampled the gape sensor output, measuring the distance between the valves, every 5 seconds; a sampling rate that our preliminary observations determined to be sufficient for characterizing gape behavior dynamics. At the end of the experiment, we calibrated each gape sensor by severing the adductor muscle to open the mussel and, using calipers, measured the sensor voltage output for valve gapes ranging from 0-20 mm at 1mm intervals (resolution of each gape sensor was < 0.1 mm) and fit an exponential function to the data.

Post-experiment sampling and morphometrics

At the end of the experiment (21 days), we carefully disassembled each density cylinder to count the number of surviving mussels at each aggregation position across all density

treatments. We then calculated the proportion of dead mussels across treatments and aggregation positions. We also measured a subset (n=30) of mussels from each aggregation position for mussel morphometrics (length, width, height, wet weight, dry weight).

Statistical Analyses

We calculated hourly means for dissolved oxygen time series for each of the four density treatment levels (Ambient, low-2L, Medium-4L, High-6L). Because each level served as a single experimental unit with repeated hourly observations, we implemented a design-based permutation framework that included two complementary tests: a Spearman's rank correlation and an omnibus permutation test based on a one-way ANOVA. We assigned density ranks to treatment levels (Ambient = 0, Low-2L = 1, Medium-4L = 2, High-6L = 3) and calculated the Spearman correlation between the density rank and the treatment-level mean DO. We then used all 4! = 24 possible permutations of treatment levels to obtain an exact one-sided *p*-value. For the ANOVA, we treated the observed *F*-statistic as a nonparametric test statistic (used solely to evaluate treatment differences rather than to estimate parameters) and permutated treatment levels across the four units (24 permutations) to generate an exact null distribution of *F*. Finally, we calculated effect sizes changes in mean DO per treatment level and pairwise differences from the Ambient condition. We applied the same analytical approach to mean hourly temperature (°C) across the four treatments.

We tested how mussel gape distance varied among density treatments (Low–2L, Medium–4L, High–6L) and aggregation positions (edge, middle, interior) using linear mixed-effects models (LMMs). To ensure independent biological replication, we first averaged gape distance within each hour for each mussel and then randomly selected one hour per mussel per

day for the duration of the experiment (9 days total). We initially fit a set of mixed models that included individual mussel ID and day as random intercepts, to represent repeated measures across mussels and across days. We then used model selection using Akaike's Information Criterion (AIC) to select best model. Models were fitted using restricted maximum likelihood (REML) in the *lme4* package in R and Type III analyses of variance with Satterthwaite's approximation for denominator degrees of freedom were used to evaluate fixed effects (*lmerTest* package). Model assumptions were evaluated using residual-versus-fitted and Q–Q plots. Post hoc comparisons of estimated marginal means (EMMs) were conducted with the *emmeans* package using Tukey correction. Planned contrasts evaluated: (i) differences among density treatments for edge-position mussels, (ii) differences among aggregation positions within the High–6L treatment, and (iii) differences among the aggregation positions closest to dissolved oxygen sensors across densities (Low-edge, Medium-middle, High-interior).

To evaluate how flow speed influenced dissolved oxygen (ΔDO) among mussel aggregations, we compared multiple nonlinear and linear models describing ΔDO as a function of flow speed (U, cm s^{-1}). For each mussel density treatment level (Low–2L, Medium–4L, High–6L), mean ΔDO was first binned into 12 adaptive flow intervals (bins 1-2 cm wide, ranging 0-20 cm s^{-1}), and bin means (± SE) were used for model fitting. Parameters of the best model were fit to bin-averaged data for each density treatment level using nonlinear least squares (nls). To quantify uncertainty, 800 parametric bootstrap samples were performed by resampling within each adaptive bin, refitting the model to each bootstrap replicate, and recalculating the fitted curve and parameters. Median bootstrapped coefficients and 95 % confidence intervals (CI) were extracted for each parameter. For each fitted model, we also report parameter standard errors (SE), *t*-values, *p*-values, and pseudo-R^2 values computed as $1 - (SS_{res}/SS_{tot})$.

We examined how mussel gape distance varied with flow speed by fitting linear models to bin-averaged data pooled across all sensors within each density treatment level. Gape distance and flow speed were averaged within 12 adaptive flow bins prior to model fitting. The model tested whether both the intercepts (baseline gape at zero flow) and slopes (change in gape per cm s^{-1}) differed among density treatment levels. Differences in model-adjusted intercepts and slopes were evaluated using estimated marginal means (EMMs; *emmeans* package), and pairwise contrasts were used to test for significant differences among treatment levels. Non-overlapping 95% confidence intervals were interpreted as evidence of significant differences in treatment levels. To assess the relationship between mussel gape distance and the magnitude of oxygen depletion within aggregations, we fit a simple linear regression between mean gape distance (mm) and mean ΔDO (mg L^{-1}, ambient – within aggregation) across all treatment levels combined. Both ΔDO and gape values were taken from bin-averaged means used in the ΔDO–flow analyses.

To evaluate how flow speed influenced the proportion of time mussels remained gaping, we used generalized linear models (GLMs) with a Gamma error distribution and log link function, appropriate for continuous, positive, and right-skewed proportional data (Bolker et al., 2009; Brooks et al., 2017). Each GLM included flow speed, density treatment level (Low–2 L, Medium–4 L, High–6 L), and their interaction as fixed effects. Separate models were run for (1) mussels positioned closest to each dissolved oxygen (DO) sensor (i.e., edge of low-2L, middle of medium-4L, and interior of high-6L densities) and (2) mussels located only along the edges of each density treatment level. For each analysis, data were first averaged at the sensor level within each adaptive flow-speed bin (same bins used above). The resulting values represented the mean proportion of time mussels remained gaping for each individual sensor across similar flow

conditions. These sensor-level means were then averaged across mussels within the same aggregation position and density treatment level to obtain a single treatment-level mean (± SE) for each flow-speed bin. Pairwise comparisons among density treatment levels were conducted using Tukey-adjusted contrasts of estimated marginal means (EMMs) from the fitted GLMs (R package *emmeans*).

Results

Mortality at the end of the total 21 days ranged from 14-23%, except for the interior, which was approximately twice as high (39%). Dissolved oxygen (DO) declined consistently with increasing mussel density, with the most pronounced reductions and fluctuations occurring in the high-density (6 L) treatment (Figure 2A–C). High-density aggregations showed larger diel swings and lower overall oxygen levels compared to the medium-, low-, and ambient-density treatments, indicating that the denser the aggregation, the stronger the oxygen depletion and the slower the reoxygenation over time. The ordered permutation test based on Spearman's rank correlation resulted in a perfect monotonic association between density rank and mean DO ($\rho = -1.00$, exact one-sided $p < 0.05$). The omnibus permutation test using one-way ANOVA produced an $F = 526.45$ with an exact right-tailed $p = 0.83$. Despite the low statistical power of our design, the effect of treatment level was large: mean DO declined by more than 50% from ambient to the high-6L density treatment. Mean hourly temperature (°C) remained consistent across density treatments, ranging from 10.5 °C to 10.6 °C across treatments (Figure S1).

Mussel gape distance varied with mussel density and aggregation position. AIC model selection indicated that the best model included density treatment and aggregation position as fixed effects, along with a random intercept for individual mussels (Table S1A). Including day as

a random effect did not improve model fit (ΔAIC = 2), indicating minimal day-to-day variation relative to individual-level differences.

Using the best-supported model, gape distance increased significantly from Low–2L to Medium–4L and from Low–2L to High–6L among mussels located at aggregation edges (Table S1B(i); both $p < 0.004$), whereas gape distance did not differ between Medium–4L and High–6L edge mussels ($p = 0.85$). Within the High–6L aggregation, gape distance was significantly greater in interior mussels compared to edge mussels (Table S1B(ii); $p < 0.05$), while differences between edge–middle and middle–interior positions were not statistically significant ($p = 0.59$ and $p = 0.33$, respectively). Comparisons of aggregation positions closest to the DO sensors showed that gape distance increased consistently with density: gape was significantly greater in Medium-middle mussels than Low-edge, greater in High-interior than Medium-middle, and greatest in High-interior compared to Low-edge mussels (Table S1B(iii); all $p < 0.0001$).

Across all mussel density treatment levels, the relationship between ΔDO (ambient – within aggregation) and flow speed followed an exponential decay pattern, with ΔDO decreasing sharply under low flow (< 4 cm s^{-1}) and asymptotically approaching a steady offset at higher flow speeds (Fig. 4; Table 3). Although the rate of decline (parameter *b*) was similar among treatments (0.24–0.28; $p < 0.05$), the magnitude of ΔDO differed substantially with mussel density (parameter *c*). The high (6L) treatment exhibited the greatest overall DO drawdown, with ΔDO > 3 mg L^{-1} even at flow speeds above 10 cm s^{-1}. In contrast, both medium (4 L) and low (2L) treatments showed lower initial DO differences and asymptotes near or below 1 mg L^{-1}. These results indicate that while all aggregations respond similarly to increasing flow, the magnitude of DO depletion within the aggregation scales strongly with mussel density, with high-density aggregations maintaining persistently lower DO levels across all flow regimes.

Mussels positioned nearest the dissolved-oxygen sensors (High: interior; Medium: middle; Low: edge) showed distinct baseline gape distances that were mainly maintained across the range of flow speeds (Fig. 5A). There was a significant flow × treatment interaction ($F_{2,33}$ = 4.65, p = 0.017), reflecting small slope differences, but gape increased only slightly with speed in all groups (slopes ≤ 0.04 mm per cm s^{-1}). The dominant pattern was a strong difference in intercepts ($F_{2,33}$ = 1773.0, p < 0.001): High density (6L) mussels held the widest openings (mean ± SE ≈ 5.81 ± 0.06 mm), whereas Medium (4L) and Low (2L) density mussels remained nearly closed (1.77 ± 0.06 mm and 0.93 ± 0.06 mm). Intercept differences were significant for all pairwise comparisons (Tukey p < 0.001). Overall, gape behavior was largely density-driven, with flow exerting a minor, positive effect (Fig. 5).

Mussels gaped wider as the difference in dissolved oxygen (ΔDO) between the aggregation and ambient water increased ($F_{1,37}$ = 59.06, p < 0.001, R^2 = 0.61; Fig. 5B). Mussels in the interior of the high-density treatment level consistently exhibited the widest gape, while those in the middle of the medium-density and at the edge of the low-density treatment levels remained more constricted (~2 mm). Within each density treatment level, gape distance did not increase further with larger ΔDO values; even when oxygen inside the aggregation was 4–6 mg L^{-1} lower than ambient, gaping remained relatively constant. When examining mussels located along the edges of each density treatment level (Fig. 5D), gape behavior was more uniform; edge mussels maintained similar gape distances regardless of aggregation density. This contrasted with the strong density-dependent differences observed for mussels positioned near the dissolved oxygen sensors, where gape distance varied markedly among treatments (Figure 5B and D).

The proportion of time mussels remained open varied significantly among density treatment levels but changed little with flow speed (Fig. 6; Table2). For mussels positioned

nearest the DO sensors—representing the interior of high-density aggregation, the middle of medium-density aggregation, and the edge of low-density aggregation—density treatment had a strong effect ($\chi^2 = 1.87$, df = 2, $p < 0.001$), whereas neither flow speed ($\chi^2 = 0.02$, df = 1, $p = 0.46$) nor its interaction with density ($\chi^2 = 0.09$, df = 2, $p = 0.27$) were significant. Mussels in the interior of the high-density (6 L) treatment level remained open nearly continuously (> 90 % of the time) across all flow speeds, those in the middle of the medium-density (4 L) treatment level were open ~85–90 % of the time, and mussels at the edge of low-density (2 L) treatment levels were open ~70 %, spending less time open overall. Pairwise contrasts confirmed that low-density mussels differed significantly from both medium and high densities (Tukey HSD, $p < 0.001$), whereas medium and high did not (Tukey HSD, $p = 0.38$).

When focusing on mussels located along the outer edges of each density treatment (Fig. 6B), patterns were similar. The effect of density remained significant (Table S2: $\chi^2 = 1.36$, df = 2, $p < 0.001$), while flow speed ($p = 0.92$) and the interaction ($p = 0.12$) were not. Edge mussels in high-density aggregations remained open ~93% of the time, those in medium-density aggregations ~87%, and those in low-density aggregations ~71%. Tukey-adjusted contrasts showed significant differences between low- and both higher-density treatment levels ($p < 0.001$), but no difference between medium- and high-density treatment levels ($p = 0.27$).

Discussion

Dissolved oxygen (DO) declined sharply within mussel aggregations relative to ambient water, with both the magnitude and variability of oxygen depletion increasing with aggregation density. High-density (6L) aggregations exhibited the lowest DO concentrations, the largest diel

fluctuations, and frequent hypoxic events, whereas DO in medium- and low-density aggregations remained 2–3 mg L^{-1} higher on average. These patterns indicate that oxygen loss within the interstitial zone was strongly driven by mussel respiration and that density and flow together governed the extent of DO depletion. Gaping behavior varied across densities and aggregation positions but remained relatively stable with short-term changes in flow or DO within a treatment. Mussels in denser aggregations gaped wider and spent more time open than those in low-density treatments, and interior mussels consistently showed the widest openings, suggesting that mussel gaping behavior differs spatially within an aggregation due local flow and DO conditions. Collectively, these findings demonstrate that structural traits such as density amplify oxygen depletion, flow modulates the magnitude and persistence of changes in oxygen driven by the mussel, and behavior varies with density and position but provides only limited buffering against low-oxygen conditions.

The relationship between DO and flow speed we observed in natural flow conditions followed an exponential decay pattern, consistent with previous flume experiments (Chapter 2; Ninokawa et al., 2020). In both studies, the steepest DO declines occurred under low flow speeds (< 5 cm s^{-1}), with depletion leveling off as flow increased. The fitted parameters for a monolayer aggregation of *M. trossulus* in Chapter 2 (a = 3.04, b = 0.31) closely matched those for the low-density (2L) treatment in this field experiment (a = 1.10, b = 0.24), indicating that the rate of decline with flow (parameter b) was similar between experiments. This similarity suggests that the physical processes controlling oxygen exchange in monolayer aggregations operate consistently across systems. However, the overall magnitude of DO depletion (parameter a) was roughly threefold greater in the flume experiment, likely reflecting differences in aggregation structure and mussel abundance (Chapter 2's monolayer contained ~1000 mussels compared to

~300 in this study's low-density treatment). Additional differences may have arisen from how flow interacts with aggregation geometry, as the flume's flat monolayer experienced steady unidirectional flow, while the cylindrical aggregations in the field were exposed to unsteady, multidirectional tidal currents that enhanced flushing. At higher densities, DO depletion remained substantially greater across all flow regimes, with ΔDO values exceeding 3 mg L^{-1} even at flow speeds above 10 cm s^{-1}, approximately three and two times higher than in the low- and medium-density treatments, respectively. These results show that while the relationship between flow and DO is consistent across laboratory and field experiments for monolayer aggregations, increasing aggregation density amplifies the magnitude of oxygen depletion. This pattern reinforces that mussel aggregations function as scale-dependent ecosystem engineers whose biogeochemical influence expands with increasing biomass (George et al., 2019; Albertson et al., 2024).

Gape distance increased with mussel density and varied across aggregation positions, showing that local crowding and microenvironmental conditions influence individual behavior. Interior mussels in dense aggregations gaped wider than those at the edges, as reduced flow and lower oxygen levels in the interior promote wider openings to maintain pumping, feeding, and respiration (Jørgensen et al., 1988). In contrast, edge mussels showed only modest changes across densities, with gape distance increasing slightly from low to medium density and then declining at the highest density. The similarity in edge behavior across density treatment levels emphasizes the importance of microhabitat position within an aggregation, as individuals at the periphery are more closely coupled to ambient hydrodynamics, while those in the interior are subject to reduced flow and more extreme biogeochemical conditions (Bell & Gosline, 1997; Jurgens & Gaylord, 2016, 2018). Another explanation for the wider gaping of interior mussels is

increased competition for food within dense aggregations. Mussels near the interior must remain open longer and filter more water because upstream neighbors intercept food particles, reducing food availability downstream (Fréchette & Bourget, 1985; Pilditch & Grant 1999; Fréchette et al. 1989).

Within an aggregation density, mussel gape distance changed little with flow speed, increasing only slightly at higher velocities (~0.04 mm per cm s^{-1}). Gape distance also increased with larger differences in DO between the aggregation and ambient water (ΔDO), but this relationship was weak and plateaued even when oxygen inside the aggregation dropped 4–6 mg L^{-1} below ambient. These patterns suggest that within a given aggregation, short-term variation in flow and DO has little influence on gape behavior. However, across densities, consistent differences in gape distance likely arise because increasing mussel biomass alters flow and oxygen conditions within the aggregation. As a result, it is difficult to separate whether behavioral differences stem primarily from a mussel's position within the aggregation or from the reduced flow and lower DO associated with higher densities.

Although gaping behavior did not change substantially with changes in flow or DO within a given density treatment over the eight-day experiment, it is important to note the high mortality rates across each density treatment after the total 21 days. During these 21 days, DO conditions across treatments retained the same patterns as those experienced in the first 8 days (except for the disturbance on the dock between June 19-21). Mortality among interior mussels was nearly twice that of other positions (39% vs. 14–23%), suggesting that sustained opening under low oxygen stress may be energetically costly or ineffective in restoring oxygen levels. Because gaping behavior was analyzed only during the first eight days, whereas mortality was

assessed after 21 days, the timing of these effects remains uncertain and warrants further research. Another potential explanation for prolonged gaping is muscle fatigue or an inability to close valves under persistent oxygen stress (Riisgård & Larsen, 2015). However, such effects are unlikely to develop within the initial eight-day observation period, but could potentially help explain differences in mortality across density treatments.

Across all treatments, mussels spent a high proportion of time open (>85%), consistent with Chapter 2 and previous studies showing that *Mytilus* maintains near-continuous gaping even under conditions that are predicted to be stressful (Miller & Dowd, 2017; Bertolini et al., 2021). The persistent gaping suggests that mussels continued pumping even under fluctuating DO levels, rather than behaviorally reducing metabolism through valve closure. In contrast, laboratory experiments on *M. edulis* have shown that mussels close their valves when DO drops below ~2 mg L^{-1} (Tang & Riisgård, 2018; Kong & Sokolova, 2025), indicating that full closure is typically a response to extreme, prolonged hypoxia. However, the hypoxic conditions held in the laboratory study were not sustained in our field experiment. In the high-density treatment, hypoxia occurred ~25% of the time during the 8-day observation period; however, individual hypoxic events were brief, averaging less than 20 minutes, with the longest hypoxic event lasting 4 hours. The dynamic, tidally driven flow regime around the dock provided intermittent flushing that limited the duration of low-oxygen exposure, allowing mussels to remain open without incurring lethal stress.

Despite the generally high levels of gaping activity, subtle positional differences in aggregation emerged in time spent open. Mussels on the edges of aggregations spent less time open (~70–75%) than those in middle or interior positions (~85–90%). This pattern likely

reflects differences in local flow and mechanical exposure: edge mussels experience higher velocities and shear stress, which can impose greater energetic costs or necessitate brief closures to reduce drag or prevent dislodgement (Bell & Gosline, 1997; Carrington et al., 2008). In contrast, interior mussels are shielded from these forces and may sustain longer feeding bouts to compensate for lower food and oxygen availability. The lack of strong flow effects across treatments also mirrors results from Chapter 2, where mussels remained open for more than 90% of the time across a range of flow speeds, indicating that gaping behavior in *M. trossulus* is relatively insensitive to short-term fluctuations in flow velocity.

The interactions among flow, DO, and gaping behavior reveal how physical and biological processes together shape oxygen dynamics within mussel aggregations. Low flow promotes oxygen depletion, particularly in dense aggregations where reduced mixing limits reoxygenation. In our experiment, gape distance increased only slightly with flow across all densities, and the proportion of time open remained high and constant, indicating that mussels did not substantially alter their behavior in response to changing flow speeds or DO levels, either within or across aggregation positions. Thus, while behavior may influence small-scale mixing, its compensatory effect is limited under the structural constraints imposed by high-density, multilayered aggregations. For example, once oxygen concentrations drop within the interstitial zone, diffusion and advection become restricted by the physical packing of shells, preventing efficient replenishment of oxygenated water. Under these conditions, external hydrodynamic flushing remains the dominant mechanism restoring oxygen within aggregations. The exponential relationship between flow and ΔDO observed here, coupled with the weak behavioral response, suggests that beyond a threshold velocity of approximately 5–8 cm s^{-1}, physical transport processes override biological control of interstitial oxygen levels.

Mussel density, flow, and behavior collectively influence interstitial oxygen dynamics, but their relative contributions differ. Density determines the magnitude and persistence of oxygen depletion, flow governs oxygen renewal, and behavior adds only minor, localized variability, particularly in dense aggregations where physical structure limits water exchange. These findings reinforce that the ecological role of mussels as ecosystem engineers depends on both environmental context and structural traits. Future studies should build on this work by examining how aggregation density and local hydrodynamics shape mussels' capacity to act as facilitators of diversity versus creators of chemically stressful habitats (Bruno et al., 2003; George et al., 2019). Because behavioral responses played a minimal role relative to density and flow, identifying the physical thresholds at which mussel aggregations shift from biologically driven to physically constrained systems will be key to predicting when and where they transition along this facilitation–inhibition continuum.

Acknowledgements

Lauren Strope and other Miller Lab members provided expert help and guidance in developing the gape sensor system. Thank you, Lara Hsia, Grace Leuchtenberger, Ava Martin,

and Eleanor Rollins for assisting with gape sensor construction. Penn Cove Shellfish LLC supplied mussels. The staff at UW Friday Harbor Laboratories offered timely logistical support. Jack Litle, Sonia Litle, Grace Leuchtenberger, Alli Cramer, Matt Reidenbach and Kelsey O'Donnell gave helpful feedback throughout the research process, and Jennifer Ruesink and Tom Daniel improved the manuscript with their comments.

Author contributions

KM and EC led the conceptual development of the study. KM designed the methodology, curated and analyzed the data, produced all graphical visualizations, drafted the original manuscript, addressed co-authors' revisions, and helped secure project funding. EC contributed to manuscript review and editing and secured project funding.

Funding

The author(s) declare that financial support was received for the research, authorship, and/or publication of this article. All aspects of the research were supported by the National Science Foundation (OCE-2050273 awarded to EC). Funding for chemical sensors and computers was provided by University of Washington Student Technology Fee (STF: 2021-33, awarded to EC and KM). KM received funding for laboratory space, housing, travel, and logistical support from UW Friday Harbor Laboratories via the Frederic H. and Kristin C. Nichols Endowed Graduate Fellowship, Emily Carrington Endowed Student Travel Support Fund, and University of Washington Biology Department awards via Friday Harbor Laboratories Award and Hoag Award.

References

Ackerman, J. D. & Nishizaki, M. T. 2004. The effect of velocity on the suspension feeding and growth of the marine mussels Mytilus trossulus and M. californianus: implications for niche separation. *J. Mar. Syst.* 49:195–207.

Albertson, L.K., Sklar, L.S., Tumolo, B.B., Cross, W.F., Collins, S.F. and Woods, H.A., 2024. The ghosts of ecosystem engineers: Legacy effects of biogenic modifications. *Functional Ecology,* 38(1), pp.52-72.

Arribas, L. P., Donnarumma, L., Palomo, M. G., & Scrosati, R. A. (2014). Intertidal mussels as ecosystem engineers: their associated invertebrate biodiversity under contrasting wave exposures. *Marine Biodiversity*, 44(2), 203-211.

Bell, E.C. and Gosline, J.M., 1997. Strategies for life in flow: tenacity, morphometry, and probability of dislodgment of two Mytilus species. *Marine Ecology Progress Series*, 159, pp.197-208.

Bertolini, C., Rubinetti, S., Umgiesser, G., Witbaard, R., Bouma, T. J., Rubino, A. & Pastres, R. 2021. How to cope in heterogeneous coastal environments: spatio-temporally endogenous circadian rhythm of valve gaping by mussels. *Sci. Total Environ.* 768:145085.

Bolker, B. M., Brooks, M. E., Clark, C. J., Geange, S. W., Poulsen, J. R., Stevens, M. H. H. & White, J. S. S. 2009. Generalized linear mixed models: a practical guide for ecology and evolution. *Trends Ecol. Evol.* 24:127–135.

Brooks, M. E., Kristensen, K., Van Benthem, K. J., Magnusson, A., Berg, C. W., Nielsen, A. & Bolker, B. M. 2017. glmmTMB balances speed and flexibility among packages for zero-inflated generalized linear mixed modeling. R J. 9:378–400.

Bruno, J. F. 2001. Habitat modification and facilitation in benthic marine communities. In Marine Community Ecology (Bertness, M. D., Gaines, S. D. & Hay, M. E., Eds.). Sinauer, Sunderland, MA, pp. 201–218.

Bruno, J. F., Stachowicz, J. J. & Bertness, M. D. 2003. Inclusion of facilitation into ecological theory. *Trends Ecol. Evol.* 18:119–125.

Carrington, E., Moeser, G. M., Thompson, S. B., Coutts, L. C. & Craig, C. A. 2008. Mussel attachment on rocky shores: the effect of flow on byssus production. *Integr. Comp. Biol.* 48:801–807.

Crimaldi, J. P., Koseff, J. R. & Monismith, S. G. 2007. Structure of mass and momentum fields over a model aggregation of benthic filter feeders. Biogeosciences 4:269–282.

Derksen-Hooijberg, M., Angelini, C., Hoogveld, J.R., Lamers, L.P., Borst, A., Smolders, A., Harpenslager, S.F., Govers, L.L. and van der Heide, T., 2019. Repetitive desiccation events weaken a salt marsh mutualism. *Journal of Ecology,* 107(5), pp.2415-2426.

Durier, G., Nadalini, J.B., Comeau, L.A., Starr, M., Michaud, S., Tran, D., St-Louis, R., Babarro, J.M., Clements, J.C. and Tremblay, R., 2022. Use of valvometry as an alert tool

to signal the presence of toxic algae Alexandrium catenella by Mytilus edulis. *Frontiers in Marine Science,* 9, p.987872.

Ellison, A. M. 2019. Foundation species, non-trophic interactions, and the value of being common. *Science* 13:254–268.

Ellison, A. M., Bank, M. S., Clinton, B. D., Colburn, E. A., Elliott, K., Ford, C. R. et al. 2005. Loss of foundation species: consequences for the structure and dynamics of forested ecosystems. *Front. Ecol. Environ.* 3:479–486.

Fréchette, M. 2012. A model of clearance rate regulation in mussels. *J. Sea Res.* 73:32–40.

Fréchette, M. & Bourget, E. 1985. Food-limited growth of Mytilus edulis L. in relation to the benthic boundary layer. *Can. J. Fish. Aquat. Sci.* 42:1166–1170.

Fréchette, M., Butman, C. A. & Geyer, W. R. 1989. The importance of boundary-layer flows in supplying phytoplankton to the benthic suspension feeder, Mytilus edulis L. *Limnol. Oceanogr.* 34:19–36.

George, M. N., Pedigo, B. & Carrington, E. 2018. Hypoxia weakens mussel attachment by interrupting DOPA cross-linking during adhesive plaque curing. *J. R. Soc. Interface* 15:20180489.

George, M. N., Andino, J., Huie, J. & Carrington, E. 2019. Microscale pH and dissolved oxygen fluctuations within mussel aggregations and their implications for mussel attachment and raft aquaculture. *J. Shellfish Res.* 38:795–809.

Hirsh, H. K., Nickols, K. J., Takeshita, Y., Traiger, S. B., Mucciarone, D. A., Monismith, S. & Dunbar, R. B. 2020. Drivers of biogeochemical variability in a central California kelp forest: implications for local amelioration of ocean acidification. *J. Geophys. Res. Oceans* 125:e2020JC016320.

Howard, J. K. & Cuffey, K. M. 2006. The functional role of native freshwater mussels in the fluvial benthic environment. *Freshw. Biol.* 51:460–474.

Jurgens, L. J., & Gaylord, B. (2016). Edge effects reverse facilitation by a widespread foundation species. Scientific Reports, 6(1), 37573.

Jurgens, L.J. and Gaylord, B., 2018. Physical effects of habitat-forming species override latitudinal trends in temperature. *Ecology Letters,* 21(2), pp.190-196.

Jones, C. G., Lawton, J. H. & Shachak, M. 1994. Organisms as ecosystem engineers. *In Ecosystem Management* (pp. 130–147). Springer, New York.

Jørgensen, C.B., Larsen, P.S., Møhlenberg, F. and Riisgård, H.U., 1988. The mussel pump: properties and modeling. *Marine Ecology Progress Series,* 45, pp.205-216.

Kong, H. & Sokolova, I. M. 2025. Effects of hypoxia and anoxia on the reproductive performance of the blue mussel Mytilus edulis. *Sci. Total Environ.* 972:179103.

Koweek, D.A., Nickols, K.J., Leary, P.R., Litvin, S.Y., Bell, T.W., Luthin, T., Lummis, S., Mucciarone, D.A. and Dunbar, R.B., 2017. A year in the life of a central California kelp forest: physical and biological insights into biogeochemical variability. *Biogeosciences*, 14(1), pp.31-44.

Lafferty, K. D. & Suchanek, T. H. 2016. Revisiting Paine's 1966 sea star removal experiment, the most-cited empirical article in *The American Naturalist. Am. Nat.* 188:365–378.

Lenth, R. V. 2024. emmeans: Estimated marginal means, aka least-squares means. R package version 1.10.2. https://CRAN.R-project.org/package=emmeans.

Menge, B. A. 1976. Organization of the New England rocky intertidal community: role of predation, competition, and environmental heterogeneity. *Ecol. Monogr*. 46:355–393.

Menge, B. A., Chan, F. & Lubchenco, J. 2008. Response of a rocky intertidal ecosystem engineer and community dominant to climate change. *Ecol. Lett.* 11:151–162.

Miller, L. P. & Dowd, W. W. 2017. Multimodal in situ datalogging quantifies inter-individual variation in thermal experience and persistent origin effects on gaping behavior among intertidal mussels (Mytilus californianus). *J. Exp. Biol.* 220:4305–4319.

Murie, K. A. & Bourdeau, P. E. 2020. Fragmented kelp forest canopies retain their ability to alter local seawater chemistry. *Sci. Rep.* 10:1–13.

Ninokawa, A., Takeshita, Y., Jellison, B. M., Jurgens, L. J. & Gaylord, B. 2020. Biological modification of seawater chemistry by an ecosystem engineer, the California mussel, Mytilus californianus. *Limnol. Oceanogr.* 65:157–172.

Nishizaki, M. & Ackerman, J. D. 2017. Mussels blow rings: jet behavior affects local mixing. *Limnol. Oceanogr.* 62:125–136.

Nixon, S. W., Oviatt, C. A., Rogers, C. & Taylor, K. 1971. Mass and metabolism of a mussel bed. *Oecologia* 8:21–30.

Pilditch, C. A. & Grant, J. 1999. Effect of variations in flow velocity and phytoplankton concentration on sea scallop (Placopecten magellanicus) grazing rates. *J. Exp. Mar. Biol. Ecol.* 240:111–136.

R Core Team. 2022. R: A language and environment for statistical computing. R Foundation for Statistical Computing, Vienna, Austria.

Reidenbach, M.A., Limm, M., Hondzo, M. and Stacey, M.T., 2010. Effects of bed roughness on boundary layer mixing and mass flux across the sediment-water interface. *Water Resources Research,* 46(7).

Riisgård, H. U. & Larsen, P. S. 2015. Physiologically regulated valve-closure makes mussels long-term starvation survivors: test of hypothesis. *J. Molluscan Stud.* 81:303–307.

Sanders, D. and van Veen, F.F., 2011. Ecosystem engineering and predation: The multi-trophic impact of two ant species. *Journal of Animal Ecology,* 80(3), pp.569-576.

Seed, R. & Suchanek, T. H. 1992. Population and community ecology of Mytilus. In The Mussel Mytilus: Ecology, Physiology, Genetics and Culture (Eds. E. Gosling). *Elsevier,* pp. 87–170.

Shakspeare, A., Moore, H., Service, M., Wilson, C., Ahmed, H., Cameron, T. C. & Steinke, M. 2023. Gaping behaviour of Blue mussels (Mytilus edulis) in relation to freshwater runoff risks. *Aquaculture Reports* 33: 101719.

Stachowicz, J. J. 2001. Mutualism, facilitation, and the structure of ecological communities. *Bioscience* 51:235–246.

Suchanek, T. H. 1978. The ecology of Mytilus edulis L. in exposed rocky intertidal communities. J. Exp. *Mar. Biol. Ecol.* 31:105–120.

Suchanek, T. H. 1979. The Mytilus californianus community: studies on the composition, structure, organization, and dynamics of a mussel bed. Univ. Washington, Ph.D. thesis.

Tang, B. & Riisgård, H. U. 2018. Relationship between oxygen concentration, respiration and filtration rate in blue mussel Mytilus edulis. J. *Oceanol. Limnol.* 36:395–404.

Tomasetti, S. J., Doall, M. H., Hallinan, B. D., Kraemer, J. R. & Gobler, C. J. 2023. Oyster reefs' control of carbonate chemistry—implications for oyster reef restoration in estuaries subject to coastal ocean acidification. *Glob. Change Biol.* 29:6572–6590.

Traiger, S. B., Cohn, B., Panos, D., Daly, M., Hirsh, H. K., Martone, M. et al. 2021. Limited biogeochemical modification of surface waters by kelp forest canopies: influence of kelp metabolism and site-specific hydrodynamics. *Limnol. Oceanogr.*

Van Duren, L. A., Herman, P. M., Sandee, A. J. & Heip, C. H. 2006. Effects of mussel filtering activity on boundary layer structure. *J. Sea Res*. 55:3–14.

Ward, J.E. and Targett, N.M., 1989. Influence of marine microalgal metabolites on the feeding behavior of the blue mussel Mytilus edulis. *Marine Biology,* 101(3), pp.313-321.

Tables and Figures

Table 1. Experimental parameters and mussel morphometrics across density treatments. A) Summary of experimental parameters, by density treatment and aggregation position within density treatment. (B) Morphometric data were taken at the end of the experiment across all density treatments (n = 30 per treatment).

A) Experimental parameters

By treatment	Low-2L	Medium-4L		High-6L		
# mussels	312	1528		3047		
Proportion of mussels dead	0.18	0.18		0.20		
Total Bed Biomass (kg)	0.78	1.68		2.94		
By position within treatment	**Edge**	**Edge**	**Middle**	**Edge**	**Middle**	**Interior**
# mussels	312	1082	446	1375	1239	433
Proportion of mussels dead	0.18	0.16	0.23	0.14	0.19	0.39
Mussels w/ gape sensors at end	3	4	2	3	2	4
B) Mussel Morphometrics (mean± SD: n=30)						
Length (mm)	59.2 (±0.8)	57.4 (±0.8)	55.7 (±1.0)	57.8 (±0.9)	58.3 (±0.9)	59.1 (±0.8)
Width (mm)	20.1 (±0.5)	20.9 (±1.3)	18.9 (±0.4)	18.9 (±0.3)	19.8 (±0.5)	19.6 (±0.3)
Height (mm)	25.4 (±0.4)	24.7 (±0.4)	26.6 (±1.1)	25.1 (±0.4)	25.9 (±0.4)	24.7 (±0.5)
Dry Body Weight (g)	1.2 (±0.1)	1.1 (±0.1)	1.2 (±0.1)	1.1 (±0.1)	1.0 (±0.1)	1.1 (±0.1)

Table 2. Summary of the best-fitting linear mixed-effects model (LMM) describing gape distance as a function of density treatment and aggregation position. The response variable is the gape distance from one randomly selected hour per mussel per day (9 days total). Fixed effects include density treatment (Low–2L, Medium–4L, High–6L) and aggregation position (edge, middle, interior). Individual mussels were used as a random intercept to account for repeated measurements of individual mussels. Num DF = numerator degrees of freedom; Den DF = denominator degrees of freedom.

Table 3. Summary of model fits describing the nonlinear relationship between the difference in dissolved oxygen (ΔDO, mg L^{-1}) and flow speed (U, cm s^{-1}) across mussel density treatments. The model is an exponential decay with offset: $a \times \exp^{(-b \times U)} + c$. Flow speeds were binned into

Fixed Effects	Sums of squares	Mean of Squares	Num DF	Den DF	F-value	P-value
Density treatment	47.86	23.93	2	155.33	14.40	<0.0001
Aggregation position	95.47	47.74	2	120.24	28.73	<0.0001
		Random Effect		Variance		Std.Dev
		ind. mussel (intercept)		2.96		1.72
		Residuals		1.66		1.29

12 adaptive intervals (see main text). Parameter estimates (a, b, c) are shown with standard errors (SE), t-values, p-values, and bootstrapped 95 % confidence intervals (CI). R^2 indicates the pseudo-R^2 of the fitted model.

Density	Parameter	Estimate	SE	t-value	p-value	(95% CI)	R^2
Large	a	4.54	0.76	6.01	0.0003	5.65 [5.37–5.92]	
(6L)	b	0.28	0.09	3.16	0.01	0.3 3[0.29–0.36]	0.86
	c	2.09	0.24	8.85	<0.0001	2.10 [1.91–2.28]	
Medium	a	3.48	0.32	11.00	<0.0001	4.28 [4.05–4.49]	
(4L)	b	0.24	0.05	5.26	<0.0001	0.29 [0.28–0.31]	0.91
	c	0.61	0.12	4.96	0.001	0.64 [0.60–0.68]	
Small	a	1.10	0.10	10.60	<0.0001	1.39 [1.29–1.50]	
(2L)	b	0.24	0.05	5.10	0.001	0.33 [0.30–0.36]	0.89
	c	0.05	0.04	1.32	0.225	0.09 [0.07–0.11]	

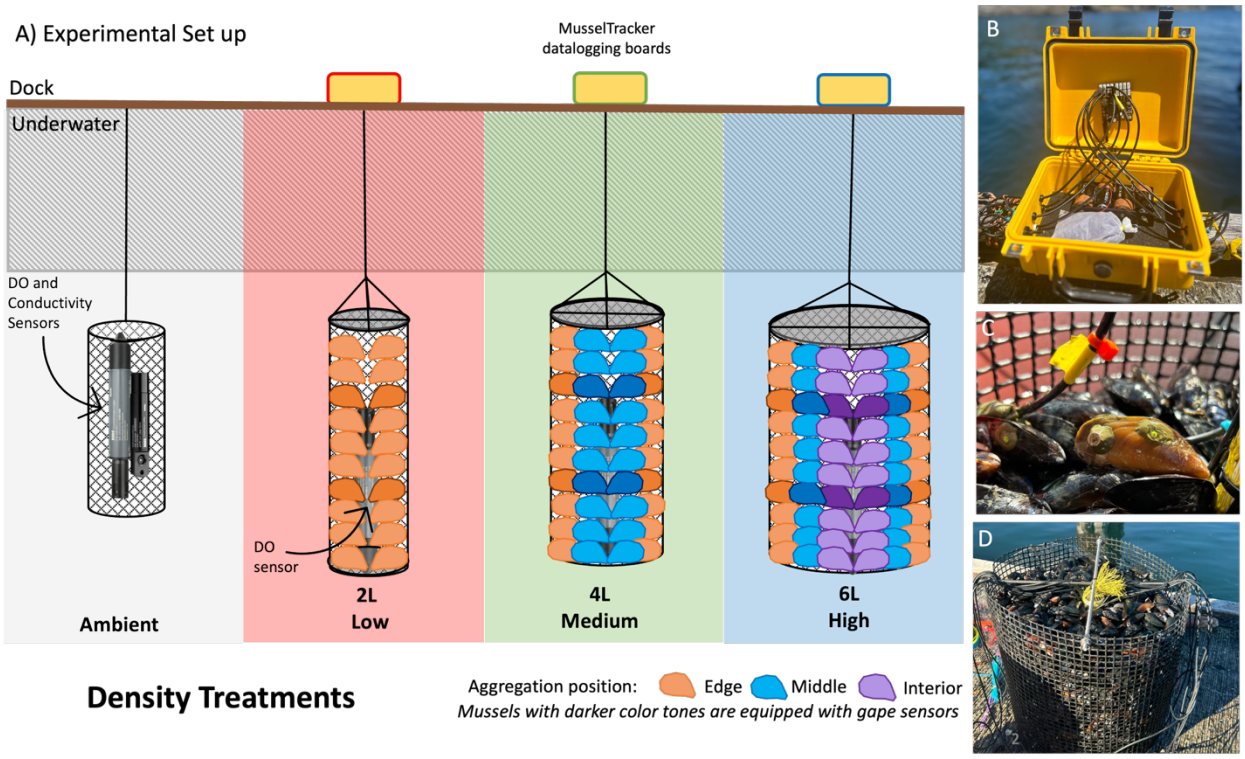

Figure 1. Schematic of experimental design and instrumentation for field experiment. A) Four mesh cylinders were suspended from the FHL dock: one contained only sensors to measure ambient water conditions (left), and each of the remaining three held mussel aggregations of *M. trossulus* at one of three biomass densities (2L = low), (4L = medium), (6L = high density). Each cylinder with mussels was instrumented with a DO sensor placed in the middle of each aggregation and a MusselTracker system to monitor gape sensors. Gape sensors were attached to four individual mussels per aggregation position: edge (orange), middle (blue), and interior (purple). (B) The MusselTracker system in a waterproof housing, with wires leading to gape sensors attached to mussels within cylinders. (C) Close-up view of two mussels fitted with gape sensors, before more mussels were added on top of them. (D) High-density (6L) mussel aggregation fully instrumented in its mesh cylinder before deployment.

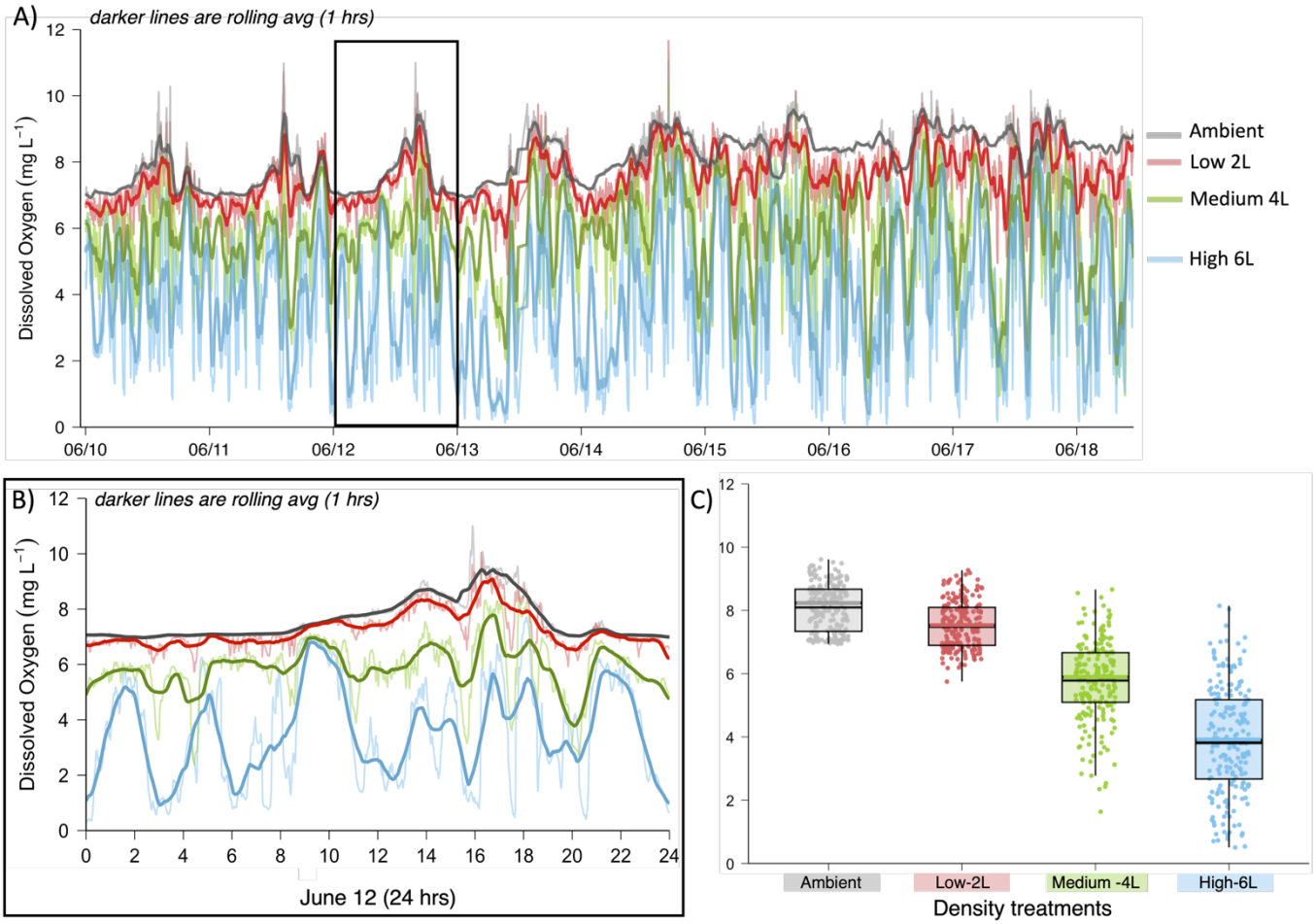

Figure 2. DO dynamics over time at the interior of each density treatment during the field experiment (June 10–18, 2024). (A) Time series of dissolved oxygen (DO, mg L^{-1}) for each treatment [low = 2L (red), medium = 4L (green), high = 6L(blue), and ambient control (grey)]. Lighter lines show 1-minute observations, and darker lines are 1-hour rolling averages. (B) Expanded view of a representative 24-hr period (June 12, black window in A) showing raw data taken every minute with hourly with 1-hour rolling means. (C) Boxplots summarizing variation in hourly mean DO (points) for each density treatment. Lines within each box represent the median (black) and mean (colored). The box indicates interquartile range (IQR; 25th–75th percentiles), and whiskers extend to data points within 1.5 × IQR.

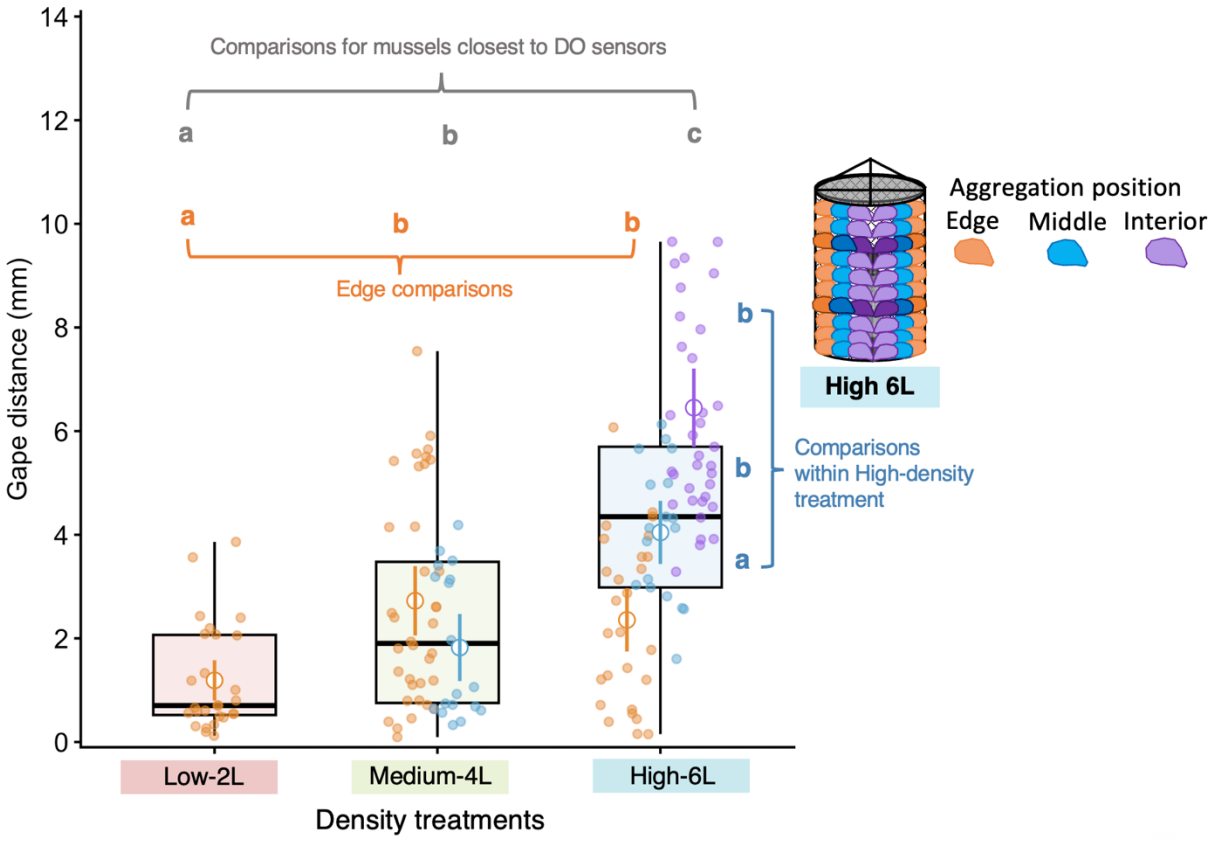

Figure 3. Mussel gape distance across density treatments and aggregation positions. Boxplots show the distribution of mean hourly gape distances across all sensors within each treatment: low (2L), medium (4L), and high (6L). Small colored points represent values for individual mussels, pooled by aggregation position (edge = orange, middle = blue, interior = purple). Larger open circles indicate mean gape ± 95% CI for each aggregation position. The schematic (right) illustrates the sensor placement within the high-density (6 L) bed, showing the horizontal stratification of mussels from the edge to the interior. Three different sets of pairwise comparisons were made, denoted by the different colored letters. If letters of the same color are different, this indicates significant differences among that pairwise comparison (Table S1: $p < 0.05$). Orange letters indicate differences among edge mussels across densities, grey letters among mussels positioned closest to the DO sensors, and blue letters among aggregation positions within the high–6L bed.

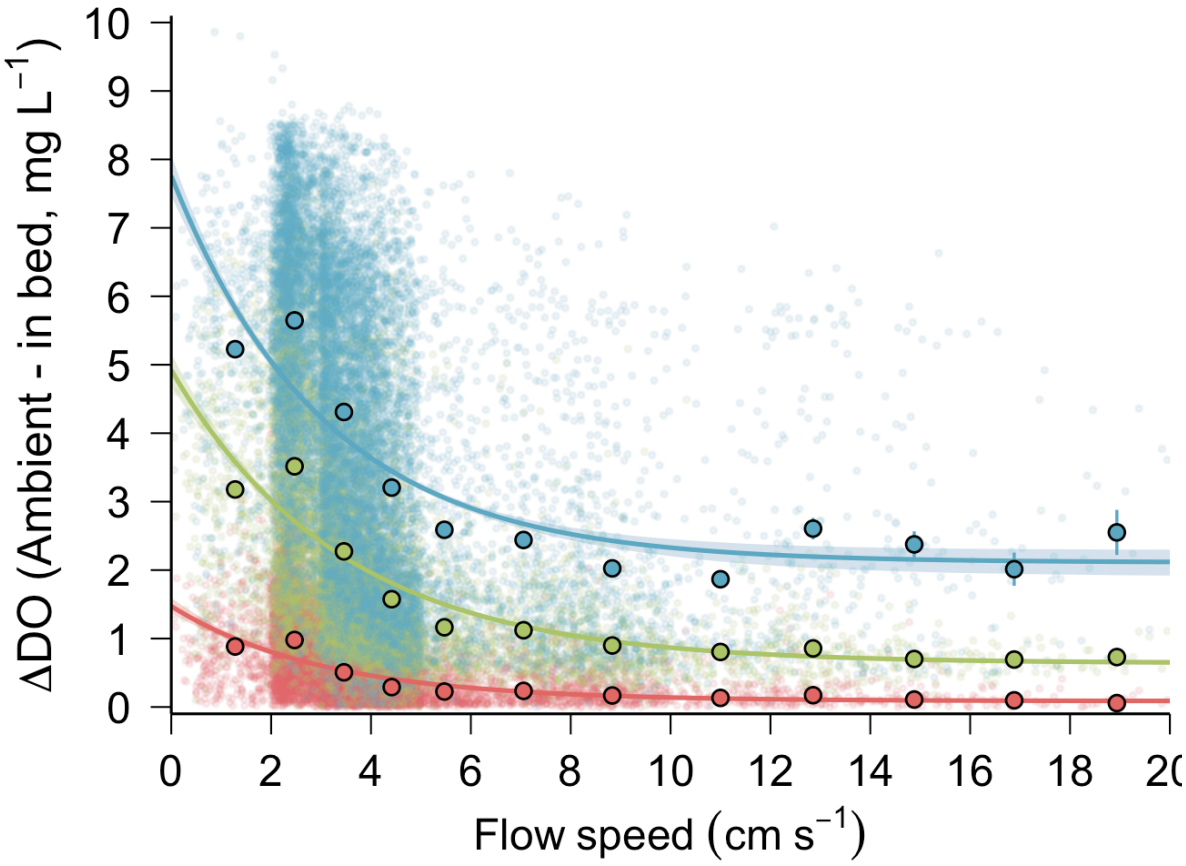

Figure 4. Flow speed effects on the difference in dissolved oxygen (ΔDO; Ambient – in aggregation) for each density treatment [low (2L-red), medium (4L-green), and high (6L-blue)]. Small points are 1-minute observations, while large filled circles are binned means ± 95% confidence intervals (CI) for each adaptive flow speed interval. Lines indicate nonlinear model fits (± 95% CI) for each density treatment.

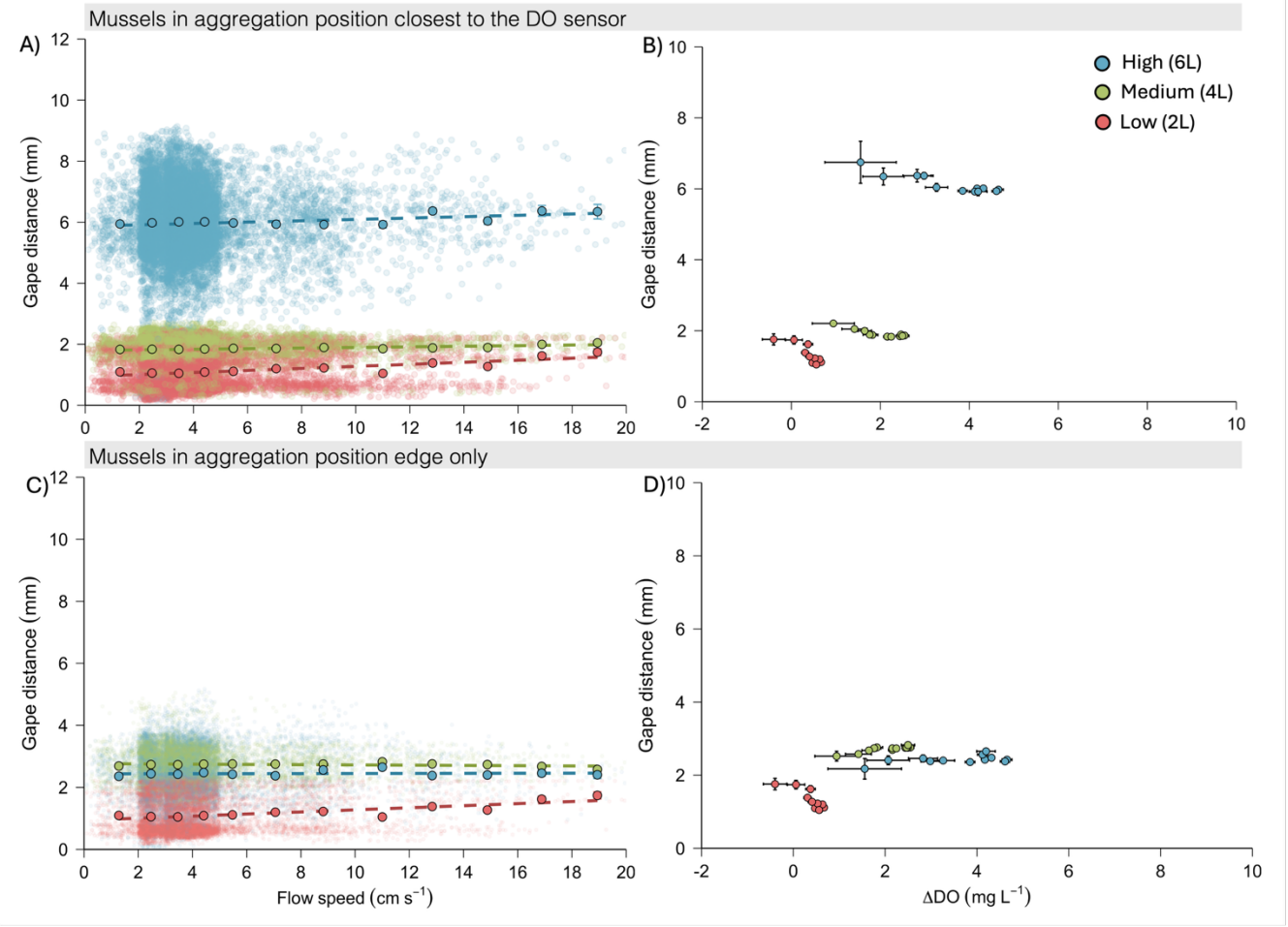

Figure 5. Effects of flow speed and dissolved oxygen differences (ΔDO) on mussel gaping behavior across density treatments and aggregation positions. (A–B) Mussels located in aggregation positions closest to the dissolved oxygen (DO) sensor—interior of high-density (6 L, blue), middle of medium-density (4 L, green), and edge of low-density (2 L, red) aggregations. (C–D) Mussels that were positioned along the edges of each density treatment. In panels A and C, small transparent points represent raw gape-distance measurements recorded every minute, and large filled circles show bin-averaged means ± standard error (SE) across adaptive flow-speed bins; dashed lines represent linear fits for each density treatment. In panels B and D, large filled circles represent bin-averaged means, with horizontal and vertical error bars indicating variability (± SE) in ΔDO and gape distance, respectively, for each corresponding flow speed.

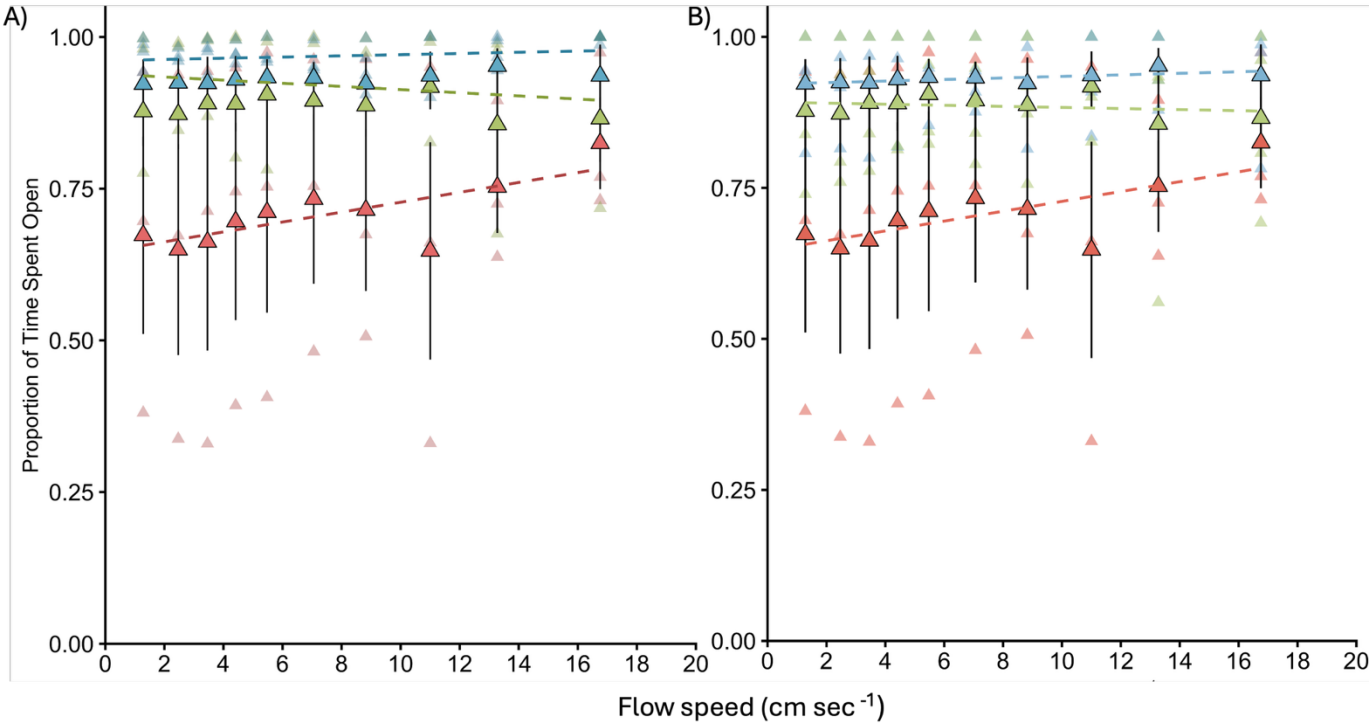

Figure 6. Proportion of time mussels remained open across flow speeds for different density treatments and aggregation positions. (A) Mussels located in aggregation positions closest to the dissolved oxygen (DO) sensor, representing individuals from the edge of low density–2L (red), the medium density–4L (green), and the interior of high density–6L (blue). (B) Mussels located along the edges of each density treatment. Light triangles show individual mussels (average proportion of time open per flow-speed bin), and dark triangles show treatment means ± SE across bins.

Supplemental Material

Table S1. **Model selection and planned pairwise comparisons for mussel gape distance across density treatments and aggregation positions.**(A) Akaike Information Criterion (AIC) results for linear mixed-effects models evaluating gape distance (mm) as a function of density treatment (Low–2L, Medium–4L, High–6L) and aggregation position (edge, middle, interior). All models were fitted using gape distance from one randomly selected hour per mussel per day (9 days total). Full Models included a random intercept for individual mussels and day to account for repeated measurements across days. ΔAIC values, model degrees of freedom (df), and model weights are shown relative to the best-fitting model. B) Planned pairwise comparisons of estimated marginal means (EMMs) from the top-ranked mixed model. Comparisons include: (i) differences among density treatments for mussels located at bed edges; (ii) differences among aggregation positions within the high-density (6 L) treatment; and (iii) differences among the aggregation positions located closest to the dissolved oxygen (DO) sensors across density treatments (Low edge, Medium middle, High interior). Differences were evaluated using Tukey-adjusted p-values.

A) AIC Model Selection for Gape Distance				
Model Description	ΔAIC		df	Model weight
Model w/ ind. mussel as re only	0		7	0.73
Full Model	2.00		8	0.27
Aggregation position only	25.31		6	<0.001
Density treatment only	48.5		6	<0.001
Random effect only	101.9		4	<0.001
B) Pairwise Comparisons				
(i) Comparison- edge positions only	estimate	SE	t.ratio	P-value
Low – Medium	**1.66**	**0.50**	**3.33**	**<0.004**
Low – High	**1.89**	**0.50**	**3.76**	**<0.001**
Medium – High	0.23	0.42	0.55	0.85
(ii) Comparison- within High–6L treatment				
Edge – Middle	-1.69	1.64	-1.03	0.59
Edge – Interior	**-4.10**	**1.37**	**-2.99**	**<0.05**
Middle – Interior	-2.41	1.55	-1.55	0.33
(iii) Comparison- aggregation position closest to DO	estimate	SE	t.ratio	P-value
Low edge – Medium middle	**-3.05**	**0.42**	**-7.24**	**<0.0001**
Medium middle - High interior	**-4.50**	**0.56**	**-7.99**	**<0.0001**
Low edge – High interior	**-7.55**	**0.68**	**-11.10**	**<0.0001**

Table S2. Summary of generalized linear model (GLM) results describing the effects of flow speed and mussel density on the proportion of time mussels remained open. Models were fit using a Gamma distribution with a log link function. (A) Mussels positioned closest to each dissolved oxygen (DO) sensor (Low–2 L, Medium–4 L, High–6 L). (B) Mussels located along the edges of each density treatment. Analysis of deviance tables show effects of flow speed (mean flow), density treatment (label), and their interaction. Estimated marginal means (EMMs) and Tukey-adjusted pairwise contrasts are provided on the log scale, with back-transformed mean proportions (± SE) and 95 % confidence intervals (CI) shown for clarity.

(A) Mussels in aggregation position closest to the DO sensor						
Factors		df	Deviance	Residual DF	Residual Deviance	P-value
Mean Flow speed		1	0.02	108	6.16	0.46
Density treatment		2	1.87	106	4.29	<0.001
Mean Flow speed× Density treatment		2	0.09	104	4.19	0.27
Estimated marginal means – pairwise contrasts						
Contrast	Estimate	SE			t-ratio	p-value
Low – Medium	-0.25	0.05			-5.53	<0.001
Low – High	-0.31	0.05			-7.24	<0.001
Medium – High	-0.05	0.05			-1.34	0.38
(B) Mussels in edge aggregation position only						
Factors		df	Deviance	Residual DF	Residual Deviance	P-value
Mean Flow speed		1	0.0004	119	6.36	0.92
Density treatment		2	1.26	117	5.00	<0.001
Mean Flow speed× Density treatment		2	0.15	115	4.84	0.12
Estimated marginal means – pairwise contrasts						
Contrast	Estimate	SE			t-ratio	p-value
Low – Medium	-0.20	0.04			-4.64	<0.001
Low – High	-0.27	0.04			-6.08	<0.001
Medium – High	-0.06	0.04			-1.56	0.27

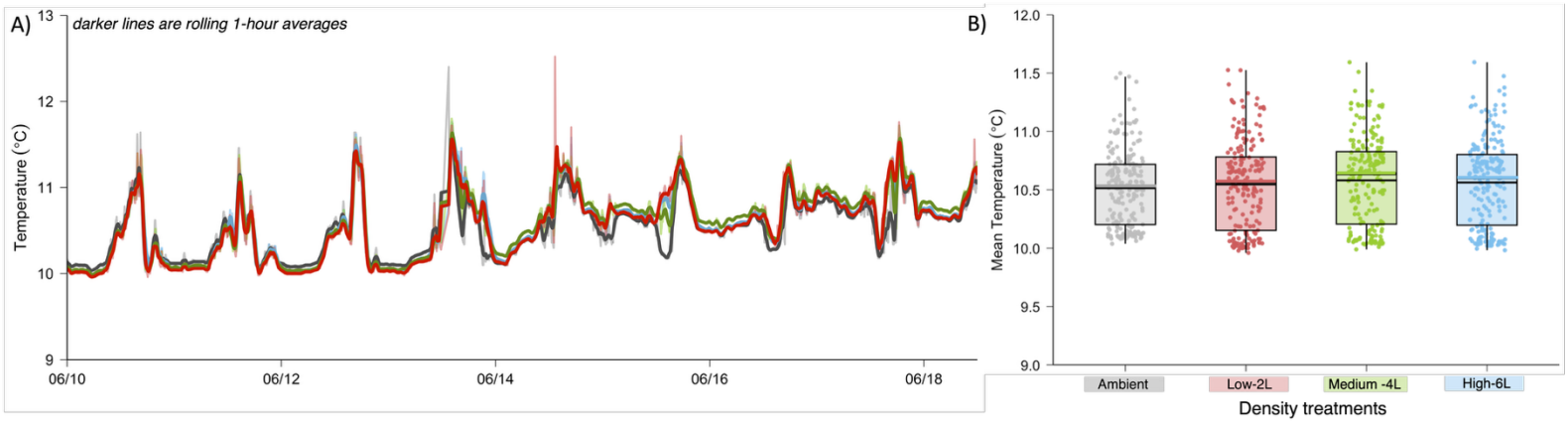

Figure S1. Temperature variation across density treatments.
(A) Time series of temperature (°C) from June 10–18 across mussel density treatments (low = 2L (red), medium = 4L (green), high = 6L (blue), and an ambient control (grey). Lighter lines show raw 1-minute measurements, and darker lines indicate 1-hour rolling averages. (B) Boxplots of hourly mean temperature across treatments. The horizontal black lines mark the median, colored lines are mean, boxes show the interquartile range (IQR; 25th–75th percentiles), and whiskers extend to data points within 1.5 × IQR. Individual points are 1-hour averages.

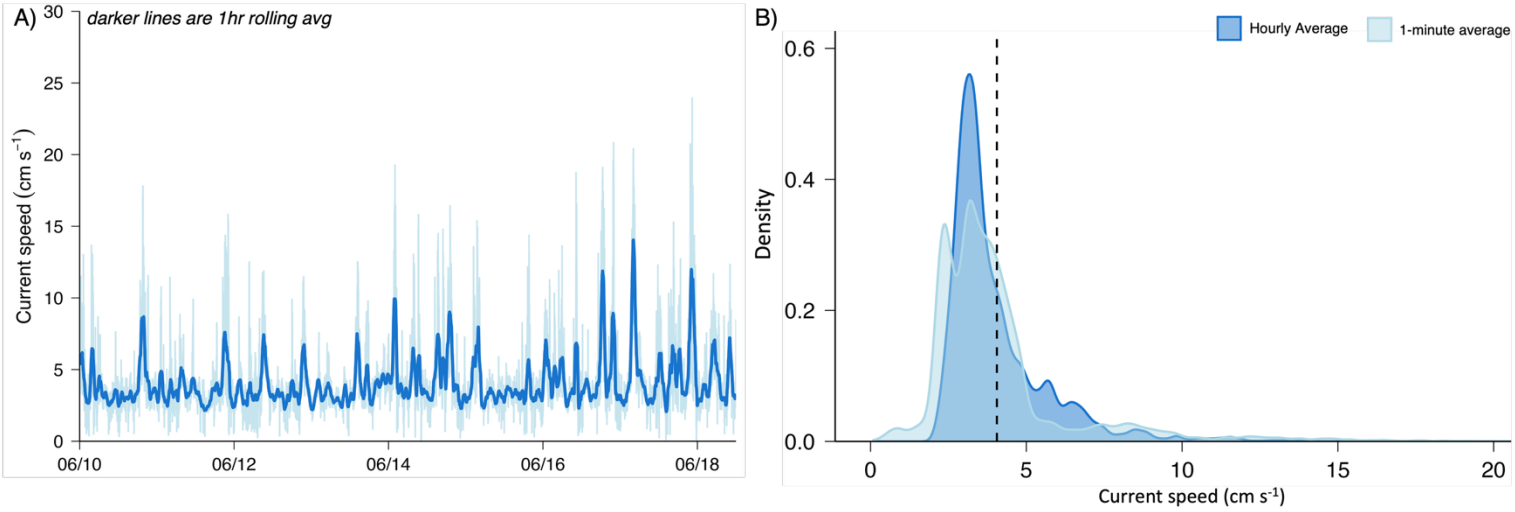

Figure S2. Current speeds across duration of the experiment. A) Time series of current speed during the experiment. The light blue line represents samples taken every minute, while the darker blue line is a 1-hour rolling average. B) Distribution of current speeds comparing the 1-minute and 1-hour datasets, the dashed black line represents the mean.